FATES Documentation

Release d2.0.0

FATES Development Team

Dec 03, 2021

CONTENTS

CHAPTER 1

TECHNICAL DOCUMENTATION FOR FATES

FATES is the "Functionally Assembled Terrestrial Ecosystem Simulator". It is an external module which can run within a given "Host Land Model" (HLM). Currently (November 2017) implementations are supported in both the Community Land Model of the Community Terrestrial Systems Model (CLM-CTSM) and in the Energy Exascale Earth Systems Model (E3SM) Land Model (ELM).

FATES was derived from the CLM Ecosystem Demography model (CLM(ED)), which was documented in:

Fisher, R. A., Muszala, S., Verteinstein, M., Lawrence, P., Xu, C., McDowell, N. G., Knox, R. G., Koven, C., Holm, J., Rogers, B. M., Spessa, A., Lawrence, D., and Bonan, G.: Taking off the training wheels: the properties of a dynamic vegetation model without climate envelopes, CLM4.5(ED), Geosci. Model Dev., 8, 3593-3619, https://doi.org/10.5194/gmd-8-3593-2015, 2015.

and this technical note was first published as an appendix to that paper.

https://pdfs.semanticscholar.org/396c/b9f172cb681421ed78325a2237bfb428eece.pdf

1.1 Authors of FATES code and technical documentation.

Rosie A. Fisher [1,2], Ryan G. Knox [3], Charles D. Koven [3], Gregory Lemieux [3], Chonggang Xu [4], Brad Christofferson [5], Jacquelyn Shuman [1], Maoyi Huang [6], Erik Kluzek [1], Benjamin Andre [1], Jessica F. Needham [3], Jennifer Holm [3], Marlies Kovenock [7], Abigail L. S. Swann [7], Stefan Muszala [1], Shawn P. Serbin [8], Qianyu Li [8], Mariana Verteinstein [1], Anthony P. Walker [11], Alan di Vittorio [3], Yilin Fang [9], Yi Xu [6]

[1] Climate and Global Dynamics Division, National Center for Atmospheric Research, Boulder, CO, USA

[2] Centre Européen de Recherche et de Formation Avancée en Calcul Scientifique, Toulouse, France

[3] Climate and Ecosystem Sciences Division, Lawrence Berkeley National Laboratory, Berkeley, CA, USA

[4] Earth and Environmental Sciences Division, Los Alamos National Laboratory, Los Alamos, NM, USA

[5] Department of Biology, University of Texas, Rio Grande Valley, Edinburg, TX, USA

[6] Atmospheric Sciences and Global Change Division, Pacific Northwest National Laboratory, Richland, WA, USA

[7] Department of Biology, University of Washington, Seattle, WA, USA

[8] Environmental and Climate Sciences Department, Brookhaven National Laboratory, Upton, NY, USA

[9] Energy and Environment Directorate, Pacific Northwest National Laboratory, Richland, WA, USA

[10] Jet Propulsion Laboratory, Pasadena, CA, USA

[11] Climate Change Science Institute, Environmental Sciences Division, Oak Ridge National Laboratory, Oak Ridge, TN, USA

1.2 Introduction

The Ecosystem Demography ('ED'), concept within FATES is derived from the work of *Moorcroft et al. (2001)*

and is a cohort model of vegetation competition and co-existence, allowing a representation of the biosphere which accounts for the division of the land surface into successional stages, and for competition for light between height structured cohorts of representative trees of various plant functional types.

The implementation of the Ecosystem Demography concept within FATES links the surface flux and canopy physiology concepts in the CLM/ELM with numerous additional developments necessary to accommodate the new model also documented here. These include a version of the SPITFIRE (Spread and InTensity of Fire) model of *Thonicke et al. (2010)*, and an adoption of the concept of *Perfect Plasticity Approximation* approach of *Purves et al. 2008*, *Lichstein et al. 2011* and *Weng et al. 2014*, in accounting for the spatial arrangement of crowns. Novel algorithms accounting for the fragmentation of coarse woody debris into chemical litter streams, for the physiological optimisation of canopy thickness, for the accumulation of seeds in the seed bank, for multi-layer multi-PFT radiation transfer, for drought-deciduous and cold-deciduous phenology, for carbon storage allocation, and for tree mortality under carbon stress, are also included and presented here.

Numerous other implementations of the Ecosystem Demography concept exist (See *Fisher et al. (2018)* for a review of these) Therefore, to avoid confusion between the concept of 'Ecosystem Demography' and the implementation of this concept in different models, the CLM(ED) implementation described by *Fisher et al. (2015)* will hereafter be called 'FATES' (the Functionally Assembled Terrestrial Ecosystem Simulator).

1.3 The representation of ecosystem heterogeneity in FATES

The terrestrial surface of the Earth is heterogeneous for many reasons, driven by variations in climate, edaphic history, ecological variability, geological forcing and human interventions. Land surface models represent this variability first by introducing a grid structure to the land surface, allowing different atmospheric forcings to operate in each grid cell, and subsequently by representing 'sub-grid' variability in the surface properties. In the CLM, the land surface is divided into numerous 'landunits' corresponding to the underlying condition of the surface (e.g. soils, ice, lakes, bare ground) and then 'columns' referring to elements of the surface that share below ground resources (water & nutrients). Within the soil landunit, for example, there are separate columns for crops, and for natural vegetation, as these are assumed to use separate resource pools. The FATES model at present only operates on the naturally vegetated column. The soil column is sub-divided into numerous tiles, that correspond to statistical fractions of the potentially vegetated land area. In the CLM 4.5 (and all previous versions of the model), sub-grid tiling operates on the basis of plant functional types (PFTs). That is, each piece of land is assumed to be occupied by only one plant functional type, with multiple PFT-specific tiles sharing a common soil water and nutrient pool. This PFT-based tiling structure is the standard method used by most land surface models deployed in climate prediction.

The introduction of the Ecosystem Demography concept introduces significant alterations to the representation of the land surface in the CLM. In FATES, the tiling structure represents the disturbance history of the ecosystem. Thus, some fraction of the land surface is characterized as 'recently disturbed', some fraction has escaped disturbance for a long time, and other areas will have intermediate disturbances. Thus the ED concept essentially discretizes the trajectory of succession from disturbed ground to 'mature' ecosystems. Within FATES, each "disturbance history class" is referred

to as a 'patch'. The word "patch" has many possible interpretations, so it is important to note that: **there is no spatial location associated with the concept of a 'patch' . It refers to a fraction of the potential vegetated area consisting of all parts of the ecosystem with similar disturbance history.**

The 'patch' organizational structure in CLM thus replaces the previous 'PFT' structure in the organization heirarchy. The original hierarchical land surface organizational structure of CLM as described in *Oleson et al. 2013* may be depicted as:

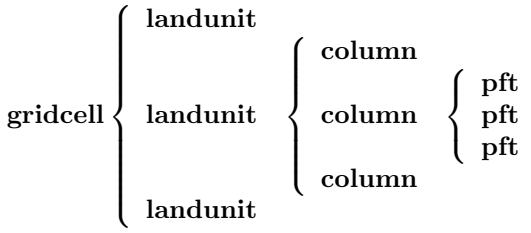

and the new structure is altered to the following:

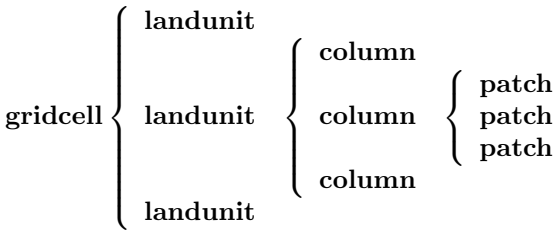

Thus, each gridcell becomes a matrix of 'patches' that are conceptualized by their 'age since disturbance' in years. This is the equivalent of grouping together all those areas of a gridcell that are 'canopy gaps', into a single entity, and all those areas that are 'mature forest' into a single entity.

1.3.1 Cohortized representation of tree populations

Each common-disturbance-history patch is a notional ecosystem that might in reality contain numerous individual plants which vary in their physiological attributes, in height and in spatial position. One way of addressing this heterogeneity is to simulate a forest of specific individuals, and to monitor their behavior through time. This is the approach taken by "gap" and individual-based models (*Smith et al. 2001*, *Sato et al. 2007*, *Uriarte et al. 2009*, *Fyllas et al. 2014*). The depiction of individuals typically implies that the outcome of the model is stochastic. This is because we lack the necessary detailed knowledge to simulate the individual plant's fates. Thus gap models imply both stochastic locations and mortality of plants. Thus, (with a genuinely random seed) each model outcome is different, and an ensemble of model runs is required to generate an average representative solution. Because the random death of large individual trees can cause significant deviations from the mean trajectory for a small plot (a typical simulated plot size is 30m x 30 m) the number of runs required to minimize these deviations is large and computationally expensive. For this reason, models that resolve individual trees typically use a physiological timestep of one day or longer (e.g. *Smith et al. 2001*, *Xiaidong et al. 2005*, *Sato et al. 2007*

The approach introduced by the Ecosystem Demography model *Moorcroft et al. 2001* is to group the hypothetical population of plants into "cohorts". In the notional ecosystem, after the land-surface is divided into common-disturbance-history patches, the population in each patch is divided first into plant functional types (the standard approach to representing plant diversity in large scale vegetation models), and then each plant type is represented as numerous height classes. Importantly, **for each PFT/height class bin, we model *one* representative individual plant, which tracks the average properties of this 'cohort' of individual plants.** Thus, each common-disturbance-history patch is typically occupied by a set of cohorts of different plant functional types, and different height classes within those plant functional types. Each cohort is associated with a number of identical trees, n_{coh} (where coh denotes the identification or index number for a given cohort)..

The complete hierarchy of elements in FATES is therefore now described as follows:

$$\textbf{gridcell}\left\{\begin{array}{l}\textbf{landunit}\\ \textbf{landunit}\left\{\begin{array}{l}\textbf{column}\\ \textbf{column}\left\{\begin{array}{l}\textbf{patch}\\ \textbf{patch}\left\{\begin{array}{l}\textbf{cohort}\\ \textbf{cohort}\\ \textbf{cohort}\end{array}\right.\\ \textbf{patch}\end{array}\right.\\ \textbf{column}\end{array}\right.\\ \textbf{landunit}\end{array}\right.$$

1.3.2 Discretization of cohorts and patches

Newly disturbed land and newly recruited seedlings can in theory be generated at each new model timestep as the result of germination and disturbance processes. If the new patches and cohorts established at *every* timestep were tracked by the model structure, the computational load would of course be extremely high (and thus equivalent to an individual-based approach). A signature feature of the ED model is the system by which *functionally equivalent* patches and cohorts are fused into single model entities to save memory and computational time.

This functionality requires that criteria are established for the meaning of *functional equivalence*, which are by necessity slightly subjective, as they represent ways of abstracting reality into a more tractable mathematical representation. As an example of this, for height-structured cohorts, we calculate the relativized differences in height (h_{coh}, m) between two cohorts of the same pft, p and q as

$$d_{hite,p,q} = \frac{\text{abs.}(h_{p-}h_q)}{\frac{1}{2}(h_p + h_q)}$$

If $d_{hite,p,q}$ is smaller than some threshold t_{ch}, and they are of the same plant functional type, the two cohorts are considered equivalent and merged to form a third cohort r, with the properties of cohort p and q averaged such that they conserve mass. The model parameter t_{ch} can be adjusted to adjust the trade-off between simulation accuracy and computational load. There is no theoretical optimal value for this threshold but it may be altered to have finer or coarser model resolutions as needed.

Similarly, for common-disturbance-history patches, we again assign a threshold criteria, which is then compared to the difference between patches m and n, and if the difference is less than some threshold value (t_p) then patches are merged together, otherwise they are kept separate. However, in contrast with height-structured cohorts, where the meaning of the difference criteria is relatively clear, how the landscape should be divided into common-disturbance-history units is less clear. Several alternative criteria are possible, including Leaf Area Index, total biomass and total stem basal area.

In this implementation of FATES we assess the amount of above-ground biomass in each PFT/plant diameter bin. Biomass is first grouped into fixed diameter bins for each PFT (ft) and a significant difference in any bin will cause patches to remain separated. This means that if two patches have similar total biomass, but differ in the distribution of that biomass between diameter classes or plant types, they remain as separate entities. Thus

$$B_{profile,m,dc,ft} = \sum_{d_{c,min}}^{d_{c,max}} (B_{ag,coh} n_{coh})$$

$B_{profile,m,dc,ft}$ is the binned above-ground biomass profile for patch m,d_c is the diameter class. $d_{c,min}$ and $d_{c,max}$ are the lower and upper boundaries for the d_c diameter class. $B_{ag,coh}$ and n_{coh} depict the biomass (KgC m^{-2}) and the number of individuals of each cohort respectively. A difference matrix between patches m and n is thus calculated as

$$d_{biomass,mn,dc,ft} = \frac{\text{abs}(B_{profile,m,hc,ft} - B_{profile,n,hc,ft})}{\frac{1}{2}(B_{profile,m,hc,ft} + B_{profile,n,hc,ft})}$$

If all the values of $d_{biomass,mn,hc,ft}$ are smaller than the threshold, t_p, then the patches m and n are fused together to form a new patch o.

To increase computational efficiency and to simplify the coding structure of the model, the maximum number of patches is capped at $P_{no,max}$. To force the fusion of patches down to this number, the simulation begins with a relatively sensitive discretization of patches (t_p = 0.2) but if the patch number exceeds the maximum, the fusion routine is repeated iteratively until the two most similar patches reach their fusion threshold. This approach maintains an even discretization along the biomass gradient, in contrast to, for example, simply fusing the oldest or youngest patches together.

The area of the new patch ($A_{patch,o}$, m^2) is the sum of the area of the two existing patches,

$$A_{patch,o} = A_{patch,n} + A_{patch,m}$$

and the cohorts 'belonging' to patches m and n now co-occupy patch o. The state properties of m and n (litter, seed pools, etc.) are also averaged in accordance with mass conservation .

1.3.3 Linked Lists: the general code structure of FATES

The number of patches in each natural vegetation column and the number of cohorts in any given patch are variable through time because they are re-calculated for each daily timestep of the model. The more complex an ecosystem, the larger the number of patches and cohorts. For a slowly growing ecosystem, where maximum cohort size achieved between disturbance intervals is low, the number of cohorts is also low. For fast-growing ecosystems where many plant types are viable and maximum heights are large, more cohorts are required to represent the ecosystem with adequate complexity.

In terms of variable structure, the creation of an array whose size could accommodate every possible cohort would mean defining the maximum potential number of cohorts for every potential patch, which would result in very large amounts of wasted allocated memory, on account of the heterogeneity in the number of cohorts between complex and simple ecosystems (n.b. this does still happen for some variables at restart timesteps). To resolve this, the cohort structure in FATES model does not use an array system for internal calculations. Instead it uses a system of *linked lists* where each cohort structure is linked to the cohorts larger than and smaller than itself using a system of pointers. The shortest cohort in each patch has a 'shorter' pointer that points to the *null* value, and the tallest cohort has a 'taller' pointer that points to the null value.

Instead of iterating along a vector indexed by coh, the code structures typically begin at the tallest cohort in a given patch, and iterate until a null pointer is encountered.

Using this structure, it is therefore possible to have an unbounded upper limit on cohort number, and also to easily alter the ordering of cohorts if, for example, a cohort of one functional type begins to grow faster than a competitor of another functional type, and the cohort list can easily be re-ordered by altering the pointer structure. Each cohort has *pointers* indicating to which patch and gridcell it belongs. The patch system is analogous to the cohort system, except that patches are ordered in terms of their relative age, with pointers to older and younger patches where cp_1 is the oldest:

1.3.4 Indices used in FATES

Some of the indices used in FATES are similar to those used in the standard CLM4.5 model; column (c), land unit(l), grid cell(g) and soil layer (j). On account of the additional complexity of the new representation of plant function, several additional indices are introduced that describe the discritization of plant type, fuel type, litter type, plant height, canopy identity, leaf vertical structure and fuel moisture characteristics. To provide a reference with which to interpret the equations that follow, they are listed here.

Table 1.1: Table of subscripts used in this document

Parameter Symbol	Parameter Name
ft	Plant Functional Type
fc	Fuel Class
lsc	Litter Size Class
coh	Cohort Index
patch	Patch Index
cl	Canopy Layer
z	Leaf Layer
mc	Moisture Class
o	Plant Organ Index
s	Nutrient Species Index

1.3.5 Cohort State Variables

The unit of allometry in the ED model is the cohort. Each cohort represents a group of plants with similar functional types and heights that occupy portions of column with similar disturbance histories. The state variables of each cohort therefore consist of several pieces of information that fully describe the growth status of the plant and its position in the ecosystem structure, and from which the model can be restarted. The state variables of a cohort are as follows:

Table 1.2: State Variables of 'cohort' sructure

Quantity	Variable name	Units	Notes
Plant Functional Type	ft_{coh}	integer	
Number of Individuals	n_{coh}	n per 10000m:math:' ^{-2}'	
Height	h_{coh}	m	
Diameter	dbh_{coh}	cm	
Carbon Mass	$C_{(o,coh)}$	Kg plant^{-1}	leaf, fine-root sapwood, storage, structural, reproductive
Nutrient Mass	$N_{(o,s,coh)}$	Kg plant^{-1}	Optional depending on hypothesis. See PARTEH documentation.
Leaf memory	$l_{memory,coh}$	KgC plant^{-1}	Leaf mass when leaves are dropped
Phenological Status	$S_{phen,coh}$	integer	1=leaves off. 2=leaves on
Canopy Layer Index	cl_{coh}	integer	1=top canopy >1=understory
Canopy trimming	$C_{trim,coh}$	fraction	1.0=max leaf area
Patch Index	p_{coh}	integer	To which patch does this cohort belong?

1.3.6 Patch State Variables

A patch, as discuss earlier, is a fraction of the landscape which contains ecosystems with similar structure and disturbance history. A patch has no spatial location. The state variables, which are 'ecosystem' rather than 'tree' scale properties, from which the model can be restarted, are as follows

Table 1.3: State variables of 'patch' structure

Quantity	Variable name	Units	Indexed By
Area	A_{patch}	m^2	
Age	age_{patch}	years	
Seed	$seed_{patch}$	KgC m^{-2}	ft
Leaf Litter	$l_{litter,patch}$	KgC m^{-2}	ft
Root Litter	$r_{litter,patch}$	KgC m^{-2}	ft
AG Coarse Woody Debris	$CWD_{AG,patch}$	KgC m^{-2}	Size Class (lsc)
BG Coarse Woody Debris	$CWD_{BG,patch}$	KgC m^{-2}	Size Class (lsc)
Canopy Spread	$S_{c,patch}$		Canopy Layer
Column Index	l_{patch}	integer	

1.3.7 Model Structure

Code concerned with the Ecosystem Demography model interfaces with the CLM model in four ways: i) During initialization, ii) During the calculation of surface processes (albedo, radiation absorption, canopy fluxes) each model time step (typically half-hourly), iii) During the main invokation of the ED model code at the end of each day. Daily cohort-level NPP is used to grow plants and alter the cohort structures, disturbance processes (fire and mortality) operate to alter the patch structures, and all fragmenting carbon pool dynamics are calculated. iv) during restart reading and writing. The net assimilation (NPP) fluxes attributed to each cohort are accumulated throughout each daily cycle and passed into the ED code as the major driver of vegetation dynamics.

1.4 Initialization of vegetation from bare ground

If the model is restarted from a bare ground state (as opposed to a pre-existing vegetation state), the state variables above are initialized as follows. First, the number of plants per PFT is allocated according to the initial seeding density (S_{init}, individuals per m^2) and the area of the patch A_{patch}, which in the first timestep is the same as the area of the notional ecosystem A_{tot}. The model has no meaningful spatial dimension, but we assign a notional area such that the values of 'n_{coh}' can be attributed. The default value of A_{tot} is one hectare (10,000 m^2), but the model will behave identically irrepective of the value of this parameter.

$$n_{coh,0} = S_{init} A_{patch}$$

Each cohort is initialized at the minimum canopy height $h_{min,ft}$, which is specified as a parameter for each plant functional type and denotes the smallest size of plant which is tracked by the model. Smaller plants are not considered, and their emergence from the recruitment processes is unresolved and therefore implicitly parameterized in the seedling establishment model.

The diameter of each cohort is then specified according to the height-diameter allometry function associated with the PFT of interest, see *Table of Allometric Functions*. The biomass pools for the newly recruited plant are then determined from the allometry equations that define the target (idealized) sizes for each pool.

Table 1.4: (INCOMPLETE) List of the parameters that define the intialization of new plants during a "cold-start" simulation.

Parameter Symbol	Parameter Name	Units	Default Value
h_{min}	Minimum plant height	m	1.5
S_{init}	Initial Planting density	Individuals m^{-2}	

1.5 Allocation and Reactive Transport (PARTEH)

The **Plant Allocation** and **Reactive Transport Extensible Hypotheses (PARTEH)** is a suite of modules that handle the processes of allocation, transport and reactions (i.e. thos processes related to movement and change, yet perhaps not the genesis) of various arbitrary species (carbon, nutrients, toxins, etc) within the various organs of live vegetation. In FATES, these processes are resolved per unit plant, for each cohort.

1.5.1 Overview

The **Plant Allocation** and **Reactive Transport Extensible Hypotheses (PARTEH)** is a suite of modules that handle the processes of allocation, transport and reactions (i.e. thos processes related to movement and change, yet perhaps not the genesis) of various arbitrary species (carbon, nutrients, toxins, etc) within the various organs of live vegetation.

The modules themselves are written in modern Fortran, with an emphasis on code extensibility (i.e. future proofing). This software can therefore be compiled and embedded in Land Surface Models (LSMs) and Dynamic Vegetation Models (DVMs). A functional unit testing infrastructure, written in python, is also used to evaluate how the different modules that define the allocation, reaction and transport hypotheses, operate under contexts of different synthetic boundary conditions.

PARTEH's Domain of Influence

Summary of Domain of Influence:

1. Single plant allocation, transport and the associated reactions
2. Not photosynthesis
3. Optional payment of respiration costs, and/or optional calculations of rates associated with transport/allocation (growth respiration)
4. Turnover losses and turnover re-translocation, coordinated with external modules
5. Accepts soil nutrient boundary fluxes, not a soil BGC model

An expanded description of PARTEH's scope follows.

PARTEH's scope is not limited to, but will likely be applied on individual plants. It may operate as a sub-component of ecosystem scaling models (such as FATES, ED, etc) where its treatment of single plant physics, will be translated into cohorts. Hypotheses may also be crafted that operate on other scales, such as pools that are disasociated from individual plants.

PARTEH is intended to work in coordination with, but not replicate, photosynthesis modules.

Since some respiratory costs are tightly connected with allocation, reactions and transport, PARTEH is designed to both support alternative hypothesis on and perform calculations of associated respiration costs, or accept respiration costs associated with allocation as an input.

PARTEH does handle the turnover of live plants. These calculations may rely on coordination with outside modules that specify the scale and scope of turnover associated with events like deciduous leaf drop, deciduous leaf flushing, fire, herbivory or storms. Turnover is inextricably linked to re-translocation, which is classified as reaction and transport. This turnover may be mediated either through continuous (background) type behavior, or event based behavior (e.g. leaf drop).

PARTEH does not simulate the fate of live vegetation turnover, for example litter decomposition, and it is expected that these carbon and nutrient loss fluxes are passed to the host-model (e.g FATES) to be accounted for.

PARTEH does not handle plant mortality. A host model may ask PARTEH for diagnostics on nutrient concentrations in various plant organs, however decisions on how this is expected to influence plant survival are handled outside of the model.

PARTEH does not handle below-ground soil-biogeochemistry. The uptake of nutrients from the soil is an expected boundary condition, however it is also expected that the soil biogeochemical model will ask PARTEH to provide information on the state of plant organs and perhaps the concentrations of species present in those organs so that is can properly determine the plant's affinity for nutrient fluxes. Further, this fluxes will likely be mediated through a vegetation scaling model (e.g. FATES scales PARTEH affinities and fluxes in its communication with a below-ground model (ECA, CNP, PFLOTRAN, etc.).

Why "Extensible Hypotheses"?

The breadth of knowledge of how plants handle reactive transport is increasing, yet many uncertainties remain. In light of so many uncertainties, it has seemed inappropriate to coalesce around a single functional hypothesis for terrestrial ecosystem modeling.

Moreover, if so many uncertainties remain, a framework that could conveniently intercompare functional hypthesese with the hopes of comparing with available data, seems useful.

This has led to a design strategy that supports extensibility in design and intercomparison of multiple functional hypotheses of Plant Reactive Transport. Thus, it is considered a suite of modules, and not a model, because it is designed to accomodate many different functional hypotheses about how plant handle nutrient dynamics.

Software Design

PARTEH is written in **modern Fortran** using some object oriented coding principles. It may be called from terrestrial ecosystem model, or it can be called using its own driver (which is written in python).

The PARTEH software is packaged with the FATES model. PARTEH software is found in two locations. In the fates/parteh folder, the main fortran code that houses the PARTEH class objects and processes is found. The fates/functional_unit_testing/parteh/ folder contains scripts for functional unit testing of the PARTEH submodule. The scripts running the tests are written in python. XML files control the tests and set parameters. There are also fortran codes that serve as wrappers and support to help make the connection between the python unit testing framework and the core PARTEH fortran code found in fates/parteh.

The module system does not yet leverage external numerical libraries such as Petsc, trilos or sundials. In the first iterations of building this module system, the numerical integration needs have been fairly simple. However, the solving of numerical integration has been written in such a way that all hypotheses currently call the same generic routines. Curently an **Euler scheme**, and a **Runge-Kutte-Fehlerg 4/5th order** are offered. By writing the modules such that they call a self-contained generic integration layer, the code is in a more ready state to upgrade to a more sophisticated external library.

The module system uses the principal of **inheritance** to help facilitate extensible softare design. Specifically, a **base-class** has been designed, which forces all the different hypotheses to be written as **extensions** of the base. Thus, each hypothesis will have a template of how to populate the various state-variables and how and when to call its procedures. Moreover, the base class contains helper procedures that connect to the external needs of PARTEH. For intance, if a model such as FATES needs to ask PARTEH how much leaf biomass exists, it can call a procedure defined by the base class which will return the leaf biomass wihtout explicitly stating which hypothesis to calculate it for. By attaching these helper functions to the base class, these operate on all extensions (different hypotheses of the base), therefore buffering the environment outside of PAREH to the choices that are made inside of PARTEH.

Conventions Used

Symbology

In the description of all hypotheses, the following symbology will be used. For a generic variable X:

Table 1.5: Table 1

Symbol	Description
$\dot{X}$	Flux rate
$\vec{X}$	Time integrated (total) flux
$\hat{X}$	Deficit or demand relative to reference
$\bar{X}$	Target quantity
$\tilde{X}$	Time integrated turnover loss

The PARTEH code will mostly be concerned with the mass pools of carbon and nutrients as state variables (those entities which maintain continuity through time and space, and are integrated). Pools will generally refer to the mass, in absolute units [kg]. Any pool can also be defined by a combination of species (carbon, nitrogen, phosphorous, etc.) and organ (leaf, fine-root, sapwood, etc). While the code is flexible enough to accomodate different isotopes of carbon, in general carbon species in this document will be denoted generically $C_{(o)}$ for any organ indexed o. Nutrients of arbitrary species s and organ o will be denoted $N_{(o,s)}$. See *Table 2*:

Table 1.6: Table 2

Symbol	Dimension	Description	Units
State Variables			
$C_{(o)}$	organ	carbon mass	[kg]
$N_{(o,s)}$	organ x species	nutrient mass	[kg]

All Parameters Are PFT Specific

A note about parameters. All parameters (thus far) used in PARTEH, can be assumed as PFT specific. In each of the describing tables, this is indicated. But the notation in describing text does not maintain a "pft" dimension, as it should just be implied.

1.5.2 Hypotheses

The bulk of the more complicated processes in PARTEH are subsumed in the allocation and transport of newly acquired resources. However, since the process of re-translocation during turnover is a reactive transport process, this falls within PARTEH's domain. Therefore, broadly, reactive transport in PARTEH is partitioned into allocation and turnover.

The PARTEH software is written to enable flexibility in the frequency and order at which allocation and turnover processes are used/called. In FATES, both are called daily and tunover (all forms) are called first.

The PARTEH software is also written such that allocation hypothesis are each relegated inside their own modules. Turnover, for which existing hypotheses are somewhat simpler than allocation, are written generically and can operate in concert with any allocation hypothesis for any arbitrary set of organs and nutrients.

Turnover Hypotheses

Overview of Turnover

In the turnover phase, biomass is removed from the plant due to turnover associated with both maintenance and event based processes.

1. Maintenance turnover is continuous, and typically applies to the constant overturn of ageing leaves and fine-roots in evergreens, and continuous branchfall in most all species
2. Event based turnover refers to phenology and/or seasonal losses of leaves and fine-roots in deciduous plants, or losses due to the damage from storms or fire.

The parameters that govern the rate of turnover are applicable to the maintenance rates. The severity of losses due to events are governed by external modules. Since a plant must be exclusively one of evergreen or deciduous, the parameters that govern retranslocation are applicable in each context. If a plant is evergreen, the leaf retranslocation parameter for that functional type is relevant to maintenance turnover process in leaves. If a plant is deciduous, the leaf retranslocation parameter is relevant to the seasonal or stress induced drop processes. The table *Turnover Parameters* describes the parameters.

Table 1.7: Turnover Parameters

Symbol	Dimension	Description	Units
τ_l	pft*	leaf maintenance turnover timescale	[years]
τ_f	pft*	fine-root maintenance turnover timescale	[years]
τ_b	pft*	branch turnover timescale	[years]
$\eta_{c(o)}$	pft* x organ	carbon retranslocation fraction	[kg/kg]
$\eta_{n(o)}$	pft* x organ	nitrogen retranslocation fraction	[kg/kg]
$\eta_{p(o)}$	pft* x organ	phosphorous retranslocation fraction	[kg/kg]

List of key parameters used for turnover processes. :math:'' Note that the parameters are specified explicitly for each pft, but the dimension will be implied in our notation as each plant is already uniquely asociated with a PFT.*

Maintenance Turnover Hypotheses

Constant Fraction Maintenance Turnover and Retranslocation

Constant fraction turnover can be applied to any arbitrary mass pool. The loss rates are governed by the turnover parameters for leaves, fine-roots and branches, as well as the re-translocation fractions. See *Turnover Parameters*

Turnover losses to leaves (organ set $o = \mathbb{O}_l$) and fineroots (organ set $o = \mathbb{O}_f$) are dictated by their turnover timescale parameters τ_l and τ_f respectively. Branchfall affects the pools of sapwood, structure, storage and reproduction (if non-zero), which have the branchfall set of organs $o = \mathbb{O}_b$. Note that with no re-translocation of nutrients, these rates apply to all nutrient species. The turnover timescale is in units of [years-1], the elapsed time Δ_{yr} is in units of years (which in practice is 1/365). Some amount of nutrient of each species s may be re-translocated directly back into the existing pool as proportions dictated by $\eta_{l(s)}$ and $\eta_{f(s)}$ in leaves and fine-root respectively. The turnover flux for

carbon $\tilde{C}$ and nutrient species $\tilde{N}$ are calculated as:

$$
\begin{aligned}
&\text{leaves} \\
&\tilde{C}_{(\mathbb{O}_l)} = C_{(\mathbb{O}_l)} \cdot \tau_l \cdot \Delta_{yr} \\
&\tilde{N}_{(\mathbb{O}_l,s)} = N_{(\mathbb{O}_l,s)} \cdot \tau_l \cdot \Delta_{yr} \cdot (1 - \eta_{c(ft,\mathbb{O}_l)}) \\
&\text{fine-roots} \\
&\tilde{C}_{(\mathbb{O}_f)} = C_{(\mathbb{O}_f)} \cdot \tau_f \cdot \Delta_{yr} \\
&\tilde{N}_{(\mathbb{O}_f,s)} = N_{(\mathbb{O}_f,s)} \cdot \tau_f \cdot \Delta_{yr} \cdot ((1 - \eta_{*(ft,\mathbb{O}_f)}) \\
&\text{branches} \\
&\tilde{C}_{(\mathbb{O}_b,s)} = C_{(\mathbb{O}_b,s)} \cdot \tau_b \cdot \Delta_{yr} \\
&\tilde{N}_{(\mathbb{O}_b,s)} = N_{(\mathbb{O}_b,s)} \cdot \tau_b \cdot \Delta_{yr}
\end{aligned}
\tag{1.1}
$$

Note that as an end-user of the FATES model, the retranslocation factors are defined in separate arrays by species. The notation we use in the above equations are simplified to indicate that the nutrient retranslocation factors specific to the species of interest, e.g. $\eta_{*(ft,\mathbb{O}_f)}$. These loss fluxes are directly removed from the state variables for any organ o and species s:

$$
\begin{aligned}
C_{(o)} &= C_{(o)} - \tilde{C}_{(o)} \\
N_{(o,s)} &= N_{(o,s)} - \tilde{N}_{(o,s)}
\end{aligned}
$$

Event Based Turnover Hypotheses

Event Based Turnover with Simple Retranslocation Hypotheses

For event-based turnover, the host model must provide PARTEH with the fractions of the biomass that should be removed from each organ in the event. Depending on the context, PARTEH will or will-not implement re-translocation of nutrients.

PARTEH will implement re-translocation for these events:

1. Deciduous leaf drop

PARTEH will not implement re-translocation for these events:

1. Fire losses
2. Herbivory
3. Storms

The procedures for both contexts are similar, where in the later, the re-translocation factors can be assumed as zero.

In all situations, when the events are triggered, a fraction mass lost must be passed in as the argument. As an example, for deciduous leaf drop, the fraction of dropped leave f_{drop} is assessed from the phenology module and passed into the PARTEH module. We define a mass M which is represented for any carbon or nutrient species present, (defined by species set $s = \mathbb{S}$), and each organ in that set $o = \mathbb{O}_l$ (perhaps there are multiple leaf organs). For all species and organs in that set, we define the turnover (or loss) mass $\vec{M}_{loss(\mathbb{S},\mathbb{O}_l)}$ and the re-translocated mass $\vec{M}_{retr(\mathbb{S},\mathbb{O}_l)}$ which is destined for storage $M_{(\mathbb{S},st)}$.

$$
\begin{aligned}
\vec{M}_{loss(\mathbb{S},\mathbb{O}_l)} = &\quad (1 - \eta_{*(ft,\mathbb{O}_l)}) \cdot M_{(\mathbb{S},\mathbb{O}_l)} \cdot f_{drop} \\
\vec{M}_{retr(\mathbb{S},\mathbb{O}_l)} = &\quad \eta_{*(ft,\mathbb{O}_l)} \cdot M_{(\mathbb{S},\mathbb{O}_l)} \cdot f_{drop}
\end{aligned}
\tag{1.2}
$$

Both fluxes decrement the pool of interest, while the loss flux leaves the live plant's control volume, and the retranslocated mass increments storage carbon.

$$\begin{aligned} M_{(\mathbb{S},\mathbb{O}_l)} = &\quad M_{(\mathbb{S},\mathbb{O}_l)} - (\vec{M}_{loss(\mathbb{S},\mathbb{O}_l)} + \vec{M}_{retr(\mathbb{S},\mathbb{O}_l)}) \\ M_{(\mathbb{S},st)} = &\quad M_{(\mathbb{S},st)} + \vec{M}_{retr(\mathbb{S},\mathbb{O}_l)} \end{aligned} \tag{1.3}$$

Allocation Hypotheses

Allocation Hypothesis 1: Allometrically Guided, Carbon Only

Hypothesis 1, the carbon-only allometric hypotheses, assumes there is a single carbon species for each of the six plant organ pools:

1. Leaf
2. Fine-root
3. Sapwood
4. Structural wood
5. Storage
6. Reproductive

This method was designed to be called daily, which is true when called for the FATES model.

The carbon-only allometric hypotheses contains no nutrient species, no growth limitations based on nutrients, and asumes that tissues will grow in proportion to each other based on a set of allometric functions. These allometric functions are tied to diameter d. For PARTEH, these allometric functions are those used by FATES. The allometric functions will calculate a target mass for each pool, which essentially is the maximum carrying capacity for that pool based on the plant's size (stem diameter). In the case of grasses, diameter is still used. And even though it does not have a physical meaning, it is still a usefull mediator to tie all the proportional pools together. For mature trees, the diameter should reflect the diameter at breast height. Target leaf mass is slightly more complicated. The target leaf mass is based also on a trimming function which scales down the maximum leaf biomass to remove unproductive leaves from shaded lower boughs. Allometric schemes are based off of previous research, which will be noted in intercomparisons.

This documentation will use the generic symbol C for carbon masses and fluxes for organs indexed by o. Also see *Conventions Used*.

Table 1.8: Table H1-1

Symbol	Dimension	Description	Units
State Variables			
$C_{(o)}$	organ	carbon mass	[kg]
Input/Output Boundary Conditions			
d	scalar	Reference Stem Diameter	[cm]
Input Boundary Conditions			
C_{gain}	scalar	Daily carbon gain	[kg]
f_{trim}	scalar	Canopy Trim Fraction	[0-1]
Parameters			
p_{tm}	pft*	maintenance replacement priority	[0-1]

List of key states, boundary conditions and parameters in hypothesis 1, allometric based carbon-only model. In this notation, o is used to index the organ dimension. :math:'' Note that the pft index for the maintenance replacement priority is specified for each PFT, but the dimension will be implied in our notation as each plant is uniquely asociated with a PFT.*

Assumptions of Other Processes

Daily Carbon Gain

It is assumed that over the sub-daily time-steps, net gains photosynthesis and losses from total plant respiration (growth and maintenance) are calculated and integrated (or accumulated). The net sum of these terms results in a daily net carbon gain C_{gain}.

Turnover and Phenology

It is assumed that for the current day, all turnover from live plants has already been removed, and/or any flushing associated with leaf-out (or bud-burst) has already been transferred (most likely from storage).

Different methodologies for calculating turnover exist. Event based turnover is covered in *Event Based Turnover Hypotheses*, and maintenance turnover is covered in *Maintenance Turnover Hypotheses*.

The PARTEH software system provides helper functions to remove, add and transfer carbon and nutrients during these different processes. It is up to various external modules such as fire and phenology to determine the timing and relative magnitudes of the pools being reduced or flushed.

Order of Operations

Allocation for this hypothesis can be partitioned roughly into two parts, replenishing the plants' existing pools with respect to a target mass that is defined by the stature (size) of the plant (this may be thought of of bringing the plant back to allometric targets). And then, if resources are still available, the plant will grow in stature where allocation seeks to grow the pools out concurrently with each other.

1. *Replenish Pools with Respect to Target Levels*
2. *Grow Stature Concurrently*

Replenish Pools with Respect to Target Levels

The plant will go through a sequence of allocations into the different plant tissues, ultimately attempting to get each organ's total carbon pool up to the target mass, $\grave{C}_{(o)}$. These targets are goverened by the stature of the plant, and can be thought of as the desireable pool sizes that the plant would likely have if it were prepared to grow in stature. Losses from turnover, may have drawn down the masses away from the target values associated with their current stature. Sometimes this is considered being "off allometry". In this hypothesis, the base assumption is that the targets are dictated by allometry, but other methods of determining these targets are possible as well. Allometric targets are dicated here, by a function of plant diameter d , plant functional type pft, and the canopy trim fraction f_{trim}. This last variable, can be described as the fraction of the crown that this particular plant desires to fill out, compared to a prototypical plant in idealized conditions. This fraction changes slowly over yearly time-scales, responding to the relative productivity of the plant's crown layers with respect to their respiration costs.

$$\grave{C}_{(o)} = \text{func}(d, \text{pft}, f_{trim}) \tag{1.4}$$

Replace Maintenance Turnover

The first step in replenishing carbon pools is the replacement of maintenance turnover losses in evergreen plants. Evergreen plants continually loose leaf and fine-root tissues over the course of the year. We first define an organ set: $o = \mathbb{O}_{lf}$, which is comprised of leaves and fine-roots. The demand for replacement of each organ in this set

$\check{C}_{(\mathbb{O}_{lf})}$, is governed by the amount of carbon each organ lost to turnover on this day $\vec{C}_{turn(\mathbb{O}_{lf})}$. A parameter governs this prioritization. When $p_{tm} = 1$, an attempt is made to replace all carbon lost from maintenance turnover. When $p_{tm} = 0$,no attempt is made to replace this turnover.

$$\check{C}_{(\mathbb{O}_{lf})} = \quad p_{tm} \cdot \vec{C}_{turn(\mathbb{O}_{lf})} \tag{1.5}$$

The total carbon demanded in this step $\check{C}_1$ is summed for both leaf and fine-root tissues:

$$\check{C}_1 = \sum_{o=\mathbb{O}_{lf}} \check{C}_{(o)} \tag{1.6}$$

The flux into these two pools $\vec{C}_{(\mathbb{O}_{lf})}$ is governed by the minimum between the how much carbon is available (the sum of carbon gain and available storage carbon $C_{(st)}$) for replacement and how much is demanded.

$$\vec{C}_{(\mathbb{O}_{lf})} = \quad \min(\check{C}_{(\mathbb{O}_{lf})}, \max(0, (C_{(st)} + C_{gain}) * (\check{C}_{(\mathbb{O}_{lf})}/\check{C}_1))) \tag{1.7}$$

The carbon pools of the leaf and fine-root organs are then incremented, and the daily carbon gain is decremented.

$$\begin{aligned} C_{(\mathbb{O}_{lf})} = &\quad C_{(\mathbb{O}_{lf})} + \vec{C}_{(\mathbb{O}_{lf})} \\ C_{gain} = &\quad C_{gain} - \sum_{o=\mathbb{O}_{lf}} \vec{C}_{(o)} \end{aligned} \tag{1.8}$$

Note that this step may push the daily carbon gain to a negative value. Carbon will be transferred in the next step to "pay" for this negative carbon balance.

Bi-directional Storage Transfer

In the next step, either of two things will happen. If the daily carbon gain C_{gain} is now negative (which may simply be due to more respiration than primary production or because of its payments in the previous step), carbon will be drawn from storage $C_{(st)}$ to bring the carbon gain to zero. At which point the daily allocations are complete and the module returns. Flux into storage is denoted $\vec{C}_{(st)}$.

$$\begin{aligned} \text{if} \quad C_{gain} < 0 & \\ \vec{C}_{(st)} = &\quad C_{gain} \end{aligned} \tag{1.9}$$

If the daily carbon gain is positive, carbon will flow into storage based on a non-linear rate that increases the flux when stores are low and decreases the flux when stores are high. This is mediated by identifying the fraction of storage with its allometric maximum f_{st}, as well as limiting transfer to not exceed the storage demand $\check{C}_{(st)}$.

$$\begin{aligned} \text{if} \quad C_{gain} >= 0 & \\ \check{C}_{(st)} = &\quad \grave{C}_{(st)} - C_{(st)} \\ f_{st} = &\quad C_{(st)}/\grave{C}_{(st)} \\ \vec{C}_{(st)} = &\quad \min(\check{C}_{(st)}, C_{gain} \cdot \max(e^{-f_{st}^4} - e^{-1}, 0)) \end{aligned} \tag{1.10}$$

And the pools are likewise incremented like they were in the first step.

$$\begin{aligned} C_{gain} = &\quad C_{gain} - \vec{C}_{(st)} \\ C_{(st)} = &\quad C_{(st)} + \vec{C}_{(st)} \end{aligned} \tag{1.11}$$

Replenish Remaining Allometric Deficit of Leaves and Fine-roots

In this next step, leaves and fine-roots, again get preferrential access to any available carbon from the daily gains to replenish their pools towards the target values. For leaf and fineroot organs, in index set $\mathbb{O}_{lf}$, we estimate the deficit from target $\check{C}_{(\mathbb{O}_{lf})}$, and their sum deficit $\check{C}_2$.

$$\check{C}_{(\mathbb{O}_{lf})} = \grave{C}_{(\mathbb{O}_{lf})} - C_{(\mathbb{O}_{lf})} \tag{1.12}$$

$$\check{C}_2 = \sum_{o=\mathbb{O}_{lf}} \check{C}_{(o)} \tag{1.13}$$

The flux into leaves and fine-roots is handled proportional to their demands, and based on the minimum between the carbon available and the total demanded from both pools.

$$\begin{aligned} \vec{C}_{(\mathbb{O}_{lf})} &= \min(\check{C}_{(\mathbb{O}_{lf})}, C_{gain} \cdot \check{C}_{(\mathbb{O}_{lf})}/\check{C}_2) \\ C_{(\mathbb{O}_{lf})} &= C_{(\mathbb{O}_{lf})} + \vec{C}_{(\mathbb{O}_{lf})} \\ C_{gain} &= C_{gain} - \sum_{o=\mathbb{O}_{lf}} \vec{C}_{(o)} \end{aligned} \tag{1.14}$$

Replenish Remaining Live Pools Toward Allometric Targets

After the prioritized replenishment of leaves and fine-roots, remaining daily carbon gain is allocated to sapwood and storage tissues. The math in this process is the same as in the previous section, *Replenish Remaining Allometric Deficit of Leaves and Fine-roots*. The only difference is the set of relevant organs changes.

Replenish Structural Pool Toward Allometric Target

Due to branchfall, the plant's current structural carbon pool may be lower than the target size dictated by allometry and stature. Following the algorithm of the previous two sections, *Replenish Remaining Allometric Deficit of Leaves and Fine-roots* and *Replenish Remaining Live Pools Toward Allometric Targets*, any remaining daily carbon gain is transferred into the structural pool.

At this point, if any daily carbon gain C_{gain} remains, the plant must be "on-allometry". With this assumption, concurrent stature growth can proceed.

Grow Stature Concurrently

Note, it possible that some pools may be larger than their allometric targets. This is due to numerical imprecisions, and also may be an artifact of the fusion process in demographic scaling routines (FATES/ED). While it has not been explicitly stated yet, many of the previous calculations in this chapter prevent negative fluxes out of the carbon pools in such cases. In this step, we define the set of organs o that match allometry with some precision, but not above. This is the stature growth set, $\mathbb{O}_{sg}$.

The allometric functions governing the target sizes of the carbon pools also provide the rate of change in the pool with respect to plant diameter. These functions can be related to the plants diameter, and uses parameterizations that are tuned to the plant's functional type. Since the plant is on allometry, the actual carbon pools should match the target pools, to some precision. Therefore, for any diameter d, we also know for each organ o in $\mathbb{O}_{sg}$ we can obtain the differential from the allometry module. A description of the allometry module is provided in the allometry chapter.

$$\frac{dC_{(\mathbb{O}_{sg})}}{dd} = \text{function}(d, \text{pft}) \tag{1.15}$$

This concurrent growth step is facilitated by numerical integration, where we integrate over the independant variable, remaining daily carbon gain C_{gain}. For any given point in the integration process, we first identify the sum change in carbon with respect to diameter $\frac{dC_{sg}}{dd}$

$$\frac{dC_{sg}}{dd} = \sum_{o=\mathbb{O}_{sg}} \frac{dC_{(o)}}{dd} \tag{1.16}$$

With the sum change in flux, we can then identify the proportional amount of carbon demanded from any individual pool, relative to the total carbon allocated over all pools in the set.

$$\frac{dC_{(\mathbb{O}_{sg})}}{dC_{sg}} = \frac{dC_{(\mathbb{O}_{sg})}}{dd} / \frac{dC_{sg}}{dd} \tag{1.17}$$

It is also at this time, that reproductive carbon flux is allocated. This is a special case, that does not use allometric scaling, and instead retrieves a reproductive allocation fraction f_{repro} that it retrieves from parameterization or a more sophisticated seed/flower allocation algorithm. The fraction $\frac{d\dot{C}_{(\mathbb{O}_{sg})}}{dC_{sg}}$ changes dynamically as the plant grows along its allometric curve, and could potentially require numerical solvers that enforce improved stability or precision. For most cases, since plant growth is slow, and the interval of integration is small compared to the size of the derivatives, a simple Euler integration suffices. The integration for organs in set $\mathbb{O}_{sg}$, and reproduction are defined as follows.

$$\vec{C}_{(\mathbb{O}_{sg})} = \int_{dC=0}^{C_{gain}} \frac{d\dot{C}_{(\mathbb{O}_{sg})}}{dC_{sg}} (1 - f_{repro}) \quad dC \tag{1.18}$$

$$\vec{C}_{(repro)} = \int_{dC=0}^{C_{gain}} f_{repro} \quad dC \tag{1.19}$$

Following this calculation, the integrated fluxes (including reproduction) are summed up, and then normalized such that their sum matches C_{gain} to ensure that the exact amount of remaining carbon is used up. The change in diameter can also be determined by simply relating one of the integrations back to diameter.

$$\Delta d = \int_{dC=0}^{C_{gain}} \frac{d\dot{C}_{(\mathbb{O}_{sg})}}{dC_{sg}} \frac{dd}{dC_{(\mathbb{O}_{sg})}} (1 - f_{repro}) \quad dC \tag{1.20}$$

Allocation Hypothesis 2: Allometrically Guided, Carbon and Nutrients with Prioritization and Flexible Target Stoichiometry

This hypothesis assumes there is a single carbon species, and an arbitrary number of nutrient species for each of the six plant organ pools:

1. Leaf
2. Fine-root
3. Sapwood
4. Structural wood
5. Storage
6. Reproductive

The PARTEH code for hypothesis two currently only enables Nitrogen and Phosphorous. The code can be easily extended to handle other nurtient species, however this would increase the number of parameters used and complicate things for a broader user base. Without an imediate need for other species, they have been left out. This documentation will use the generic symbol N for all nutrients of any species indexed by s in organs indexed by o.

The state variables, boundary conditions and parameters for hypothesis 2 are described in *Table H2-1*.

Table 1.9: Table H2-1

Symbol	Dimension	Description	Units
State Variables			
$C_{(o)}$	organ	carbon mass	[kg]
$N_{(o,s)}$	organ x species	nutrient mass	[kg]
Input/Output Boundary Conditions			
R_{md}	scalar	Maint. Resp. Deficit	[kg]
d	scalar	Reference Stem Diameter	[cm]
Input Boundary Conditions			
f_{trim}	scalar	Canopy Trim Fraction	[0-1]
C_{gain}	scalar	Daily carbon gain	[kg]
$N_{gain(s)}$	species	Daily nutrient gain	[kg]
Output Boundary Conditions			
C_{exu}	scalar	Daily carbon exudation	[kg]
$N_{exu(s)}$	species	Daily nutrient exudation	[kg]
R_g	scalar	Growth Respiration	[kg]
Parameters			
$\alpha_{(o,s)}$	pft* x organ x species	ideal stoichiometric ratios	[kg/kg]
$\beta_{(o,s)}$	pft* x organ x species	minimum stoichiometric ratios	[kg/kg]
p_{tm}	pft*	tissue vs. resp. prioritization	[0-1]
$\omega_{(o)}$	pft* x organ	prioritization level	[1-6]
$r_{g(o)}$	pft* x organ	unit growth respiration rate	[kg/kg]

List of key states, boundary conditions and parameters in hypothesis 2, allometric multi-nutrient species with fixed target stoichiometry. In this notation, o and s are used to index the organ and species (nutrient) dimensions. :math:'' Note that the parameters are specified explicitly for each pft, but the dimension will be implied in our notation as each plant is already uniquely asociated with a PFT.*

Order of Operations

It is assumed that over the sub-daily time-steps, photosynthesis, respiration and nutrient uptake has been accumulated. These provide net carbon and nutrient gains at the end of the day to drive allocations. The first daily procedure is the removal of biomass from the plant due to turnover coming from leaf-fall, branchfall and turnover of fine-roots. The second daiy procedure seeks to replenish the plants existing pools with respect to a target mass that is defined by the stature (size) of the plant (this may be thought of of bringing the plant back to allometric targets). Next, if resources are still available the plant will grow in stature, where allocation seeks to grow the pools out concurrently with each other. If any nutrient resources remain, they will be allocated towards ideal stoichiometric proportions, which may or may not be greater than the proportionalities needed during stature growth. And finally, all excess materials are sent to storage pools (if not full) and then exuded through roots.

1. (sub-daily) *Accumulate Carbon and Nutrients*
2. (daily) Perform Allocations to Pools
    a. *Remove Biomass From All Pools as Turnover*
    b. *Replenish Pools with Respect to Target Levels*
    c. *Grow Stature Concurrently*
    d. *Allocate Nutrients Towards Ideal Stoichiometric Ratios*
    e. *Send Excess Quantities to Storage or Exude to Soil*

VISUALIZATION

Accumulate Carbon and Nutrients

Photosynthesis and maintenance respiration are sensitive to light levels and tissue temperatures, which vary over sub-daily timescales. In CLM/ELM, this "fast" time-step is 30 minutes. It is assumed that the host-model (e.g. FATES) will handle the calculation of GPP and maintenance respiration, and integrate these quantities over the course of the day. There is some flexibility in how PARTEH handles allocations with these two constraints. Along with nutrient inputs, the host model must provide the boundary conditions of daily carbon gain C_{gain}, and optionally, the maintenance respiration deficit R_{md}.

There are two scenarios that this hypothesis accomodates:

1. The host model calculates the difference between daily integrated GPP and maintenance respiration and passes it as C_{gain}, which may be positive or negative. No maintenance respiration is tracked, because it is paid instantly, and thus $R_{md} = 0$.
2. The host model passes GPP as C_{gain} (always positive), and maintains a running account of maintenance respiration deficit, thereby adding the daily integrated maintenance respiration to R_{md}. The PARTEH model will then attempt to pay for R_{md}, and passing back the updated deficit to the host.

The third key boundary condition provided by the host, is the daily integrated flux of nutrients from soil to fine-roots, $N_{gain(s)}$, for each nutrient species s. Depending on the soil biogeochemistry model in use, PARTEH can provide information about the state of the plant, to help the soil biogeochemistry module determine the plant's affinity in a competitive nutrient environment.

Remove Biomass From All Pools as Turnover

Different methodologies for calculating turnover exist, and are executed prior to allocations. Event based turnover is covered in *Event Based Turnover Hypotheses*, and maintenance turnover is covered in *Maintenance Turnover Hypotheses*.

Replenish Pools with Respect to Target Levels

The organs of each plant have target masses for carbon $\grave{C}_{(o)}$ and nutrients $\grave{N}_{(o,s)}$. These targets are goverened by the stature of the plant, and can be thought of as the desireable pool sizes that the plant would like to have to be ready for further growth in stature. Turnover, as described in the previous section, draws down the masses away from the target values associated with their current stature. Sometimes this is considered being "off allometry". In this hypothesis, the base assumption is that the targets are dictated by allometry, but other methods of determining these targets are possible as well. Allometric targets are typically a function of plant diameter dbh , plant functional type pft, and an indicator of how much trimming of unproductive lower boughs a plant has executed trimming.

$$\grave{C}_{(o)} = \text{func}(\text{dbh}, \text{pft}, \text{trimming}) \tag{1.21}$$

For nutrient species, the targets are based on a parameter that describes the minimum stoichiometric ratios with carbon $\beta_{(o,s)}$ that are required for the plant to grow in stature.

$$\grave{N}_{(o,s)} = \quad \grave{C}_{(o)} \cdot \beta_{(o,s)} \tag{1.22}$$

In this step, the plant must allocate resources to bring its pools up to the targets before growing out the plant's stature again. This process relies on calculating the targets, and then the carbon $\check{C}_{(o)}$ and nutrient $\check{N}_{(o,s)}$ demands to reach those targets.

Given these targets, the demands for each carbon $\check{C}_{(o)}$ and nutrient $\check{N}_{(o,s)}$ pool are calculated. In the case of carbon, a growth tax is applied to allocation, which contributes to the demand. Here, that tax is governed by a unit growth

parameter $r_{g(o)}$, however more complicated growth tax functions could be used as well. Likewise, a pool may already be at or above its current target. Only positive demands are used, so a floor of 0 is imposed on the demand.

$$\check{C}_{(o)} = \max(0, (\grave{C}_{(o)} - C_{(o)}) \cdot (1 + r_{g(o)})) \tag{1.23}$$

$$\check{N}_{(o,s)} = \max(0, \grave{N}_{(o,s)} - N_{(o,s)}) \tag{1.24}$$

Each plant organ is then associated with any priority level, 0 through 6. Organs associated with priority 1 will get first access to carbon and nutrients and organs associated with priority order will get the remainder. The priority order levels are ascended sequentially, we indicate the valid set of organ indices in the current priority order level pr as set $\mathbb{O}_{pr}$. Note that priority level 0 is a special bypass level. This is used for reproductive allocation, which currently is only generated during the stature growth step. Note, it is not required that ANY organs are classified as priority 1.

The first priority level ($pr = 1, \mathbb{O}_1$) has two approaches based on the boundary conditions provided.

1. It is assumed that maintenance respiration costs have not been paid yet by the host model, and thus the maintenance respiration deficit R_{md} exists and is non-zero, and that daily carbon gains are greater than or equal to zero. This is detailed in *Priority 1 Carbon Fluxes with explicit Maintenance Respiration Deficit*.
2. It is assumed that boundary condition for C_{gain} has already decucted maintenance respiration costs. Here, R_{md} is always zero, and if the plant is not metabolically dormant, C_{gain} may be positive or negative. This is detailed in :ref:"p1_implicit_rmd_section'.

Priority 1 Carbon Fluxes with explicit Maintenance Respiration Deficit

First, we assess how much total demand is coming from the priority 1 carbon pools.

$$\check{C}_1 = \sum_{o=\mathbb{O}_1} \check{C}_{(o)} \tag{1.25}$$

The total carbon that can be translocated from storage is $\vec{C}_{st-tran}$. Any number of models could be used to determine how resistant the storage is to pay off high-priority tissues and maintenance respiration costs. Below is an example of a simple function where the transferable carbon decreases as the square of the pool's proportion with its target. Where storage is denoted organ index $o = st$:

$$C_{st-tran} = C_{(st)} \cdot \min(1, C_{(st)}/\grave{C}_{(st)}) \tag{1.26}$$

The total carbon that is transferred $\vec{C}_{tot}$ is the minimum between the demanded and what can be transferred from both storage and carbon gains C_{gain}. The fraction of how much is transferred versus demanded, f_{tot}, is also useful.

$$\begin{aligned} \vec{C}_{tot} &= \min(\check{C}_1 + R_{md}, C_{st-tran} + C_{gain}) \\ f_{tot} &= \vec{C}_{tot}/(\check{C}_1 + R_{md}) \end{aligned} \tag{1.27}$$

Preference can be specified to allocate available carbon to either maintenance respiration, or the priority 1 pools. To do so, we define a redistribution flux $\vec{C}_{RD}$ that scales the transfer between the two options. The parameter p_{tm}, which varies betwen 0 and 1, sets the relative priority of each. When the parameter is greater than 0.5, $\vec{C}_{RD}$ re-directs flux from relieving maintenance respiration deficit ($\vec{C}_{md}$) towards priority 1 tissues ($\vec{C}_1$). Alternatively, when the parameter

is less than 0.5, $\vec{C}_{RD}$ is redictect from replacing priority 1 tissues into maintenance respiration deficit.

$$\begin{aligned}
&\text{for } p_{tm} > 0.5 \\
&\quad \vec{C}_{RD} = \quad \min((p_{tm} - 0.5)/0.5 \cdot f_{tot} \cdot R_m, (1 - f_{tot}) \cdot \check{C}_1) \\
&\quad \vec{C}_1 = \quad f_{tot} \cdot \check{C}_1 + \vec{C}_{RD} \\
&\quad \vec{R}_{md} = \quad f_{tot} \cdot R_{md} - \vec{C}_{RD} \\
&\text{for } p_{tm} < 0.5 \\
&\quad \vec{C}_{RD} = \quad \min((0.5 - p_{tm})/0.5 \cdot f_{tot} \cdot \check{C}_1, (1 - f_{tot}) \cdot R_{md}) \\
&\quad \vec{C}_1 = \quad f_{tot} \cdot \check{C}_1 - C_{RD} \\
&\quad \vec{R}_{md} = \quad f_{tot} \cdot R_{md} + \vec{C}_{RD}
\end{aligned} \tag{1.28}$$

The total flux of carbon into each priority 1 pool is then governed, linearly, by the fraction of which their demand constitutes the whole demand. For any carbon pool in organ found in priority set $\mathbb{O}_1$.

$$\vec{C}_{(\mathbb{O}_1)} = \vec{C}_1 \cdot \check{C}_{(\mathbb{O}_1)}/\check{C}_1 \tag{1.29}$$

With the fluxes known, increment the priority 1 carbon pools, increment their growth respiration. For each organ in set $\mathbb{O}_1$:

$$\begin{aligned}
C_{(\mathbb{O}_1)} = \quad & C_{(\mathbb{O}_1)} + \vec{C}_{(\mathbb{O}_1)}/(1 + r_{g(\mathbb{O}_1)}) \\
R_{g(\mathbb{O}_1)} = \quad & R_{g(\mathbb{O}_1)} + \vec{C}_{(\mathbb{O}_1)} \cdot r_{g(\mathbb{O}_1)}/(1 + r_{g(\mathbb{O}_1)})
\end{aligned} \tag{1.30}$$

Decrement maintenance respiration deficit, daily carbon gain, and potentially, storage carbon (where $o = st$).

$$\begin{aligned}
R_{md} = \quad & R_{md} - \vec{R}_{md} \\
\vec{C}_{gain} = \quad & \min(C_{gain}, \vec{C}_{tot}) \\
C_{gain} = \quad & C_{gain} - \vec{C}_{gain} \\
C_{(st)} = \quad & C_{(st)} - \max(0, \vec{C}_{tot} - \vec{C}_{gain})
\end{aligned} \tag{1.31}$$

Priority 1 Carbon Fluxes with Implicit Maintenance Respiration

Recall that as an alternative to *Priority 1 Carbon Fluxes with explicit Maintenance Respiration Deficit*, carbon gains may subsume maintenance respiration. With this assumption, the equations in the previous section are valid in all cases, except for when $C_{gain} < 0$. For this condition, it is assumed that storage carbon will pay off the negative carbon gain and bring it back to zero. Caution must be made, in so much that calculations of maintenance respiration are conducted so that the plant does create impossible conditions where storage carbon becomes zero. PARTEH will fail gracefully in this condition. The remainder of this section specifically details the condition where $C_{gain} < 0$.

The flux from storage brings negative daily carbon gain up to zero.

$$\begin{aligned}
\vec{C}_{gain} = \quad & -C_{gain} \\
C_{(st)} = \quad & C_{(st)} - \vec{C}_{gain} \\
C_{gain} = \quad & 0
\end{aligned} \tag{1.32}$$

Any extra flux that can transferred out of storage and into priority 1 tissues, would then be calculated by using the same function that determines the maximum transferrable carbon, as in (1.26). However, in this case $C_{st-trans}$ is calculated after the carbon to replace the negative C_{gain} is removed in (1.32). The demand for carbon to priority 1 tissues follows the same methods as *Priority 1 Carbon Fluxes with explicit Maintenance Respiration Deficit*.

$$\begin{aligned}
&\text{if} \quad C_{gain} < 0 \\
&\qquad \vec{C}_1 = \quad \min(C_{st-trans}, \check{C}_1)
\end{aligned} \tag{1.33}$$

Transfer from storage into priority 1 tissues also follows the same logic as *Priority 1 Carbon Fluxes with explicit Maintenance Respiration Deficit*, specifically (1.29). And finally, decrement storage again, as per total flux into priority 1 organs $\vec{C}_1$.

$$C_{(st)} = \quad C_{(st)} + \vec{C}_1 \tag{1.34}$$

Priority 1 Nutrient Fluxes

With the priority 1 carbon pools updated, the fluxes of nutrients into those pools can proceed. The targets $\grave{N}_{(o,s)}$, and subsequently the deficit from the target $\check{N}_{(o,s)}$, is set by the organ of interest's current (and newly updated) carbon mass. For all nutrient species s, and all organs o in set $\mathbb{O}_1$, the targets and demands are updated via (1.22) and (1.24).

The total demand for each nutrient species s across priority 1 tissues is thus:

$$\check{N}_{1(s)} = \quad \sum_{o=\mathbb{O}_1} \check{N}_{(o,s)} \tag{1.35}$$

And therefore the fluxes for each species s and each organ in priority set $\mathbb{O}_1$ are transferred into their respective pools.

$$\begin{aligned} \vec{N}_{(\mathbb{O}_1,s)} &= \quad \min(N_{gain(s)}, \check{N}_{1(s)}) \cdot (\check{N}_{(\mathbb{O}_1,s)} / \check{N}_{1(s)}) \\ N_{(\mathbb{O}_1,s)} &= \quad N_{(\mathbb{O}_1,s)} + \vec{N}_{(\mathbb{O}_1,s)} \end{aligned} \tag{1.36}$$

The daily nutrient gains for each species are correspondingly decremented.

$$N_{gain(s)} = \quad N_{gain(s)} - \min(N_{gain(s)}, \check{N}_{1(s)}) \tag{1.37}$$

Carbon and Nutrient Fluxes after Priority Level 1

At this point, all priority 1 fluxes have been allocated. The next priority level fluxes are enacted sequentially, and the procedure is much the same as priority 1, without the complications of shunting carbon to maintenance respiration or paying back negative carbon gains, or **transfering from storage to pay for priority 1 demands**.

For each priority level pr, a new set of organs is sub-set into group $\mathbb{O}_{pr}$, thereby calculating fluxes of carbon and nutrients and decrementing C_{gain} and $N_{gain(s)}$ correspondingly. The algorithm follows generally:

1. Sum the carbon demands of the set, via (1.25)
2. Calculate carbon fluxes based on relative demand, similar to (1.29)
3. Increment carbon pools, growth respiration and decrement carbon gain, via (1.30) and (1.31) (ignoring parts where storage is translocated)
4. Re-assess nutrient demands, via (1.24)
5. Sum the nutrient demands of the set, similar too (1.35)
6. Calculate nutrient fluxes and perform transfers, similar to (1.36) and (1.37)

Grow Stature Concurrently

If there is at some of each daily carbon gain, and daily nutrient gain for all species remaining, the plant will grow out its stature. This method assumes that the organs will grow out concurrently.

As a default, the carbon in these organs will be allocated as dictated by the derivatives of the allometric functions. Other hypotheses, such as those that seek to optimize root tissues to increase nutrient acquisition will break from this.

Of important note, is that for either reasons governed outside of the PARTEH framework, or because of numerical integration errors, some organs may have slightly more carbon than their allometric target. In doing so, we remove these organs from the set to be grown out. Structural carbon is an exception, and is always "on-allometry", since it is directly tied to stature and dbh. This is actually forced by adjusting the plant's diameter to match the structural carbon in cases where structural carbon was higher than its allometric target.

Broadly, the first objective in this section, is to determine which species, be it carbon or nutrient, will limit growth. To do this, we calculate an approximation of how much equivalent growth in carbon each of them could provide, by extrapolating the derivatives at the current plant's stature. The derivatives for target carbon per change in diameter, $\frac{dC_{(o)}}{dd}$, are provided by allometric functions. In the following set of organs, we exlude reproduction (which does not have a derivative wrt size), creating subset of organs $\mathbb{O}_{sg}$.

$$\frac{dC_{sg}}{dd} = \sum_{o=\mathbb{O}_{sg}} \frac{d\grave{C}_{(o)}}{dd} \tag{1.38}$$

With this sum, we can determine the relative fraction of carbon that is sent to each organ in set $\mathbb{O}_{sg}$, that is directed to stature growth, denoted: $f_{sg(\mathbb{O}_{sg})}$. The fraction of flux that is directed towards reproductive organs, $f_{sg(o=repro)}$ is special, and is **calculated from an external module**.

For the other organs, in set $\mathbb{O}_{sg}$:

$$f_{sg(\mathbb{O}_{sg})} = \frac{d\grave{C}_{(\mathbb{O}_{sg})}}{dd} / \frac{dC_{sg}}{dd} \cdot (1 - f_{sg(repro)}) \tag{1.39}$$

The approximated amount of carbon would be transferred into plant tissues $\vec{C}^*_{sg}$, is calculated via assembling these relative fractions, and divesting the total available carbon gain of the growth respiration rates for each pool. Note the asterisk in the symbology is meant to reflect an approximate value.

$$\vec{C}^*_{sg} = C_{gain} \cdot \left(\frac{f_{sg(repro)}}{1 + r_{g(repro)}} + \sum_{o=\mathbb{O}_{sg}} \frac{f_{sg(o)}}{1 + r_g(o)} \right) \tag{1.40}$$

The approximated amount of nutrient of each species s that would be transferred into plant tissues $\vec{N}^*_{sg(s)}$, is calculated much in the same way, however there is no growth respiration tax. Also, it is possible that a nutrient pool may have a mass that is already greater than the mass equivalent to the target associated with the minimum stoichiometry. Such cases must be accounted for, because they will reduce the likelihood of nutrient needs in that organ limiting growth.

$$\begin{aligned} \vec{N}^*_{sg(s)} &= N_{gain(s)} \cdot \left(f_{sg(repro)} / \beta_{(repro,s)} + \sum_{o=\mathbb{O}_{sg}} f_{sg(o)} / \beta_{(o,s)} \right) \\ &+ \max(0, N_{(repro,s)} - \grave{N}_{(repro,s)}) / \beta_{(repro,s)} \\ &+ \sum_{o=\mathbb{O}_{sg}} \max(0, N_{(o,s)} - \grave{N}_{(o,s)}) / \beta_{(o,s)} \end{aligned} \tag{1.41}$$

The actual carbon that is then set aside for stature growth $\vec{C}_{sg}$, based on the minimum of approximations $\vec{C}^*_{sg}$ and $\vec{N}^*_{sg(s)}$.

$$\vec{C}_{sg} = C_{gain} \cdot \min(\vec{C}^*_{sg}, \vec{N}^*_{sg(s)}) / \vec{C}^*_{sg} \tag{1.42}$$

Carbon fluxes into each of the plant's organs are conducted via numerical integration, which is a coupled set of ordinary differential equations, integrated over $\vec{C}_{sg}$. For each organ in set $\mathbb{O}_{sg}$.

Where the rate of change of carbon for a given organ is its proportionality relative to the whole:

$$\frac{dC_{(\mathbb{O}_{sg})}}{dC_{sg}} = \overbrace{\frac{dC_{(\mathbb{O}_{sg})}}{dd} \cdot \frac{dd}{dC_{sg}}}^{\text{Continuous allometry equations}} \tag{1.43}$$

$$\vec{C}_{sg(\mathbb{O}_{sg})} = \int_{dC_{sg}=0}^{\vec{C}_{sg}} \frac{dC_{(\mathbb{O}_{sg})}}{dC_{sg}} dC_{sg} \tag{1.44}$$

The fluxes are then transferred to increment the carbon pools, increment the growth respiration and decrement the carbon gain.

Allocate Nutrients Towards Ideal Stoichiometric Ratios

Send Excess Quantities to Storage or Exude to Soil

1.6 Allometry and Growth Along Allometric Curves

In the previous section, *Allocation and Reactive Transport (PARTEH)*, we covered the equations that describe how growth is implemented, as well the order of operations and logic of that forumlation. In this section, we will discuss the various allometric functions that generate the relative rates of change, as well as the target biomass quantities $\grave{X}$.

1.6.1 "Forced" Growth Along Allometric Curves

Growth specified by current PARTEH hypotheses follow along the allometric curves. A hypothetical example of a cohorts integration along such a curve is provided in the top panel of the diagram below. It is assumed that when a plant grows in stature, the structural biomass matches the target structural biomass for its size (DBH). This is represented by the grey dot sitting on the allometry line for structural biomass.

A state of being "on allometry" is consistent with the cohort (grey dot) existing on the allometric curve.

It is expected, and it is represented in the model, that due to either continuous or event based turnover, that biomass pools are continually depleted, thus pulling the grey dot straight down, away from the allometry line. Recall from the PARTEH description, that the first step in the growth algorithm is to use available carbon to replace these lost biomass pools (without increasing dbh) so that it is "on allometry".

Also, all numerical integration has some amount of truncation error (step error). When FATES conducts the stature growth integration step, it typically uses Euler integration, because it is fast and simple. As a result, all biomass pools are projected along the tangent of the allometric curves from where they started. When the curvature parameters that govern these relationships are greater than 1, this results in continual "undershooting" of the actual target quantity. This is not a liability, firstly because growth is forced to be mass conservative. And secondly, to re-iterate the explanation above, upon the next growth step the algorithm will spend carbon to first get the pools back "on allometry", before it projects along the tangent again. This is represented in the lower panel.

However, we also have to accomodate for cases where the actual amount of biomass in the cohort's pools are larger than the target sizes dictated by the cohort's diameter. This can be visualized by the cohort residing somewhere above the line. This can happen for two reasons, 1) cohort fusion or 2) growth along allometric curves with curvature parameters (exponents) less than 1.

For woody plants, if a non-structural biomass pool is greater than the target pool size, the solution is simple. That pool is flagged to be ignored during the stature growth step, and eventually the cohort's dbh will increase such that the target size exceeds its actual size again. This is visualized in the top panel of the diagram below.

There is a caveat here. The diameter must be "tied" to one of the biomass pools. And for woody plants, we choose structural carbon. And thus, we cannot flag to ignore structural carbon during stature growth since it is inextricably linked to diameter. Therefore, cohorts that have structural biomass that is greater than the target biomass dictated by its diameter, will have their DBH forceably increased (without increasing any biomass) until the allometric target matches the actual biomass. See the lower panel in the diagram below.

Note, the explanation above was explained for woody plants, which tie diameter to structural biomass. For non-woody plants, such as grasses, we tie leaf biomass to diameter instead.

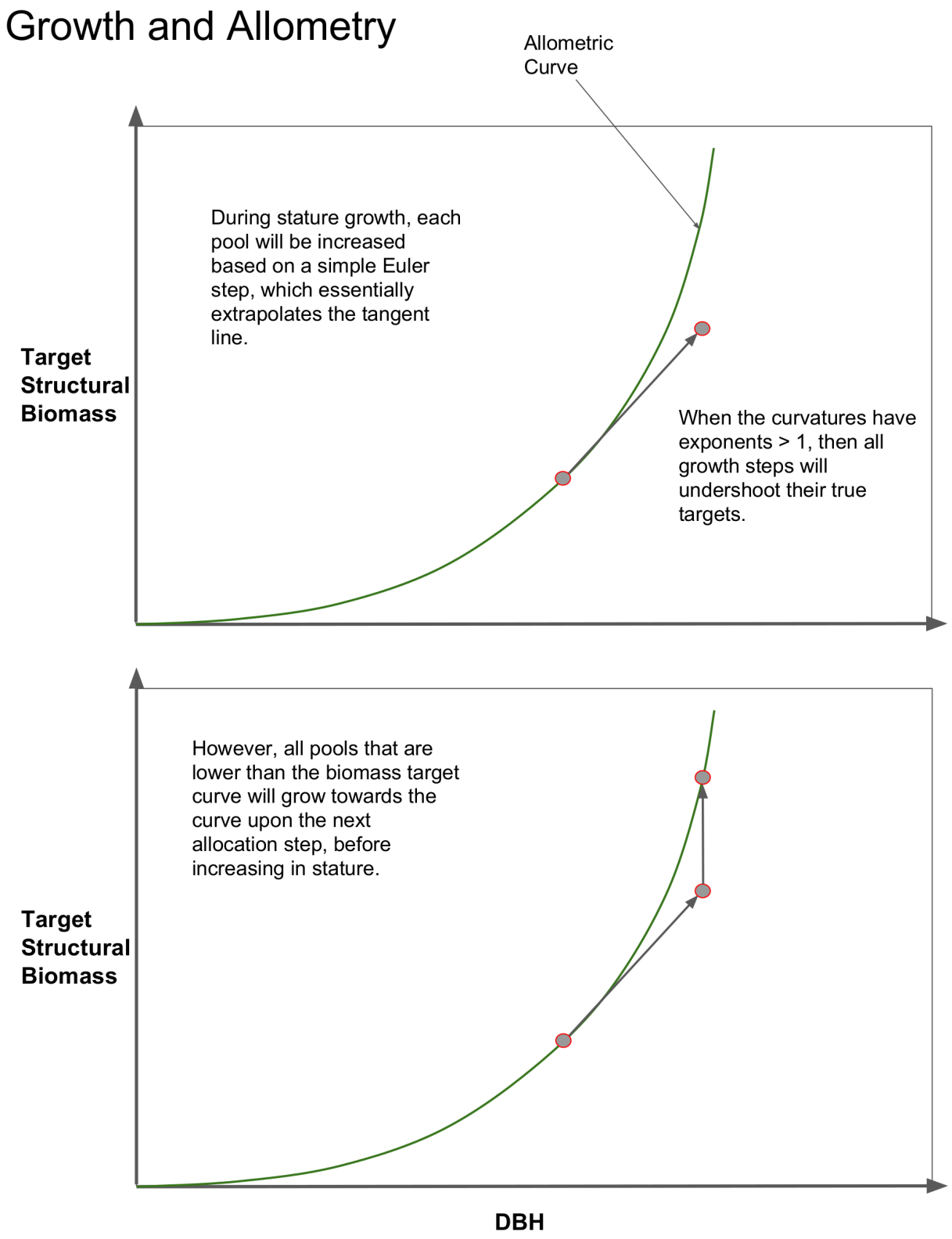
Growth and Allometry
Allometric Curve
During stature growth, each pool will be increased based on a simple Euler step, which essentially extrapolates the tangent line.
When the curvatures have exponents > 1, then all growth steps will undershoot their true targets.
Target Structural Biomass
However, all pools that are lower than the biomass target curve will grow towards the curve upon the next allocation step, before increasing in stature.
Target Structural Biomass
DBH

Growth and Allometry

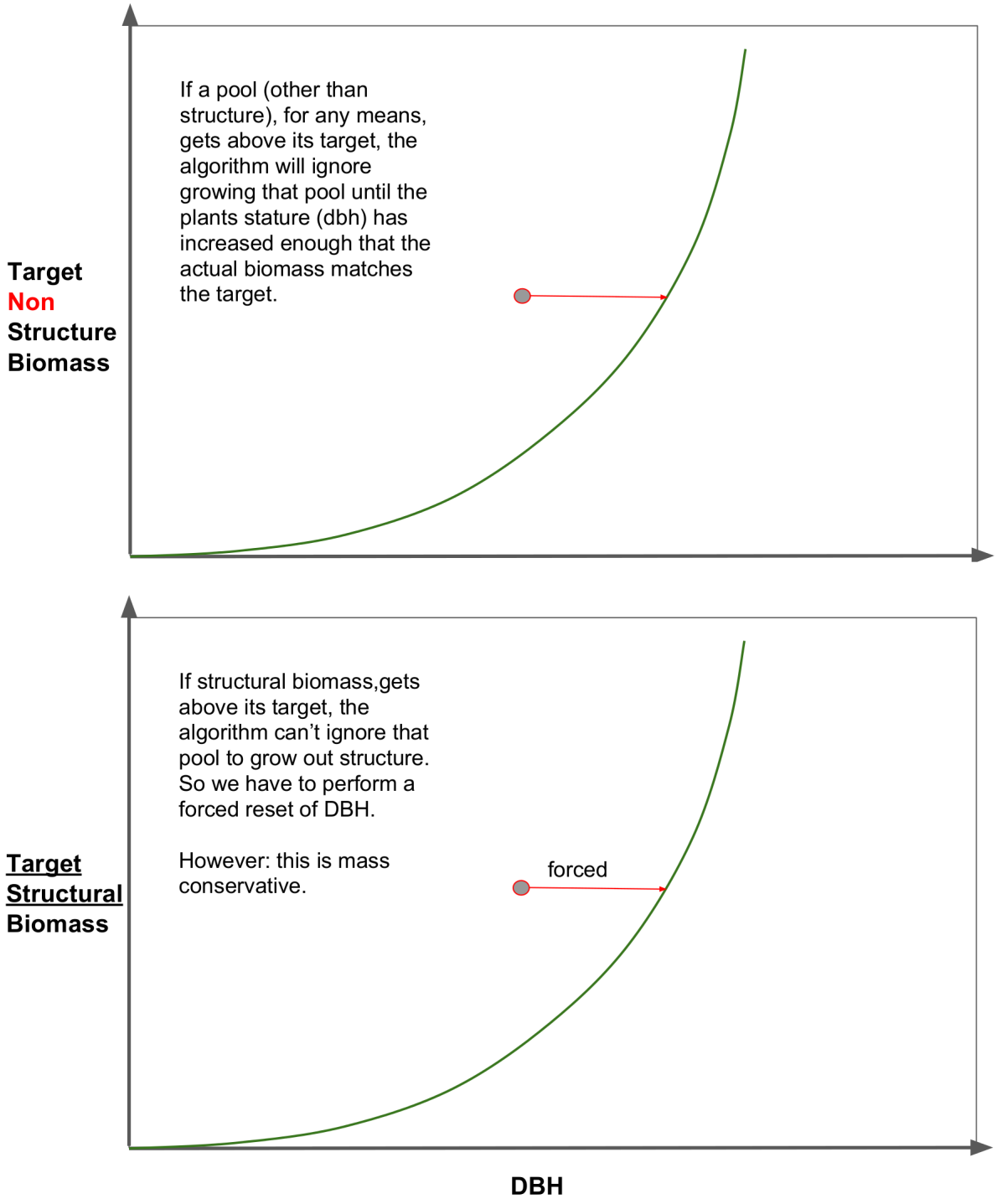

1.6.2 Allometric Relationships

FATES-PARTEH (in its base hypotheses) uses allometry to dictate the target biomass quantities of structure, sapwood, leaf, fine-root, reproduction and storage. Further, FATES also uses allometric relationships to define a cohort's height and crown area. All of these target quantities are tied to diameter. Biomass pools may also be functionally dependent on other biomass pools, as long as a cyclical relationship is not generated, and can ultimately be related to diameter or other external factors. For instance, target root biomass is typically defined as proportional to leaf biomass. Target leaf biomass is dependent on height and a canopy trimming function, while crown area and above ground biomass are each also dependent on height.

The FATES code is written in a way that offers flexibility in how these relationships are cast. Each of these forumulations uses one or more user defined constant parameters, but it also allows for completely different functional forms. All of FATES allometric relationships can be found in the file FatesAllometryMod.F90.

Important note. Most allometry relationships from field research define total above ground biomass (AGB) as their estimated quantity instead of structural biomass. In FATES, since AGB is not a state-variable, it must be derived from the portions of several state variables. However, we make a simplification in FATES, and assume that the allometric relationships for AGB only contain structural wood and sapwood, and do not contain leaves, storage or reproductive tissues. Diagnostics on AGB will include all terms. Thus the allometric target for AGB contains the state targets and the fraction of above ground biomass (pft constant parameter) f_a.

$$\grave{C}_{(AGB)} = (\grave{C}_{(structure)} + \grave{C}_{(sapwood)}) * f_{agb} \tag{1.45}$$

Note that the diameter to height relationships all use an effective diameter, d_*. This is the minimum between the actual plant diameter, and the PFT specific parameter that specifies the diameter at which maximum height occurs d_{hmax}.

$$d_* = \min(d, d_{hmax}) \tag{1.46}$$

The following table details the different allometric relationships that governs growth and stature, and the optional relationships and parameters associated with those relationships.

Table 1.10: Table of Allometric Functions

Reference	Function
Diameter to Height	
Power Function	$h = p_1 \cdot d_*^{p_2}$
Obrien et al (1995)	$h = 10^{(log10(d_*) \cdot p_1 + p_2)}$
Poorter et al (2006)	$h = p_1 \cdot (1 - e^{p_2 \cdot d_*^{p_3}})$
Martinez Cano et al (2019)	$h = (p_1 \cdot d_*^{p_2})/(p_3 + d_*^{p_2})$
Target Above Ground Biomass	
Saldarriaga et al. (1998)	$\grave{C}_{agb} = f_{agb} \cdot p_1 \cdot h^{p_2} \cdot d^{p_3} \cdot \rho^{p_4}$
2 Parameter power function	$\grave{C}_{agb} = p_1/\text{c2b} \cdot d^{p_2}$
Chave et al. (2014)	$\grave{C}_{agb} = p_1/\text{c2b} \cdot (\rho \cdot d^2 \cdot h)^{p_2}$
Target Leaf Biomass (TBD)	
Target Sapwood Biomass (TBD)	
Target Fine-root Biomass (TBD)	
Target Storage Biomass (TBD)	

List of allometric relationships, their functional forms, and relevant parameters.

1.7 Canopy Structure and the Perfect Plasticity Approximation

During initialization and every subsequent daily ED timestep, the canopy structure model is called to determine how the leaf area of the different cohorts is arranged relative to the incoming radiation, which will then be used to drive the radiation and photosynthesis calculations. This task requires that some assumptions are made about 1) the shape and depth of the canopy within which the plant leaves are arranged and 2) how the leaves of different cohorts are arranged relative to each other. This set of assumptions are critical to model performance in ED-like cohort based models, since they determine how light resources are partitioned between competing plants of varying heights, which has a very significant impact on how vegetation distribution emerges from competition *Fisher et al. 2010*.

The standard ED1.0 model makes a simple 'flat disk' assumption, that the leaf area of each cohort is spread in an homogenous layer at one exact height across entire the ground area represented by each patch. FATES has diverged from this representation due to (at least) two problematic emergent properties that we identified as generating unrealistic behaviours espetially for large-area patches.

1. Over-estimation of light competition . The vertical stacking of cohorts which have all their leaf area at the same nominal height means that when one cohort is only very slightly taller than it's competitor, it is completely shaded by it. This means that any small advantage in terms of height growth translates into a large advantage in terms of light competition, even at the seedling stage. This property of the model artificially exaggerates the process of light competition. In reality, trees do not compete for light until their canopies begin to overlap and canopy closure is approached.

2. Unrealistic over-crowding. The 'flat-disk' assumption has no consideration of the spatial extent of tree crowns. Therefore it has no control on the packing density of plants in the model. Given a mismatch between production and mortality, entirely unrealistic tree densities are thus possible for some combinations of recruitment, growth and mortality rates.

To account for the filling of space in three dimensions using the one-dimensional representation of the canopy employed by CLM, we implement a new scheme derived from that of *Purves et al. 2008*. Their argument follows the development of an individual-based variant of the SORTIE model, called SHELL, which allows the location of individual plant crowns to be highly flexible in space. Ultimately, the solutions of this model possess an emergent property whereby the crowns of the plants simply fill all of the available space in the canopy before forming a distinct understorey.

Purves et al. developed a model that uses this feature, called the 'perfect plasticity approximation', which assumes the plants are able to perfectly fill all of the available canopy space. That is, at canopy closure, all of the available horizontal space is filled, with negligible gaps, owing to lateral tree growth and the ability of tree canopies to grow into the available gaps (this is of course, an over-simplified but potential useful ecosystem property). The 'perfect plasticity approximation' (PPA) implies that the community of trees is subdivided into discrete canopy layers, and by extension, each cohort represented by FATES model is assigned a canopy layer status flag, C_L. In this version, we set the maximum number of canopy layers at 2 for simplicity, although is possible to have a larger number of layers in theory. $C_{L,coh}$ = 1 means that all the trees of cohort coh are in the upper canopy (overstory), and $C_{L,coh}$ = 2 means that all the trees of cohort coh are in the understorey.

In this model, all the trees in the canopy experience full light on their uppermost leaf layer, and all trees in the understorey experience the same light (full sunlight attenuated by the average LAI of the upper canopy) on their uppermost leaves, as described in the radiation transfer section (more nuanced versions of this approach may be investigated in future model versions). The canopy is assumed to be cylindrical, the lower layers of which experience self-shading by the upper layers.

To determine whether a second canopy layer is required, the model needs to know the spatial extent of tree crowns. Crown area, A_{crown}, m^2, is defined as

$$A_{crown,coh} = \pi (dbh_{coh} S_{c,patch,cl})^{1.56}$$

where A_{crown} is the crown area of a single tree canopy (m:math:^{-2}) and $S_{c,patch,cl}$ is the 'canopy spread' parameter (m cm^-1) of this canopy layer, which is assigned as a function of canopy space filling, discussed below. In contrast

to *Purves et al. 2008* , we use an exponent, identical to that for leaf biomass, of 1.56, not 2.0, such that tree leaf area index does not change as a function of diameter.

To determine whether the canopy is closed, we calculate the total canopy area as:

$$A_{canopy} = \sum_{coh=1}^{nc,patch} A_{crown,coh}.n_{coh}$$

where nc_{patch} is the number of cohorts in a given patch. If the area of all crowns A_{canopy} (m^2) is larger than the total ground area of a patch (A_{patch}), which typically happens at the end of the day, after growth and updated crown allometry is resolved in the model, then some fraction of each cohort is demoted to the understorey.

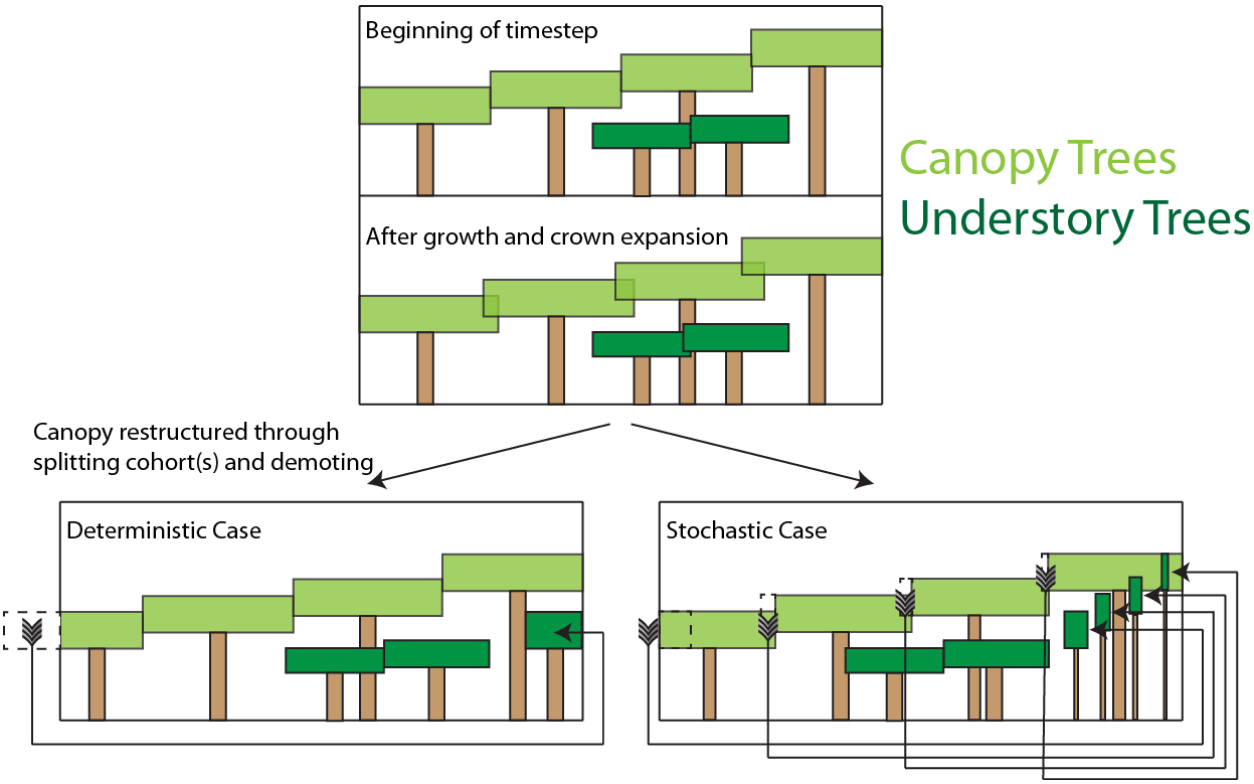

Under these circumstances, the *extra* crown area A_{loss} (i.e., A_{canopy} - A_p) is moved into the understorey. For each cohort already in the canopy, we determine a fraction of trees that are moved from the canopy (L_c) to the understorey. L_c is calculated as *Fisher et al. 2010*

$$L_c = \frac{A_{loss,patch} w_{coh}}{\sum_{coh=1}^{nc,patch} w_{coh}},$$

where w_{coh} is a weighting of each cohort. There are two possible ways of calculating this weighting coefficient. The first, as described in *Fisher et al. 2010*, is to probabilistically weight cohorts based on their height h (m) and the competitive exclusion coefficient C_e

$$w_{coh} = h_{coh} C_e.$$

The higher the value of C_e the greater the impact of tree diameter on the probability of a given tree obtaining a position in the canopy layer. That is, for high C_e values, competition is highly deterministic. The smaller the value of C_e, the greater the influence of random factors on the competitive exclusion process, and the higher the probability that slower growing trees will get into the canopy. Appropriate values of C_e are poorly constrained but alter the outcome of competitive processes.

The second way of weighting the cohorts is a more determinstic method based on a strict rank-ordering of the cohorts by height, where all cohorts shorter than that cohorts whose cumulative (from the tallest cohort) rank-ordered crown area equals the area of the patch area are demoted to the lower canopy layer. This is derived from the original PPA algorithm described in *Purves et al. 2008*.

The process by which trees are moved between canopy layers is complex because 1) the crown area predicted for a cohort to lose may be larger than the total crown area of the cohort, which requires iterative solutions, and 2) on some occasions (e.g. after fire, or if the parameter which sets the disturbed area as a function of the fractional crown area of canopy tree mortality is less than one), the canopy may open up and require 'promotion' of cohorts from the understorey, and 3) canopy area may change due to the variations of canopy spread values ($S_{c,patch,cl}$, see the section below for details) when

fractions of cohorts are demoted or promoted. Further details can be found in the code references in the footnote.

1.7.1 Horizontal Canopy Spread

Purves et al. 2008 estimated the ratio between canopy and stem diameter c_p as 0.1 m cm^{-1} for canopy trees in North American forests, but this estimate was made on trees in closed canopies, whose shape is subject to space competition from other individuals. Sapling trees have no constraints in their horizontal spatial structure, and as such, are more likely to display their leaves to full sunlight. Also, prior to canopy closure, light interception by leaves on the sides of the canopy is also higher than it would be in a closed canopy forest. If the 'canopy spread' parameter is constant for all trees, then we simulate high levels of self-shading for plants in unclosed canopies, which is arguably unrealistic and can lower the productivity of trees in areas of unclosed canopy (e.g. low productivity areas of boreal or semi-arid regions where LAI and canopy cover might naturally be low). We here interpret the degree of canopy spread, S_c as a function of how much tree crowns interfere with each other in space, or the total canopy area A_{canopy}. However A_{canopy} itself is a function of S_c, leading to a circularity. S_c is thus solved iteratively through time.

Each daily model step, A_{canopy} and the fraction of the gridcell occupied by tree canopies in each canopy layer

($A_{f,cl}$ = $A_{canopy,cl}$/A_{patch}) is

calculated based on S_c from the previous timestep. If A_f is greater than a threshold value A_t, S_c is increased by a small increment i. The threshold A_t is, hypothetically, the canopy fraction at which light competition begins to impact on tree growth. This is less than 1.0 owing to the non-perfect spatial spacing of tree canopies. If $A_{f,cl}$ is greater than A_t, then S_c is reduced by an increment i, to reduce the spatial extent of the canopy, thus.

$$S_{c,patch,cl,t+1} = \begin{cases} S_{c,patch,cl,t} + i & \text{for } A_{f,cl} < A_t \\ S_{c,patch,cl,t} - i & \text{for } A_{f,cl} > A_t \end{cases}$$

The values of S_c are bounded to upper and lower limits. The lower limit corresponds to the observed canopy spread parameter for canopy trees $S_{c,min}$ and the upper limit corresponds to the largest canopy extent $S_{c,max}$

$$S_{c,patch,cl} = \begin{cases} S_{c,min} & \text{for } S_{c,patch,cl} < S_{c,\min} \\ S_{c,max} & \text{for } S_{c,patch,cl} > S_{c,\max} \end{cases}$$

This iterative scheme requires two additional parameters (i and A_t). i affects the speed with which canopy spread (and hence leaf are index) increase as canopy closure is neared. However, the model is relatively insensitive to the choice of either i or A_t.

1.7.2 Definition of Leaf and Stem Area Profile

Within each patch, the model defines and tracks cohorts of multiple plant functional types that exist either in the canopy or understorey. Light on the top leaf surface of each cohort in the canopy is the same, and the rate of decay

through the canopy is also the same for each PFT. Therefore, we accumulate all the cohorts of a given PFT together for the sake of the radiation and photosynthesis calculations (to avoid separate calculations for every cohort).

Therefore, the leaf area index for each patch is defined as a three-dimensional array $lai_{cl,ft,z}$ where C_l

is the canopy layer, ft is the functional type and z is the leaf layer within each canopy. This three-dimensional structure is the basis of the radiation and photosynthetic models. In addition to a leaf area profile matrix, we also define, for each patch, the area which is covered by leaves at each layer as $carea_{cl,ft,z}$.

Each plant cohort is already defined as a member of a single canopy layer and functional type. This means that to generate the $x_{cl,ft,z}$ matrix, it only remains to divide the leaf area of each cohort into leaf layers. First, we determine how many leaf layers are occupied by a single cohort, by calculating the 'tree LAI' as the total leaf area of each cohort divided by its crown area (both in m^2)

$$tree_{lai,coh} = \frac{C_{leaf,coh} \cdot \mathrm{sla}_{ft}}{A_{crown,coh}}$$

where sla_{ft} is the specific leaf area in m^2 KgC^{-1} and C_{leaf} is in kGC per plant.

Stem area index (SAI) is ratio of the total area of all woody stems on a plant to the area of ground covered by the plant. During winter in deciduous areas, the extra absorption by woody stems can have a significant impact on the surface energy budget. However, in previous *big leaf* versions of the CLM, computing the circumstances under which stem area was visible in the absence of leaves was difficult and the algorithm was largely heuristic as a result. Given the multi-layer canopy introduced for FATES, we can determine the leaves in the higher canopy layers will likely shade stem area in the lower layers when leaves are on, and therefore stem area index can be calculated as a function of woody biomass directly.

Literature on stem area index is particularly poor, as it's estimation is complex and not particularly amenable to the use of, for example, assumptions of random distribution in space that are typically used to calculate leaf area from light interception. *Kucharik et al. 1998* estimated that SAI visible from an LAI2000 sensor was around 0.5 m^2 m^-2. Low et al. 2001 estimate that the wood area index for Ponderosa Pine forest is 0.27-0.33. The existing CLM(CN) algorithm sets the minimum SAI at 0.25 to match MODIS observations, but then allows SAI to rise as a function of the LAI lost, meaning than in some places, predicted SAI can reach value of 8 or more. Clearly, greater scientific input on this quantity is badly needed. Here we determine that SAI is a linear function of woody biomass, to at very least provide a mechanistic link between the existence of wood and radiation absorbed by it. The non-linearity between how much woody area exists and how much radiation is absorbed is provided by the radiation absorption algorithm. Specifically, the SAI of an individual cohort ($\mathrm{tree}_{sai,coh}$, m^2 m^{-2}) is calculated as follows,

$$\mathrm{tree}_{sai,coh} = k_{sai} \cdot C_{struc,coh},$$

where k_{sai} is the coefficient linking structural biomass to SAI. The number of occupied leaf layers for cohort coh ($n_{z,coh}$) is then equal to the rounded up integer value of the tree SAI ($tree_{sai,coh}$) and LAI ($tree_{lai,coh}$) divided by the layer thickness (i.e., the resolution of the canopy layer model, in units of vegetation index (lai+sai) with a default value of 1.0, δ_{vai}),

$$n_{z,coh} = \frac{\mathrm{tree}_{lai,coh} + \mathrm{tree}_{sai,coh}}{\delta_{vai}}.$$

The fraction of each layer that is leaf (as opposed to stem) can then be calculated as

$$f_{leaf,coh} = \frac{\mathrm{tree}_{lai,coh}}{\mathrm{tree}_{sai,coh} + \mathrm{tree}_{lai,coh}}.$$

Finally, the leaf area in each leaf layer pertaining to this cohort is thus

$$lai_{z,coh} = \begin{cases} \delta_{vai} \cdot f_{leaf,coh} \frac{A_{canopy,coh}}{A_{canopy,patch}} & \text{for } i = 1, ..., i = n_{z,coh} - 1 \\ \delta_{vai} \cdot f_{leaf,coh} \frac{A_{canopy,coh}}{A_{canopy,patch}} \cdot r_{vai} & \text{for } i = n_{z,coh} \end{cases}$$

and the stem area index is

$$sai_{z,coh} = \begin{cases} \delta_{vai} \cdot (1 - f_{leaf,coh}) \frac{A_{canopy,coh}}{A_{canopy,patch}} & \text{for } i = 1, ..., i = n_{z,coh} - 1 \\ \delta_{vai} \cdot (1 - f_{leaf,coh}) \frac{A_{canopy,coh}}{A_{canopy,patch}} \cdot r_{vai} & \text{for } i = n_{z,coh} \end{cases}$$

where r_{vai} is the remainder of the canopy that is below the last full leaf layer

$$r_{vai} = (\text{tree}_{lai,coh} + \text{tree}_{sai,coh}) - (\delta_{vai} \cdot (n_{z,coh} - 1)).$$

$A_{canopy,patch}$ is the total canopy area occupied by plants in a given patch (m:math:^{2}) and is calculated as follows,

$$A_{canopy,patch} = \min \left(\sum_{coh=1}^{coh=ncoh} A_{canopy,coh}, A_{patch} \right).$$

The canopy is conceived as a cylinder, although this assumption could be altered given sufficient evidence that canopy shape was an important determinant of competitive outcomes, and the area of ground covered by each leaf layer is the same through the cohort canopy. With the calculated SAI and LAI, we are able to calculate the complete canopy profile. Specifically, the relative canopy area for the cohort coh is calculated as

$$area_{1:nz,coh} = \frac{A_{crown,coh}}{A_{canopy,patch}}.$$

The total occupied canopy area for each canopy layer (cl), plant functional type (ft) and leaf layer (z) bin is thus

$$c_{area,cl,ft,z} = \sum_{coh=1}^{coh=ncoh} area_{1:nz,coh}$$

where $ft_{coh} = ft$ and $cl_{coh} = cl$.

All of these quantities are summed across cohorts to give the complete leaf and stem area profiles,

$$lai_{cl,ft,z} = \sum_{coh=1}^{coh=ncoh} lai_{z,coh}$$

$$sai_{cl,ft,z} = \sum_{coh=1}^{coh=ncoh} sai_{z,coh}$$

1.7.3 Burial of leaf area by snow

The calculations above all pertain to the total leaf and stem area indices which charecterize the vegetation structure. In addition, the model must know when the vegetation is covered by snow, and by how much, so that the albedo and energy balance calculations can be adjusted accordingly. Therefore, we calculated a 'total' and 'exposed' lai and sai profile using a representation of the bottom and top canopy heights, and the depth of the average snow pack. For each leaf layer z of each cohort, we calculate an 'exposed fraction $f_{exp,z}$ via consideration of the top and bottom heights of that layer $h_{top,z}$ and $h_{bot,z}$ (m),

$$h_{top,z} = h_{coh} - h_{coh} \cdot f_{crown,ft} \cdot \frac{z}{n_{z,coh}}$$

$$h_{bot,z} = h_{coh} - h_{coh} \cdot f_{crown,ft} \cdot \frac{z+1}{n_{z,coh}}$$

where $f_{crown,ft}$ is the plant functional type (ft) specific fraction of the cohort height that is occupied by the crown. Specifically, the 'exposed fraction $f_{exp,z}$ is calculated as follows,

$$f_{exp,z} \begin{cases} = 1.0 & h_{bot,z} > d_{snow} \\ = \frac{d_{snow} - h_{bot,z}}{h_{top,z} - h_{bot,z}} & h_{top,z} > d_{snow}, h_{bot,z} < d_{snow} \\ = 0.0 & h_{top,z} < d_{snow} \end{cases}$$

The resulting exposed ($elai, esai$) and total ($tlai, tsai$) leaf and stem area indicies are calculated as

$$\begin{array}{ll} elai_{cl,ft,z} & = lai_{cl,ft,z} \cdot f_{exp,z} \\ esai_{cl,ft,z} & = sai_{cl,ft,z} \cdot f_{exp,z} \\ tlai_{cl,ft,z} & = lai_{cl,ft,z} \\ tsai_{cl,ft,z} & = sai_{cl,ft,z} \end{array} ,$$

and are used in the radiation interception and photosynthesis algorithms described later.

Parameter Symbol	Parameter Name	Units	Notes	Indexed by
:math:' delta_ {vai}'	Thickness of single canopy layer	m^{-2}m: math:^{-2}		
C_e	Competitive Exclusion Parameter	none		
$c_{p,min}$	Minimum canopy spread	m^2 cm:math:' ^{-1}'		
$c_{p,max}$	Competitive Exclusion Parameter	m^2 cm:math:' ^{-1}'		
i	Incremental change in c_p	m^2 cm:math:' ^{-1}' y^{-1}		
A_t	Threshold canopy closure	none		
$f_{crown,ft}$	Crown fraction	none		ft
k_{sai}	Stem area per unit woody biomass	m^2 KgC^-1		

1.8 Radiation Transfer

1.8.1 Fundamental Radiation Transfer Theory

The first interaction of the land surface with the properties of vegetation concerns the partitioning of energy into that which is absorbed by vegetation, reflected back into the atmosphere, and absorbed by the ground surface. Older versions of the CLM have utilized a "two-stream" approximation *Sellers 1985*, *Sellers et al. 1986* that provided an empirical solution for the radiation partitioning of a multi-layer canopy for two streams, of diffuse and direct light. However, implementation of the Ecosystem Demography model requires a) the adoption of an explicit multiple layer canopy b) the implementation of a multiple plant type canopy and c) the distinction of canopy and under-storey layers, in-between which the radiation streams are fully mixed. The radiation mixing between canopy layers is necessary as the position of different plants in the under-storey is not defined spatially or relative to the canopy trees above. In this new scheme, we thus implemented a one-dimensional scheme that traces the absorption, transmittance and reflectance of each canopy layer and the soil, iterating the upwards and downwards passes of radiation through the canopy until a pre-defined accuracy tolerance is reached. This approach is based on the work of *Norman 1979*.

Here we describe the basic theory of the radiation transfer model for the case of a single homogenous canopy, and in the next section we discuss how this is applied to the multi layer multi PFT canopy in the FATES implementation. The code considers the fractions of a single unit of incoming direct and a single unit of incoming diffuse light, that are absorbed at each layer of the canopy for a given solar angle (α_s, radians). Direct radiation is extinguished through the canopy according to the coefficient k_{dir} that is calculated from the incoming solar angle and the dimensionless leaf angle distribution parameter (χ) as

$$k_{dir} = g_{dir} / \sin(\alpha_s)$$

where

$$g_{dir} = \phi_1 + \phi_2 \cdot \sin(\alpha_s)$$

and

$$\phi_1 = 0.5 - 0.633\chi_l - 0.33\chi_l^2$$
$$\phi_2 = 0.877(1 - 2\phi_1)$$

The leaf angle distribution is a descriptor of how leaf surfaces are arranged in space. Values approaching 1.0 indicate that (on average) the majority of leaves are horizontally arranged with respect to the ground. Values approaching -1.0 indicate that leaves are mostly vertically arranged, and a value of 0.0 denotes a canopy where leaf angle is random (a 'spherical' distribution).

According to Beer's Law, the fraction of light that is transferred through a single layer of vegetation (leaves or stems) of thickness δ_{vai}, without being intercepted by any surface, is

$$tr_{dir} = e^{-k_{dir}\delta_{vai}}$$

and the incident direct radiation transmitted to each layer of the canopy ($dir_{tr,z}$) is thus calculated from the cumulative leaf area (L_{above}) shading each layer (z):

$$dir_{tr,z} = e^{-k_{dir}L_{above,z}}$$

The fraction of the leaves f_{sun} that are exposed to direct light is also calculated from the decay coefficient k_{dir}.

$$f_{sun,z} = e^{-k_{dir}L_{above,z}}$$
and
$$f_{shade,z} = 1 - f_{sun,z}$$

where $f_{shade,z}$ is the fraction of leaves that are shaded from direct radiation and only receive diffuse light.

Diffuse radiation, by definition, enters the canopy from a spectrum of potential incident directions, therefore the unintercepted transfer (tr_{dif}) through a leaf layer of thickness δ_l is calculated as the mean of the transfer rate from each of 9 different incident light directions (α_s) between 0 and 180 degrees to the horizontal.

$$tr_{dif} = \frac{1}{9}\sum_{\alpha_s=5\pi/180}^{\alpha_s=85\pi/180} e^{-k_{dir,l}\delta_{vai}}$$

$$tr_{dif} = \frac{1}{9}\pi\sum_{\alpha s=0}^{\pi/2} \frac{e^{-gdir}\alpha_s}{\delta_{vai}\cdot\sin(\alpha_s)\sin(\alpha_s)\cos(\alpha_s)}$$

The fraction (1-tr_{dif}) of the diffuse radiation is intercepted by leaves as it passes through each leaf layer. Of this, some fraction is reflected by the leaf surfaces and some is transmitted through. The fractions of diffuse radiation reflected from ($refl_{dif}$) and transmitted though ($tran_{dif}$) each layer of leaves are thus, respectively

$$refl_{dif} = (1 - tr_{dif})\rho_{l,ft}$$
$$tran_{dif} = (1 - tr_{dif})\tau_{l,ft} + tr_{dif}$$

where $\rho_{l,ft}$ and $\tau_{l,ft}$ are the fractions of incident light reflected and transmitted by individual leaf surfaces.

Once we know the fractions of light that are transmitted and reflected by each leaf layer, we begin the process of distributing light through the canopy. Starting with the first leaf layer (z=1), where the incident downwards diffuse

radiation (dif_{down}) is 1.0, we work downwards for n_z layers, calculating the radiation in the next layer down ($z+1$) as:

$$dif_{down,z+1} = \frac{dif_{down,z} tran_{dif}}{1 - r_{z+1} refl_{dif}}$$

Here, $dif_{down,z} tran_{dif}$ calculates the fraction of incoming energy transmitted downwards onto layer $z+1$. This flux is then increased by the additional radiation r_z that is reflected upwards from further down in the canopy to layer z, and then is reflected back downwards according to the reflected fraction $refl_{dif}$. The more radiation in $r_{z+1} refl_{dif}$, the smaller the denominator and the larger the downwards flux. r is also calculated sequentially, starting this time at the soil surface layer (where $z = n_z + 1$)

$$r_{nz+1} = alb_s$$

where alb_s is the soil albedo characteristic. The upwards reflected fraction r_z for each leaf layer, moving upwards, is then *Norman 1979*

$$r_z = \frac{r_{z+1} \times tran_{dif}^2}{(1 - r_{z+1} refl_{dif}) + refl_{dif}}.$$

The corresponding upwards diffuse radiation flux is therefore the fraction of downwards radiation that is incident on a particular layer, multiplied by the fraction that is reflected from all the lower layers:

$$dif_{up,z} = r_z dif_{down,z+1}$$

Now we have initial conditions for the upwards and downwards diffuse fluxes, these must be modified to account for the fact that, on interception with leaves, direct radiation is transformed into diffuse radiation. In addition, the initial solutions to the upwards and downwards radiation only allow a single 'bounce' of radiation through the canopy, so some radiation which might be intercepted by leaves higher up is potentially lost. Therefore, the solution to this model is iterative. The iterative solution has upwards and a downwards components that calculate the upwards and downwards fluxes of total radiation at each leaf layer ($rad_{dn,z}$ and $rad_{up,z}$) . The downwards component begins at the top canopy layer ($z = 1$). Here we define the incoming solar diffuse and direct radiation ($solar_{dir}$ and $solar_{dir}$ respectively).

$$dif_{dn,1} = solar_{dif}$$
$$rad_{dn,z+1} = dif_{dn,z} \cdot tran_{dif} + dif_{up,z+1} \cdot refl_{dif} + solar_{dir} \cdot dir_{tr,z}(1 - tr_{dir})\tau_l.$$

The first term of the right-hand side deals with the diffuse radiation transmitted downwards, the second with the diffuse radiation travelling upwards, and the third with the direct radiation incoming at each layer ($dir_{tr,z}$) that is intercepted by leaves ($1 - tr_{dir}$) and then transmitted through through the leaf matrix as diffuse radiation (τ_l). At the bottom of the canopy, the light reflected off the soil surface is calculated as

$$rad_{up,nz} = dif_{\mathrm{down,z}} \cdot \mathrm{salb_{dif}} + solar_{dir} \cdot dir_{tr,z} salb_{dir}.$$

The upwards propagation of the reflected radiation is then

$$rad_{up,z} = dif_{up,z+1} \cdot tran_{dif} + dif_{dn,z} \cdot refl_{dif} + solar_{dir} \cdot dir_{tr,z}(1 - tr_{dir})\rho_l.$$

Here the first two terms deal with the diffuse downwards and upwards fluxes, as before, and the third deals direct beam light that is intercepted by leaves and reflected upwards. These upwards and downwards fluxes are computed for multiple iterations, and at each iteration, $rad_{up,z}$ and $rad_{down,z}$ are compared to their values in the previous iteration. The iteration scheme stops once the differences between iterations for all layers is below a predefined tolerance factor, (set here at 10^{-4}). Subsequently, the fractions of absorbed direct ($abs_{dir,z}$) and diffuse ($abs_{dif,z}$) radiation for each leaf layer then

$$abs_{dir,z} = solar_{dir} \cdot dir_{tr,z} \cdot (1 - tr_{dir}) \cdot (1 - \rho_l - \tau_l)$$

$$abs_{dif,z} = (dif_{dn,z} + dif_{up,z+1}) \cdot (1 - tr_{dif}) \cdot (1 - \rho_l - \tau_l).$$

and, the radiation energy absorbed by the soil for the diffuse and direct streams is is calculated as

$$abs_{soil} = dif_{down,nz+1} \cdot (1 - salb_{dif}) + solar_{dir} \cdot dir_{tr,nz+1} \cdot (1 - salb_{dir}).$$

Canopy level albedo is denoted as the upwards flux from the top leaf layer

$$alb_{canopy} = \frac{dif_{up,z+1}}{solar_{dir} + solar_{dif}}$$

and the division of absorbed energy into sunlit and shaded leaf fractions, (required by the photosynthesis calculations), is

$$abs_{sha,z} = abs_{dif,z} \cdot f_{sha}$$

$$abs_{sun,z} = abs_{dif,z} \cdot f_{sun} + abs_{dir,z}$$

1.8.2 Resolution of radiation transfer theory within the FATES canopy structure

The radiation transfer theory above, was described with reference to a single canopy of one plant functional type, for the sake of clarity of explanation. The FATES model, however, calculates radiative and photosynthetic fluxes for a more complex hierarchical structure within each patch/time-since-disturbance class, as described in the leaf area profile section. Firstly, we denote two or more canopy layers (denoted cl). The concept of a 'canopy layer' refers to the idea that plants are organized into discrete over and under-stories, as predicted by the Perfect Plasticity Approximation (*Purves et al. 2008*, *Fisher et al. 2010*). Within each canopy layer there potentially exist multiple cohorts of different plant functional types and heights. Within each canopy layer, cl, and functional type, ft, the model resolves numerous leaf layers z, and, for some processes, notably photosynthesis, each leaf layer is split into a fraction of sun and shade leaves, f_{sun} and f_{sha}, respectively.

The radiation scheme described in Section is solved explicitly for this structure, for both the visible and near-infrared wavebands, according to the following assumptions.

- A *canopy layer* (cl) refers literally to the vertical layer within the canopy this cohort resides in. The top canopy layer has index 1. A closed canopy forest will therefore by definition have at least two layers, and perhaps more.
- A *leaf layer* (z) refers to the discretization of the LAI within the canopy of a given plant functional type.
- All PFTs in the same canopy layer have the same solar radiation incident on the top layer of the canopy
- Light is transmitted through the canopy of each plant functional type independently
- Between canopy layers, the light streams from different plant functional types are mixed, such that the (undefined) spatial location of plants in lower canopy layers does not impact the amount of light received.
- Where understorey layers fill less area than the overstorey layers, radiation is directly transferred to the soil surface.
- All these calculations pertain to a single patch, so we omit the *patch* subscript for simplicity in the following discussion.

Within this framework, the majority of the terms in the radiative transfer scheme are calculated with indices of cl, ft and z. In the following text, we revisit the simplified version of the radiation model described above, and explain how it is modified to account for the more complex canopy structure used by FATES.

Firstly, the light penetration functions, k_{dir} and g_{dir} are described as functions of ft, because the leaf angle distribution, χ_l, is a pft-specific parameter. Thus, the diffuse irradiance transfer rate, tr_{dif} is also ft specific because g_{dir}, on which it depends, is a function of χ_l.

The amount of direct light reaching each leaf layer is a function of the leaves existing above the layer in question. If a leaf layer 'z' is in the top canopy layer (the over-storey), it is only shaded by leaves of the same PFT so k_{dir} is unchanged from equation. If there is more than one canopy layer ($cl_{max} > 1$), then the amount of direct light reaching the top leaf surfaces of the second/lower layer is the weighted average of the light attenuated by all the parallel tree canopies in the canopy layer above, thus.

$$dir_{tr(cl,:,1)} = \sum_{ft=1}^{npft} (dir_{tr(cl,ft,z_{max})} \cdot c_{area(cl-1,ft,z_{max})})$$

where pft_{wt} is the areal fraction of each canopy layer occupied by each functional type and z_{max} is the index of the bottom canopy layer of each pft in each canopy layer (the subscripts

cl and ft are implied but omitted from all z_{max} references to avoid additional complications)

Similarly, the sunlit fraction for a leaf layer 'z' in the second canopy layer (where $cl > 1$) is

$$f_{sun(cl,ft,z)} = W_{sun(cl)} \cdot e^{k_{dir(ft,laic,z)}}$$

where $W_{sun,cl}$ is the weighted average sunlit fraction in the bottom layer of a given canopy layer.

$$W_{sun(cl)} = \sum_{ft=1}^{npft} (f_{sun(cl-1,ft,zmax)} \cdot c_{area(cl-1,ft,zmax)})$$

Following through the sequence of equations for the simple single pft and canopy layer approach above, the $refl_{dif}$ and $tran_{dif}$ fluxes are also indexed by cl, ft, and z. The diffuse radiation reflectance ratio r_z is also calculated in a manner that homogenizes fluxes between canopy layers. For the canopy layer nearest the soil (cl = cl_{max}). For the top canopy layer (cl=1), a weighted average reflectance from the lower layers is used as the baseline, in lieu of the soil albedo. Thus:

$$r_{z(cl,:,1)} = \sum_{ft=1}^{npft} (r_{z(cl-1,ft,1)} pft_{wt(cl-1,ft,1)})$$

For the iterative flux resolution, the upwards and downwards fluxes are also averaged between canopy layers, thus where $cl > 1$

$$rad_{dn(cl,ft,1)} = \sum_{ft=1}^{npft} (rad_{dn(cl-1,ft,zmax)} \cdot pft_{wt(cl-1,ft,zmax)})$$

and where cl =1, and $cl_{max} > 1$

$$rad_{up(cl,ft,zmax)} = \sum_{ft=1}^{npft} (rad_{up(cl+1,ft,1)} \cdot pft_{wt(cl+1,ft,1)})$$

The remaining terms in the radiation calculations are all also indexed by cl, ft and z so that the fraction of absorbed radiation outputs are termed $abs_{dir(cl,ft,z)}$ and $abs_{dif(cl,ft,z)}$. The sunlit and shaded absorption rates are therefore

$$abs_{sha(cl,ft,z)} = abs_{dif(cl,ft,z)} \cdot f_{sha(cl,ft,z)}$$

and

$$abs_{sun(cl,ft,z)} = abs_{dif(cl,ft,z)} \cdot f_{sun(cl,ft,z)} + abs_{dir(cl,ft,z)}$$

The albedo of the mixed pft canopy is calculated as the weighted average of the upwards radiation from the top leaf layer of each pft where cl=1:

$$alb_{canopy} = \sum_{ft=1}^{npft} \frac{dif_{up(1,ft,1)} pft_{wt(1,ft,1)}}{solar_{dir} + solar_{dif}}$$

The radiation absorbed by the soil after passing through through under-storey vegetation is:

$$abs_{soil} = \sum_{ft=1}^{npft} pft_{wt(1,ft,1)}(dif_{down(nz+1)}(1 - salb_{dif}) + solar_{dir} dir_{tr(nz+1)}(1 - salb_{dir}))$$

to which is added the diffuse flux coming directly from the upper canopy and hitting no understorey vegetation.

$$abs_{soil} = abs_{soil} + dif_{dn(2,1)}(1 - \sum_{ft=1}^{npft} pft_{wt(1,ft,1)})(1 - salb_{dif})$$

and the direct flux coming directly from the upper canopy and hitting no understorey vegetation.

$$abs_{soil} = abs_{soil} + solar_{dir} dir_{tr(2,1)}(1 - \sum_{ft=1}^{npft} pft_{wt(1,ft,1)})(1 - salb_{dir})$$

These changes to the radiation code are designed to be structurally flexible, and the scheme may be collapsed down to only include on canopy layer, functional type and pft for testing if necessary.

Table 1.11: Parameters needed for radiation transfer model.

Parameter Symbol	Parameter Name	Units	indexed by
χ	Leaf angle distribution parameter	none	*ft*
ρ_l	Fraction of light reflected by leaf surface	none	*ft*
τ_l	Fraction of light transmitted by leaf surface	none	*ft*
alb_s	Fraction of light reflected by soil	none	direct vs diffuse

1.9 Photosynthesis

1.9.1 Fundamental photosynthetic physiology theory

In this section we describe the physiological basis of the photosynthesis model before describing its application to the FATES canopy structure. This description in this section is largely repeated from the Oleson et al. CLM4.5 technical note but included here for comparison with its implementation in FATES. Photosynthesis in C3 plants is based on the model of *Farquhar 1980* as modified by *Collatz et al. (1991)*. Photosynthetic assimilation in C4 plants is based on the model of *Collatz et al. (1991)*. In both models, leaf photosynthesis, gpp (μmol CO_2 m^{-2} s^{-1}) is calculated as the minimum of three potentially limiting fluxes, described below:

$$\text{gpp} = \min(\text{w}_\text{j}, \text{w}_\text{c}, \text{w}_\text{p}).$$

The RuBP carboxylase (Rubisco) limited rate of carboxylation w_c (μmol CO_2 m^{-2} s^{-1}) is determined as

$$w_c = \begin{cases} \frac{V_{c,max}(c_i - \Gamma_*)}{ci + K_c(1 + o_i/K_o)} & \text{for } C_3 \text{ plants} \\ V_{c,max} & \text{for } C_4 \text{ plants} \end{cases} \qquad c_i - \Gamma_* \geq 0$$

where c_i is the internal leaf CO_2 partial pressure (Pa) and $o_i(0.209P_{atm})$ is the O_2 partial pressure (Pa). K_c and K_o are the Michaelis-Menten constants (Pa) for CO_2 and O_2. These vary with vegetation temperature T_v (^{o}C) according to an Arrhenious function described in *Oleson et al. 2013*. $V_{c,max}$ is the leaf layer photosynthetic capacity (μ mol CO_2 m^{-2} s^{-1}).

The maximum rate of carboxylation allowed by the capacity to regenerate RuBP (i.e., the light-limited rate) w_j (μmol CO_2 m^{-2} s^{-1}) is

$$w_j = \begin{cases} \frac{J(c_i-\Gamma_*)}{4ci+8\Gamma_*} & \text{for } C_3 \text{ plants} \\ 4.6\phi\alpha & \text{for } C_4 \text{ plants} \end{cases} \qquad c_i - \Gamma_* \geq 0$$

To find J, the electron transport rate (μ mol CO_2 m^{-2} s^{-1}), we solve the following quadratic term and take its smaller root,

$$\Theta_{psII} J^2 - (I_{psII} + J_{max})J + I_{psII} J_{max} = 0$$

where J_{max} is the maximum potential rate of electron transport (μmol m_{-2} s^{-1}), I_{PSII} is the is the light utilized in electron transport by photosystem II (μmol m_{-2} s^{-1}) and Θ_{PSII} is is curvature parameter. I_{PSII} is determined as

$$I_{PSII} = 0.5\Phi_{PSII}(4.6\phi)$$

where ϕ is the absorbed photosynthetically active radiation (Wm:math:^{-2}) for either sunlit or shaded leaves (abs_{sun} and abs_{sha}). ϕ is converted to photosynthetic photon flux assuming 4.6 μmol photons per joule. Parameter values are Φ_{PSII} = 0.7 for C3 and Φ_{PSII} = 0.85 for C4 plants.

The export limited rate of carboxylation for C3 plants and the PEP carboxylase limited rate of carboxylation for C4 plants w_e (also in μmol CO_2 m^{-2} s^{-1}) is

$$w_e = \begin{cases} 3T_{p,0} & \text{for } C_3 \text{ plants} \\ k_p \frac{c_i}{P_{atm}} & \text{for } C_4 \text{ plants.} \end{cases}$$

T_p is the triose-phosphate limited rate of photosynthesis, which is equal to $0.167V_{c,max0}$. k_p is the initial slope of C4 CO_2 response curve. The Michaelis-Menten constants K_c and K_o are modeled as follows,

$$K_c = K_{c,25}(a_{kc})^{\frac{T_v-25}{10}},$$

$$K_o = K_{o,25}(a_{ko})^{\frac{T_v-25}{10}},$$

where $K_{c,25}$ = 30.0 and $K_{o,25}$ = 30000.0 are values (Pa) at 25 ^{o}C, and a_{kc} = 2.1 and a_{ko} =1.2 are the relative changes in $K_{c,25}$ and $K_{o,25}$ respectively, for a 10^{o}C change in temperature. The CO_2 compensation point Γ_* (Pa) is

$$\Gamma_* = \frac{1}{2}\frac{K_c}{K_o}0.21o_i$$

where the term 0.21 represents the ratio of maximum rates of oxygenation to carboxylation, which is virtually constant with temperature *Farquhar, 1980*.

1.9.2 Resolution of the photosynthesis theory within the FATES canopy structure.

The photosynthesis scheme is modified from the CLM4.5 model to give estimates of photosynthesis, respiration and stomatal conductance for a three dimenstional matrix indexed by canopy level (C_l), plant functional type (ft) and leaf layer (z). We conduct the photosynthesis calculations at each layer for both sunlit and shaded leaves. Thus, the model also generates estimates of w_c, w_j and w_e indexed in the same three dimensional matrix. In this implementation, some properties (stomatal conductance parameters, top-of-canopy photosynthetic capacity) vary with plant functional type, and some vary with both functional type and canopy depth (absorbed photosynthetically active radiation, nitrogen-based variation in photosynthetic properties). The remaining drivers of photosynthesis (P_{atm}, K_c, o_i, K_o, temperature, atmospheric CO_2) remain the same throughout the canopy. The rate of gross photosynthesis

($gpp_{cl,ft,z}$)is the smoothed minimum of the three potentially limiting processes (carboxylation, electron transport, export limitation), but calculated independently for each leaf layer:

$$\mathrm{gpp}_{cl,ft,z} = \min(\mathrm{w_{c,cl,ft,z}}, \mathrm{w_{j,cl,ft,z}}, \mathrm{w_{e,cl,ft,z}}).$$

For $w_{c,cl,ft,z}$,, we use

$$w_{c,cl,ft,z} = \begin{cases} \frac{V_{c,max,cl,ft,z}(c_{i,cl,ft,z}-\Gamma_*)}{c_{i,cl,ft,z}+K_c(1+o_i/K_o)} & \text{for } C_3 \text{ plants} \\ V_{c,max,cl,ft,z} & \text{for } C_4 \text{ plants} \end{cases} \qquad c_{i,cl,ft,z} - \Gamma_* \geq 0$$

where $V_{c,max}$ now varies with PFT, canopy depth and layer (see below). Internal leaf CO_2 ($c_{i,cl,ft,z}$) is tracked seperately for each leaf layer. For the light limited rate w_j, we use

$$w_j = \begin{cases} \frac{J(c_i-\Gamma_*)4.6\phi\alpha}{4ci+8\Gamma_*} & \text{for C}_3 \text{ plants} \\ 4.6\phi\alpha & \text{for C}_4 \text{ plants} \end{cases}$$

where J is calculated as above but based on the absorbed photosynthetically active radiation($\phi_{cl,ft,z}$) for either sunlit or shaded leaves in Wm^{-2}. Specifically,

$$\phi_{cl,ft,z} = \begin{cases} abs_{sun,cl,ft,z} & \text{for sunlit leaves} \\ abs_{sha,cl,ft,z} & \text{for shaded leaves} \end{cases}$$

The export limited rate of carboxylation for C3 plants and the PEP carboxylase limited rate of carboxylation for C4 plants w_c (also in μmol CO_2 m^{-2} s^{-1}) is calculated in a similar fashion,

$$w_{e,cl,ft,z} = \begin{cases} 0.5V_{c,max,cl,ft,z} & \text{for } C_3 \text{ plants} \\ 4000V_{c,max,cl,ft,z}\frac{c_{i,cl,ft,z}}{P_{atm}} & \text{for } C_4 \text{ plants.} \end{cases}$$

1.9.3 Variation in plant physiology with canopy depth

Both $V_{c,max}$ and J_{max} vary with vertical depth in the canopy on account of the well-documented reduction in canopy nitrogen through the leaf profile, see *Bonan et al. 2012* for details). Thus, both $V_{c,max}$ and J_{max} are indexed by by C_l, ft and z according to the nitrogen decay coefficient K_n and the amount of vegetation area shading each leaf layer V_{above},

$$\begin{aligned} V_{c,max,cl,ft,z} &= V_{c,max0,ft}e^{-K_{n,ft}V_{above,cl,ft,z}}, \\ J_{max,cl,ft,z} &= J_{max0,ft}e^{-K_{n,ft}V_{above,cl,ft,z}}, \end{aligned}$$

where $V_{c,max,0}$ and $J_{max,0}$ are the top-of-canopy photosynthetic rates. V_{above} is the sum of exposed leaf area index (elai$_{cl,ft,z}$) and the exposed stem area index (esai$_{cl,ft,z}$)(m^2 m^{-2}). Namely,

$$V_{cl,ft,z} = \mathrm{elai}_{cl,ft,z} + \mathrm{esai}_{cl,ft,z}.$$

The vegetation index shading a particular leaf layer in the top canopy layer is equal to

$$V_{above,cl,ft,z} = \textstyle\sum_1^z V_{cl,ft,z} \quad \text{for } cl = 1.$$

For lower canopy layers, the weighted average vegetation index of the canopy layer above (V_{canopy}) is added to this within-canopy shading. Thus,

$$V_{above,cl,ft,z} = \textstyle\sum_1^z V_{cl,ft,z} + V_{canopy,cl-1} \quad \text{for } cl > 1,$$

where V_{canopy} is calculated as

$$V_{canopy,cl} = \sum_{ft=1}^{npft} \sum_{z=1}^{nz(ft)} (V_{cl,ft,z} \cdot pft_{wt,cl,ft,1}).$$

K_n is the coefficient of nitrogen decay with canopy depth. The value of this parameter is taken from the work of *Lloyd et al. 2010* who determined, from 204 vertical profiles of leaf traits, that the decay rate of N through canopies of tropical rainforests was a function of the V_{cmax} at the top of the canopy. They obtain the following term to predict K_n,

$$K_{n,ft} = e^{0.00963 V_{c,max0,ft} - 2.43},$$

where V_{cmax} is again in μmol CO_2 m^{-2} s^{-1}.

1.9.4 Water Stress on gas exchange

The top of canopy leaf photosynthetic capacity, $V_{c,max0}$, is also adjusted for the availability of water to plants as

$$V_{c,max0,25} = V_{c,max0,25} \beta_{sw},$$

where the adjusting factor β_{sw} ranges from one when the soil is wet to zero when the soil is dry. It depends on the soil water potential of each soil layer, the root distribution of the plant functional type, and a plant-dependent response to soil water stress,

$$\beta_{sw} = \sum_{j=1}^{nj} w_j r_j,$$

where w_j is a plant wilting factor for layer j and r_j is the fraction of roots in layer j.The plant wilting factor w_j is

$$w_j = \begin{cases} \frac{\psi_c - \psi_j}{\psi_c - \psi_o} \left(\frac{\theta_{sat,j} - \theta_{ice,j}}{\theta_{sat,j}} \right) & \text{for } T_i > \text{-2C} \\ 0 & \text{for } T_j \geq \text{-2C} \end{cases}$$

where ψ_i is the soil water matric potential (mm) and ψ_c and ψ_o are the soil water potential (mm) when stomata are fully closed or fully open, respectively. The term in brackets scales w_i the ratio of the effective porosity (after accounting for the ice fraction) relative to the total porosity. w_i = 0 when the temperature of the soil layer (T_i) is below some threshold (-2:math:^{o}C) or when there is no liquid water in the soil layer ($\theta_{liq,i} \leq 0$). For more details on the calculation of soil matric potential, see the CLM4.5 technical note.

Variation of water stress and water uptake within tiles

The remaining drivers of the photosynthesis model remain constant (atmospheric CO_2 and O^2 and canopy temperature) throughout the canopy, except for the water stress index β_{sw}. β_{sw} must be indexed by ft, because plants of differing functional types have the capacity to have varying root depth, and thus access different soil moisture profile and experience differing stress functions. Thus, the water stress function applied to gas exchange calculation is now calculated as

$$\beta_{sw,ft} = \sum_{j=1}^{nj} w_{j,ft} r_{j,ft},$$

where w_j is the water stress at each soil layer j and $r_{j,ft}$ is the root fraction of each PFT's root mass in layer j. Note that this alteration of the β_{sw} parameter also necessitates recalculation of the vertical water extraction profiles. In the original model, the fraction of extraction from each layer ($r_{e,j,patch}$) is the product of a single root distribution,

because each patch only has one plant functional type. In FATES, we need to calculate a new weighted patch effective rooting depth profile $r_{e,j,patch}$ as the weighted average of the functional-type level stress functions and their relative contributions to canopy conductance. Thus for each layer j, the extraction fraction is summed over all PFTs as

$$r_{e,j,patch} = \sum_{ft=1}^{ft=npft} \frac{w_{j,ft}}{\sum_{j=1}^{=nj} w_{j,ft}} \frac{G_{s,ft}}{G_{s,canopy}},$$

where nj is the number of soil layers, $G_{s,canopy}$is the total canopy (see section 9 for details) and $G_{s,ft}$ is the canopy conductance for plant functional type ft,

$$G_{s,ft} = \sum_{1} w_{ncoh,ft} gs_{can,coh} n_{coh}.$$

1.9.5 Aggregation of assimilated carbon into cohorts

The derivation of photosynthetic rates per leaf layer, as above, give us the estimated rate of assimilation for a unit area of leaf at a given point in the canopy in μmol CO_2 m^{-2} s_{-1}. To allow the integration of these rates into fluxes per individual tree, or cohort of trees (gCO:math:_2 tree^{-1} s^{-1}), they must be multiplied by the amount of leaf area placed in each layer by each cohort. Each cohort is described by a single functional type, ft and canopy layer C_l flag, so the problem is constrained to integrating these fluxes through the vertical profile (z).

We fist make a weighted average of photosynthesis rates from sun (gpp$_{sun}$, μmol CO_2 m^{-2} s^{-1}) and shade leaves (gpp$_{shade}$, μmol CO_2 m^{-2} s^{-1}) as

$$\text{gpp}_{cl,ft,z} = \text{gpp}_{sun,cl,ft,z} f_{sun,cl,ft,z} + \text{gpp}_{sha,cl,ft,z}(1 - f_{sun,cl,ft,z}).$$

The assimilation per leaf layer is then accumulated across all the leaf layers in a given cohort (*coh*) to give the cohort-specific gross primary productivity (GPP_{coh}),

$$GPP_{coh} = 12 \times 10^{-9} \sum_{z=1}^{nz(coh)} gpp_{cl,ft,z} A_{crown,coh} \text{elai}_{cl,ft,z}$$

The elai$_{l,cl,ft,z}$ is the exposed leaf area which is present in each leaf layer in m^2 m^{-2}. (For all the leaf layers that are completely occupied by a cohort, this is the same as the leaf fraction of δ_{vai}). The fluxes are converted from μmol into mol and then multiplied by 12 (the molecular weight of carbon) to give units for GPP$_{coh}$ of KgC cohort^{-1} s^{-1}. These are integrated for each timestep to give KgC cohort^{-1} day^{-1}

Table 1.12: Parameters needed for photosynthesis model.

Parameter Symbol	Parameter Name	Units	indexed by
$V_{c,max0}$	Maximum carboxylation capacity	μ mol CO $_2$ m $^{-2}$ s $^{-1}$	*ft*
r_b	Base Rate of Respiration	gC gN$^{-1}s^{-1}$)	
q_{10}	Temp. Response of stem and root respiration		
$R_{cn,leaf,ft}$	CN ratio of leaf matter	gC/gN	*ft*
$R_{cn,root,ft}$	CN ratio of root matter	gC/gN	*ft*
f_{gr}	Growth Respiration Fraction	none	
ψ_c	Water content when stomata close	Pa	*ft*
ψ_o	Water content above which stomata are open	Pa	*ft*

1.10 Plant respiration

Plant respiration per individual $R_{plant,coh}$ (KgC individual $^{-1}$ s^{-1}) is the sum of two terms, growth and maintenance respiration $R_{g,coh}$ and $R_{m,coh}$

$$R_{plant} = R_{g,coh} + R_{m,coh}$$

Maintenance respiration is the sum of the respiration terms from four different plant tissues, leaf, $R_{m,leaf,coh}$, fine root $R_{m,froot,coh}$, coarse root $R_{m,croot,coh}$and stem $R_{m,stem,coh}$, all also in (KgC individual $^{-1}$ s^{-1}) .

$$R_{m,coh} = R_{m,leaf,coh} + R_{m,froot,coh} + R_{m,croot,coh} + R_{m,stem,coh}$$

To calculate canopy leaf respiration, which varies through we canopy, we first determine the top-of-canopy leaf respiration rate ($r_{m,leaf,ft,0}$, gC s^{-1} m^{-2}) is calculated from a base rate of respiration per unit leaf nitrogen derived from *Ryan et al. 1991*. The base rate for leaf respiration (r_b) is 2.525 gC/gN s^{-1},

$$r_{m,leaf,ft,0} = r_b N_{a,ft}(1.5^{(25-20)/10})$$

where r_b is the base rate of metabolism (2.525 x 10^6 gC/gN s^{-1}. This base rate is adjusted assuming a Q_{10} of 1.5 to scale from the baseline of 20C to the CLM default base rate temperature of 25C. For use in the calculations of net photosynthesis and stomatal conductance, leaf respiration is converted from gC s^{-1} m^{-2}, into μmol CO_2 m^{-2} s^{-1} ($/12 \cdot 10^{-6}$).

This top-of-canopy flux is scaled to account for variation in N_a through the vertical canopy, in the same manner as the $V_{c,max}$ values are scaled using V_{above}.

$$r_{leaf,cl,ft,z} = r_{m,leaf,ft,0} e^{-K_{n,ft} V_{above,cl,ft,z}} \beta_{ft} f(t)$$

Leaf respiration is also adjusted such that it is reduced by drought stress, β_{ft}, and canopy temperature, $f(t_{veg})$. For details of the temperature functions affecting leaf respiration see the CLM4 technical note, Section 8, Equations 8.13 and 8.14. The adjusted leaf level fluxes are scaled to individual-level (gC individual $^{-1}$ s^{-1}) in the same fashion as the $\mathrm{GPP_{coh}}$ calculations

$$\mathrm{R_{m,leaf,coh}} = 12 \times 10^{-9} \sum_{z=1}^{\mathrm{nz(coh)}} \mathrm{r_{leaf,cl,ft,z} A_{crown} elai_{cl,ft,z}}$$

The stem and the coarse-root respiration terms are derived using the same base rate of respiration per unit of tissue Nitrogen.

$$R_{m,croot,coh} = 10^{-3} r_b t_c \beta_{ft} N_{\mathrm{livecroot,coh}}$$

$$R_{m,stem,coh} = 10^{-3} r_b t_c \beta_{ft} N_{\mathrm{stem,coh}}$$

Here, t_c is a temperature relationship based on a q_{10} value of 1.5, where t_v is the vegetation temperature. We use a base rate of 20 here as, again, this is the baseline temperature used by *Ryan et al. 1991*. The 10^{-3} converts from gC invididual^{-1} s^{-1} to KgC invididual^{-1} s^{-1}

$$t_c = q_{10}^{(t_v - 20)/10}$$

The tissue N contents for live sapwood are derived from the leaf CN ratios, and for fine roots from the root CN ratio as:

$$N_{\mathrm{stem,coh}} = \frac{B_{\mathrm{sapwood,coh}}}{R_{cn,leaf,ft}}$$

and

$$N_{\mathrm{livecroot,coh}} = \frac{B_{\mathrm{root,coh}} w_{frac,ft}}{R_{cn,root,ft}}$$

where $B_{\mathrm{sapwood,coh}}$ and $B_{\mathrm{root,coh}}$ are the biomass pools of sapwood and live root biomass respectively (KgC individual) and $w_{frac,ft}$ is the fraction of coarse root tissue in the root pool (0.5 for woody plants, 0.0 for grasses and crops). We assume here that stem CN ratio is the same as the leaf C:N ratio, for simplicity. The final maintenance respiration term is derived from the fine root respiration, which accounts for gradients of temperature in the soil profile and thus calculated for each soil layer j as follows:

$$R_{m,froot,j} = \frac{(1 - w_{frac,ft}) B_{\mathrm{root,coh}} b_r \beta_{ft}}{10^3 R_{cn,leaf,ft}} \sum_{j=1}^{nj} t_{c,soi,j} r_{i,ft,j}$$

$t_{c,soi}$ is a function of soil temperature in layer j that has the same form as that for stem respiration, but uses vertically resolved soil temperature instead of canopy temperature. In the CLM4.5, only coarse and not fine root respriation varies as a function of soil depth, and we maintain this assumption here, although it may be altered in later versions.

The source of maintenance respiration is the plant's carbon storage pool, which is updated daily. For plants that are in long-term negative carbon balance, FATES assumes a tradoff between reduced maintenance respiration expenditures and increased carbon-starvation mortality (see section 'Plant Mortality'). This reduction of maintenance respiration during carbon starvation is consistent with observations of trees under acute carbon stress (Sevanto et al., 2014). Because the physiologic basis and form of this process is poorly constrained, we use heuristic functions here to define these processes. First, we define a target carbon storage pool ($\grave{C}_{store,coh}$):

$$\grave{C}_{store,coh} = r_{store} \grave{C}_{leaf,coh}$$

where r_{store} is a pft-specific parameter that linearly relates the target storage pool to the target leaf biomass $\grave{C}_{leaf,coh}$. If a given plant is unable to achieve its target carbon storage because of having a negative NPP at any given time, then its actual storage pool $C_{store,coh}$ will drop below the target storage pool $\grave{C}_{store,coh}$. Then FATES sets the fractional rate of maintenance respiration (R) on the ratio of $C_{store,coh}$ to $\grave{C}_{leaf,coh}$:

$$R = \begin{cases} (1 - q^{(C_{store,coh}/\grave{C}_{leaf,coh})})/(1-q) & C_{store,coh} < \grave{C}_{leaf,coh} \\ 1 & C_{store,coh} >= \grave{C}_{leaf,coh} \end{cases}$$

where q is a parameter that governs the curvature of the respiration reduction function. This parameter is specific to a given PFT.

The growth respiration, $R_{g,coh}$ is a fixed fraction f_{gr} of the carbon remaining after maintenance respiration has occurred.

$$R_{g,coh} = \max(0, GPP_{g,coh} - R_{\mathrm{m,coh}}) \mathrm{f_{gr}}$$

Table 1.13: Parameters needed for plant respiration model.

Parameter Symbol	Parameter Name	Units	indexed by
$-K_{n,ft}$	Rate of reduction of N through the canopy	none	
r_b	Base Rate of Respiration	gC gN$^{-1}s^{-1}$)	
q_{10}	Temp. Response of stem and root respiration		
$R_{cn,leaf,ft}$	CN ratio of leaf matter	gC/gN	*ft*
$R_{cn,root,ft}$	CN ratio of root matter	gC/gN	*ft*
f_{gr}	Growth Respiration Fraction	none	*ft*
q	Low-Storage Maintenance Respiration Reduction Param.	none	*ft*

1.11 Stomatal Conductance

1.11.1 Fundamental stomatal conductance theory

Within FATES, leaf-level stomatal conductance is representated by two main approaches. The first calculates stomatal conductance (1/resistance) using the Ball-Berry model as implemented in CLM4.5 (http://www.cesm.ucar.edu/models/cesm1.2/clm/CLM45_Tech_Note.pdf) and described by *Collatz et al. (1991)* and *Sellers et al. 1996*. The model relates stomatal conductance (i.e., the inverse of resistance) to net leaf photosynthesis, scaled by the relative humidity at the leaf surfaceand the CO_2 concentration at the leaf surface. The primary difference between the CLM implementation and that used by *Collatz et al. (1991)* and *Sellers et al. (1996)* is that they used net photosynthesis (i.e., leaf photosynthesis minus leaf respiration) instead of gross photosynthesis. As implemented here, stomatal conductance equals the minimum conductance (b) when gross photosynthesis (A) is zero. Leaf stomatal conductance is

$$\frac{1}{r_s} = m_{ft}\frac{A}{c_s}\frac{e_s}{e_i}P_{atm} + b_{ft}\beta_{sw}$$

where r_s is leaf stomatal resistance (s m^2 leaf area μmol H_2O^{-1}), b_{ft} in units of μmol H_2O m^{-2} leaf area s^{-1} is a plant functional type dependent parameter equivalent to g_0 in the Ball-Berry model literature. This parameter is also scaled by the water stress index β_{sw}. Similarly, m_{ft} is the slope of the relationship (i.e. stomatal slope, or the g_1 term in the stomatal literature) between stomatal conductance and the stomatal index, comprised of the leaf assimilation rate, A (μmol CO$_2$ m^{-2} leaf area s^{-1}), c_s is the CO$_2$ partial pressure at the leaf surface (Pa), e_s is the vapor pressure at the leaf surface (Pa), e_i is the saturation vapor pressure (Pa) inside the leaf at the vegetation temperature T_v (K), and b_{ft} is the conductace (μmolH_2O m^{-2} leaf area s^{-1}) when A = 0.

The second (default) representation of stomatal conductance in FATES follows the Unified Stomatal Optimization (USO) theory, otherwise known as the Medlyn model of stomatal conductance (*Medlyn et al. 2011*). The Medlyn model calculates stomatal conductance (i.e., the inverse of resistance) based on net leaf photosynthesis, the vapor pressure deficit, and the CO2 concentration at the leaf surface. Leaf stomatal resistance is calculated as:

$$\frac{1}{r_s} = g_s = b_{ft}\beta_{sw} + 1.6(1 + \frac{m_{ft}}{\sqrt{D_s}})\frac{A_n}{C_s/P_{atm}}$$

Table 1.14: Variables use in the Medlyn equation

Parameter Symbol	Parameter Name	Units	indexed by
r_s	Leaf stomatal resistance	s m^2 leaf area μmol H_2O^{-1}	
g_s	Leaf stomatal conductance	μmol H_2O m^2 leaf area s^{-1}	
b_{ft}	Minimum stomatal conductance or the cuticular conductance	μmol H_2O m^2 leaf area s^{-1}	*ft*
β_{sw}	Soil water stress factor	none	
D_s	Vapor pressure deficit at the leaf surface	kPa	
m_{ft}	Stomatal slope	kPa$^{0.5}$	*ft*
A_n	Leaf net photosynthesis	μmol CO_2 m^{-2} leaf area s^{-1}	
C_s	CO_2 partial pressure at the leaf surface	Pa	
P_{atm}	Atmospheric pressure	Pa	

In both models leaf resistance is converted from units of s m$^2\mu$molH_2O^{-1} to s m^{-1} as: 1 s m^{-1} = 1 $\times$ $10^{-9}\mathrm{R_{gas}}\theta_{\mathrm{atm}}P_{\mathrm{atm}}$ (μmol^{-1} m^2 s), where R$_{gas}$ is the universal gas constant (J K^{-1} kmol^{-1}) and θ_{atm} is the atmospheric potential temperature (K).

Both b_{ft} and m_{ft} are PFT-specific parameters. The default values for the Ball-Berry and Medlyn stomatal conductance model representations are provide below:

Table 1.15: Variables use in the Medlyn equation

PFT Name	Ball-Berry m_{ft} (unitless)	Medlyn m_{ft} (kPa$^{0.5}$)
Broadleaf evergreen tropical tree	8	4.1
Needleleaf evergreen extratropical tree	8	2.3
Needleleaf colddecid extratropical tree	8	2.3
Broadleaf evergreen extratropical tree	8	4.1
Broadleaf hydrodecid tropical tree	8	4.4
Broadleaf colddecid extratropical tree	8	4.4
Broadleaf evergreen extratropical shrub	8	4.7
Broadleaf hydrodecid extratropical shrub	8	4.7
Broadleaf colddecid extratropical shrub	8	4.7
Arctic C_3 grass	8	2.2
Cool C_3 grass	8	5.3
C_4 grass	8	1.6

For both the Ball-Berry and Medlyn stomatal models the default b_{ft} is 1000 for all PFTs.

1.11.2 Numerical implementation of the Medlyn stomatal conductance model

Photosynthesis is calculated assuming there is negligible capacity to store CO_2 and water vapor at the leaf surface so that

$$A_n = \frac{c_a - c_i}{(1.4r_b + 1.6r_s)P_{atm}} = \frac{c_a - c_s}{1.4r_b P_{atm}} = \frac{c_s - c_i}{1.6r_s P_{atm}}$$

The terms 1.4 and 1.6 are the ratios of diffusivity of CO_2 to H_2O for the leaf boundary layer resistance and stomatal resistance. The transpiration fluxes are related as:

$$\frac{e_a - e_i}{r_b + r_s} = \frac{e_a - e_s}{r_b} = \frac{e_s - e_i}{r_s}$$

$$e_a = \frac{P_{atm} q_s}{0.622}$$

Parameter Symbol	Parameter Name	Units	indexed by
c_a	Atmospheric CO_2 pressure	Pa	
c_i	Internal leaf CO_2 partial pressure	Pa	
r_b	Leaf boundary layer resistance	s m^2 leaf area μmol H_2O^{-1}	
e_a	Vapor pressure of air	Pa	
e_i	Saturation vapor pressure	Pa	
e_s	Vapor pressure at the leaf surface	Pa	
q_s	Specific humidity of canopy air	kg kg $^{-1}$	

In the Medlyn model, an initial guess of c_i is obtained assuming the ratio between c_i and c_a (0.7 for C_3 plants and 0.4 for C_4 plants) to calculate A_n based on *Farquhar 1980*. Solving for c_s:

$$c_s = c_a - 1.4 r_b P_{atm} A_n$$

e_s can be represented as:

$$e_s = \frac{e_a r_s + e_i r_b}{r_b + r_s}$$

Where e_i is a function of temperature

Substitution of e_s following $D_s = e_i - e_s$ gives an expression for stomatal resistance (r_s) as a function of photosynthesis (A_n), given here in terms of conductance with $g_s = \frac{1}{r_s}$ and $g_b = \frac{1}{r_b}$

$$(g_s)^2 + bg_s + c = 0$$

where

$$b = -[2(b_{ft} \times \beta_{sw} + d) + \frac{(m_{ft})^2 d^2}{g_b D_a}]$$

$$c = (b_{ft} \times \beta_{sw})^2 + [2g_0 \times \beta_{sw} + d(1 - \frac{{m_{ft}}^2}{D_a})]d$$

and

$$d = \frac{1.6A_n}{c_s/P_{atm}}$$

$$D_a = \frac{e_i - e_a}{1000}$$

Stomatal conductance is the larger of the two roots that satisfies the quadratic equation. Values for c_i are given by:

$$c_i = c_a - (1.4r_b + 1.6r_s)P_{atm}A_n$$

The equations for c_i, c_s, r_s, and A_n are solved iteratively until c_i converges. Iteration will be exited if convergence criteria is met or if at least five iterations are completed.

1.11.3 Resolution of stomatal conductance theory in the FATES canopy structure

The stomatal conductance is calculated, as with photosynthesis, for each canopy, PFT and leaf layer. The HLM code requires a single canopy conductance estimate to be generated from the multi-layer multi-PFT array. In previous iterations of the HLM, sun and shade-leaf specific values have been reported and then averaged by their respective leaf areas. In this version, the total canopy condutance $G_{s,canopy}$, is calculated as the sum of the cohort-level conductance values.

$$G_{s,canopy} = \sum \frac{gs_{can,coh} n_{coh}}{A_{patch}}$$

Cohort conductance is the sum of the inverse of the leaf resistances at each canopy layer ($r_{s,z}$) multipled by the area of each cohort.

$$gs_{can,coh} = \sum_{z=1}^{z=nv,coh} \frac{A_{crown,coh}}{r_{s,cl,ft,z} + r_b}$$

1.12 Control of Leaf Area Index

The leaf area A_{leaf} (m^2) of each cohort is calculated from leaf biomass $C_{leaf,coh}$ (kgC individual^{-1}) and specific leaf area (SLA, m^2 kg C^{-1}). Leaf biomass $C_{leaf,coh}$ is controlled by the processes of phenology, allocation and turnover, described in detail in the PARTEH submodule.

$$A_{leaf,coh} = C_{leaf,coh} \cdot SLA_{ft}$$

However, using this model, where leaf area and crown area are both functions of diameter, the leaf area index of each tree in a closed canopy forest is always the same (where $S_{c,patch}$ = $S_{c,min}$, irrespective of the growth conditions. To allow greater plasticity in tree canopy structure, and for tree leaf area index to adapt to prevailing conditions, we implemented a methodology for removing those leaves in the canopy that exist in negative carbon balance. That is, their total annual assimilation rate is insufficient to pay for the turnover and maintenance costs associated with their supportive root and stem tissue, plus the costs of growing the leaf. The tissue turnover maintenance cost (KgC $m^{-2} y^{-1}$ of leaf is the total maintenance demand divided by the leaf area:

$$L_{cost,coh} = \frac{t_{md,coh}}{C_{leaf,coh} \cdot \text{SLA}}$$

The net uptake for each leaf layer $U_{net,z}$ in (KgC m^{-2} $year^{-1}$) is

$$U_{net,coh,z} = g_{coh,z} - r_{m,leaf,coh,z}$$

where g_z is the GPP of each layer of leaves in each tree (KgC m^{-2} $year^{-1}$), $r_{m,leaf,z}$ is the rate of leaf dark respiration (also KgC m^{-2} $year^{-1}$). We use an iterative scheme to define the cohort specific canopy trimming fraction $C_{trim,coh}$, on an annual time-step, where

$$C_{leaf,coh} = C_{trim} \times 0.0419 dbh_{coh}^{1.56} d_w^{0.55}$$

If the annual maintenance cost of the bottom layer of leaves (KgC m-2 year-1) is less than then the canopy is trimmed by an increment ι_l(0.01), which is applied until the end of next calander year. Because this is an optimality model, there is an issue of the timescale over which net assimilation is evaluated, the timescale of response, and the plasticity of plants to respond to these pressures. These properties should be investigated further in future efforts.

$$C_{trim,y+1} = \begin{cases} \max(\mathrm{C_{trim,y}} - \iota_\mathrm{l}, 1.0) & \text{for}(\mathrm{L_{cost,coh}} > \mathrm{U_{net,coh,nz}}) \\ \min(\mathrm{C_{trim,y}} + \iota_\mathrm{l}, \mathrm{L_{trim,min}}) & \text{for}(\mathrm{L_{cost,coh}} < \mathrm{U_{net,coh,nz}}) \end{cases}$$

We impose an arbitrary minimum value on the scope of canopy trimming of $L_{trim,min}$ (0.5). If plants are able simply to drop all of their canopy in times of stress, with no consequences, then tree mortality from carbon starvation is much less likely to occur because of the greatly reduced maintenance and turnover requirements.

Table 1.16: Parameters needed for leaf area control model.

Parameter Symbol	Parameter Name	Units	indexed by
ι_l	Fraction by which leaf mass is reduced next year	none	
$L_{trim,min}$	Minimum fraction to which leaf mass can be reduced	none	

1.13 Phenology

1.13.1 Cold Deciduous Phenology

Cold Leaf-out timing

The phenology model of *Botta et al. 2000* is used in FATES to determine the leaf-on timing. The Botta et al. model was verified against satellite data and is one of the only globally verified and published models of leaf-out phenology. This model differs from the phenology model in the CLM4.5. The model simulates leaf-on date as a function of

the number of growing degree days (GDD), defined by the sum of mean daily temperatures (T_{day} ^{o}C) above a given threshold T_g (0 ^{o}C).

$$GDD = \sum \max(T_{day} - T_g, 0)$$

Budburst occurs when GDD exceeds a threshold (GDD_{crit}). The threshold is modulated by the number of chilling days experienced (NCD) where the mean daily temperature falls below a threshold determined by *Botta et al. 2000*<*botta2000*> as 5^{o}C. A greater number of chilling days means that fewer growing degree days are required before budburst:

$$GDD_{crit} = a + be^{c.NCD}$$

where a = -68, b= 638 and c=-0.01 *Botta et al. 2000*<*botta2000*>. In the Northern Hemisphere, counting of degree days begins on 1st January, and of chilling days on 1st November. The calendar opposite of these dates is used for points in the Southern Hemisphere.

If the growing degree days exceed the critical threshold, leaf-on is triggered by a change in the gridcell phenology status flag $S_{phen,grid}$ where '2' indicates that leaves should come on and '1' indicates that they should fall.

$$S_{phen,grid} = 2 \quad \text{if } S_{phen,grid} = 1 \text{ and } GDD_{grid} \geq GDD_{crit}$$

Cold Leaf-off timing

The leaf-off model is taken from the Sheffield Dynamic Vegetation Model (SDGVM) and is similar to that for LPJ *Sitch et al. 2003* and IBIS *Foley et al. 1996* models. The average daily temperatures of the previous 10 day period are stored. Senescence is triggered when the number of days with an average temperature below 7.5^{o} ($n_{colddays}$) rises above a threshold values $n_{crit,cold}$, set at 5 days.

$$S_{phen,grid} = 1 \quad \text{if } S_{phen,grid} = 2 \text{ and } n_{colddays} \geq n_{crit,cold}$$

Global implementation modifications

Because of the global implementation of the cold-deciduous phenology scheme, adjustments must be made to account for the possibility of cold-deciduous plants experiencing situations where no chilling period triggering leaf-off ever happens. If left unaccounted for, these leaves will last indefinitely, resulting in highly unrealistic behaviour. Therefore, we implement two additional rules. Firstly, if the number of days since the last senescence event was triggered is larger than 364, then leaf-off is triggered on that day. Secondly, if no chilling days have occured during the winter accumulation period, then leaf-on is not triggered. This means that in effect, where there are no cold periods, leaves will fall off and not come back on, meaning that cold-deciduous plants can only grow in places where there is a cold season.

Further to this rule, we introduce a 'buffer' time periods after leaf-on of 30 days, so that cold-snap periods in the spring cannot trigger a leaf senescence. The 30 day limit is an arbitrary limit. In addition, we constrain growing degree day accumulation to the second half of the year (Jult onwards in the Northern hemisphere, or Jan-June in the Southern) and only allow GDD accumulation while the leaves are off.

1.13.2 Drought-deciduous Phenology: TBD

In the current version of the model, a drought deciduous algorithm exists, but is not yet operational, due to issue detected in the existing CN and soil moisture modules, which also affect the behaviour of the native ED drought deciduous model. This is a priority to address before the science tag is released.

1.13.3 Carbon Dynamics of deciduous plants

In the present version, leaf expansion and senescence happen over the course of a single day. This is clearly not an empirically robust representation of leaf behaviour, whereby leaf expansion occurs over a period of 10-14 days, and senescence over a similar period. This will be incorporated in later versions. When the cold or drought phenological status of the gridcell status changes ($S_{phen,grid}$) from '2' to '1', and the leaves are still on ($S_{phen,coh}$ =2), the leaf biomass at this timestep is 'remembered' by the model state variable $l_{memory,coh}$. This provides a 'target' biomass for leaf onset at the beginning of the next growing season (it is a target, since depletion of stored carbon in the off season may render achieving the target impossible).

$$l_{memory,coh} = C_{leaf,coh}$$

Leaf carbon is then added to the leaf litter flux $l_{leaf,coh}$ (KgC individual^{-1})

$$l_{leaf,coh} = C_{leaf,coh}$$

The alive biomass is depleted by the quantity of leaf mass lost, and the leaf biomass is set to zero

$$C_{alive,coh} = C_{alive,coh} - C_{leaf,coh}$$

$$C_{leaf,coh} = 0$$

Finally, the status $S_{phen,coh}$ is set to 1, indicating that the leaves have fallen off.

For bud burst, or leaf-on, the same occurs in reverse. If the leaves are off ($S_{phen,coh}$=1) and the phenological status triggers budburst ($S_{phen,grid}$=2) then the leaf mass is set the maximum of the leaf memory and the available store

$$C_{leaf,coh} = \max\left(l_{memory,coh}, C_{store,coh}\right)$$

this amount of carbon is removed from the store

$$C_{store,coh} = C_{store,coh} - C_{leaf,coh}$$

and the new leaf biomass is added to the alive pool

$$C_{alive,coh} = C_{alive,coh} + C_{leaf,coh}$$

Lastly, the leaf memory variable is set to zero and the phenological status of the cohort back to '2'. No parameters are currently required for this carbon accounting scheme.

Table 1.17: Parameters needed for phenology model.

Parameter Symbol	Parameter Name	Units	indexed by
$n_{crit,cold}$	Threshold of cold days for senescence	none	
T_g	Threshold for counting growing degree days	^{o}C	

1.14 Seed Dynamics and Recruitment

The production of seeds and their subsequent germination is a process that must be captured explicitly or implicitly in vegetation models. FATES contains a seed bank model designed to allow the dynamics of seed production and germination to be simulated independently. In the ED1.0 model, seed recruitment occurs in the same timestep as allocation to seeds, which prohibits the survival of a viable seed bank through a period of disturbance or low productivity (winter,

drought). In FATES, a plant functional type specific seed bank is tracked in each patch ($Seeds_{patch}$ KgC m^{-2}), whose rate of change (KgC m^{-2} y^{-1}) is the balance of inputs, germination and decay:

$$\frac{\delta Seeds_{FT}}{\delta t} = Seed_{in,ft} - Seed_{germ,ft} - Seed_{decay,ft}$$

where $Seed_{in}$, $Seed_{germ}$ and $Seed_{decay}$ are the production, germination and decay (or onset of inviability) of seeds, all in KgC m^{-2} year^{-1}.

Seeds are assumed to be distributed evenly across the site (in this version of the model), so the total input to the seed pool is therefore the sum of all of the reproductive output of all the cohorts in each patch of the correct PFT type.

$$Seed_{in,ft} = \frac{\sum_{p=1}^{n_{patch}} \sum_{i=1}^{n_{coh}} p_{seed,i}.n_{coh}}{area_{site}}$$

Seed decay is the sum of all the processes that reduce the number of seeds, taken from *Lischke et al. 2006*. Firstly, the rate at which seeds become inviable is described as a constant rate ϕ (y:math:^{-1}) which is set to 0.51, the mean of the parameters used by *Lischke et al. 2006*.

$$Seed_{decay,ft} = Seeds_{FT}.\phi$$

The seed germination flux is also prescribed as a fraction of the existing pool (α_{sgerm}), but with a cap on maximum germination rate β_{sgerm}, to prevent excessive dominance of one plant functional type over the seed pool.

$$Seed_{germ,ft} = \max(Seeds_{FT} \cdot \alpha_{sgerm}, \beta_{sgerm})$$

Table 1.18: Parameters needed for seed model.

Parameter Symbol	Parameter Name	Units	indexed by
K_s	Maximum seed mass	kgC m^{-2}	
α_{sgerm}	Proportional germination rate	none	
β_{sgerm}	Maximum germination rate	KgC m^{-2} y^{-1}	
ϕ	Decay rate of viable seeds	none	*ft*
$R_{frac,ft}$	Fraction of C_{bal} devoted to reproduction	none	*ft*

1.15 Litter Production and Fragmentation

The original CLM4.5 model contains streams of carbon pertaining to different chemical properties of litter (lignin, cellulose and labile streams, specifically). In FATES model, the fire simulation scheme in the SPITFIRE model requires that the model tracks the pools of litter pools that differ with respect to their propensity to burn (surface area-volume ratio, bulk density etc.). Therefore, this model contains more complexity in the representation of coarse woody debris. We also introduce the concept of 'fragmenting' pools, which are pools that can be burned, but are not available for decomposition or respiration. In this way, we can both maintain above-ground pools that affect the rate of burning, and the lag between tree mortality and availability of woody material for decomposition.

FATES recognizes four classes of litter. Above- and below-ground coarse woody debris (CWD_{AG}, CWD_{BG}) and leaf litter (l_{leaf} and fine root litter l_{root}). All pools are represented per patch, and with units of kGC m$^-2$. Further to this, CWD_{AG}, CWD_{BG} are split into four litter size classes (lsc) for the purposes of proscribing this to the SPITFIRE fire model (seed 'Fuel Load' section for more detail. 1-hour (twigs), 10-hour (small branches), 100-hour (large branches) and 1000-hour(boles or trunks). 4.5 %, 7.5%, 21 % and 67% of the woody biomass ($C_{store,coh} + C_{sw,coh}$) is partitioned into each class, respectively.

l_{leaf} and l_{root} are indexed by plant functional type (ft). The rational for indexing leaf and fine root by PFT is that leaf and fine root matter typically vary in their carbon:nitrogen ratio, whereas woody pools typically do not.

Rates of change of litter, all in kGC m$^-2$ year^{-1}, are calculated as

$$\frac{\delta CWD_{AG,out,lsc}}{\delta t} = CWD_{AG,in,lsc} - CWD_{AG,out,lsc}$$

$$\frac{\delta CWD_{BG,out,lsc}}{\delta t} = CWD_{BG,in,lsc} - CWD_{BG,in,lsc}$$

$$\frac{\delta l_{leaf,out,ft}}{\delta t} = l_{leaf,in,ft} - l_{leaf,out,ft}$$

$$\frac{\delta l_{root,out,ft}}{\delta t} = l_{root,in,ft} - l_{root,out,ft}$$

1.15.1 Litter Inputs

Inputs into the litter pools come from tissue turnover, mortality of canopy trees, mortality of understorey trees, mortality of seeds, and leaf senescence of deciduous plants.

$$l_{leaf,in,ft} = \Big(\sum_{i=1}^{n_{coh,ft}} n_{coh}(l_{md,coh} + l_{leaf,coh}) + M_{t,coh}.C_{leaf,coh} \Big) / \sum_{p=1}^{n_{pat}} A_{patch}$$

where $l_{md,coh}$ is the leaf turnover rate for evergreen trees and $l_{leaf,coh}$ is the leaf loss from phenology in that timestep (KgC m^{-2}. $M_{t,coh}$ is the total mortality flux in that timestep (in individuals). For fine root input. $n_{coh,ft}$ is the number of cohorts of functional type 'FT' in the current patch.

$$l_{root,in,ft} = \Big(\sum_{i=1}^{n_{coh,ft}} n_{coh}(r_{md,coh}) + M_{t,coh}.C_{root,coh} \Big) / \sum_{p=1}^{n_{pat}} A_p$$

where $r_{md,coh}$ is the root turnover rate. For coarse woody debris input ($CWD_{AG,in,lsc}$, we first calculate the sum of the mortality $M_{t,coh}.(C_{struc,coh} + C_{sw,coh})$ and turnover $n_{coh}(w_{md,coh})$ fluxes, then separate these into size classes and above/below ground fractions using the fixed fractions assigned to each (f_{lsc} and f_{ag})

$$CWD_{AG,in,lsc} = \Big(f_{lsc}.f_{ag} \sum_{i=1}^{n_{coh,ft}} n_{coh} w_{md,coh} + M_{t,coh}.(C_{struc,coh} + C_{sw,coh}) \Big) / \sum_{p=1}^{n_{pat}} A_p$$

$$CWD_{BG,in,lsc} = \Big(f_{lsc}.(1 - f_{ag}) \sum_{i=1}^{n_{coh,ft}} n_{coh} w_{md,coh} + M_{t,coh}.(C_{struc,coh} + C_{sw,coh}) \Big) / \sum_{p=1}^{n_{pat}} A_p$$

1.15.2 Litter Outputs

The fragmenting litter pool is available for burning but not for respiration or decomposition. Fragmentation rates are calculated according to a maximum fragmentation rate ($\alpha_{cwd,lsc}$ or α_{litter}) which is ameliorated by a temperature and water dependent scalar S_{tw}. The form of the temperature scalar is taken from the existing CLM4.5BGC decomposition cascade calculations). The water scaler is equal to the water limitation on photosynthesis (since the CLM4.5BGC water scaler pertains to the water potential of individual soil layers, which it is difficult to meaningfully average, given the non-linearities in the impact of soil moisture). The scaler code is modular, and new functions may be implemented trivially. Rate constants for the decay of the litter pools are extremely uncertain in literature, as few studies either separate litter into size classes, nor examine its decomposition under non-limiting moisture and temperature conditions. Thus, these parameters should be considered as part of sensitivity analyses of the model outputs.

$$CWD_{AG,out,lsc} = CWD_{AG,lsc}.\alpha_{cwd,lsc}.S_{tw}$$

$$CWD_{BG,out,lsc} = CWD_{BG,lsc}.\alpha_{cwd,lsc}.S_{tw}$$
$$l_{leaf,out,ft} = l_{leaf,ft}.\alpha_{litter}.S_{tw}$$
$$l_{root,out,ft} = l_{root,ft}.\alpha_{root,ft}.S_{tw}$$

1.15.3 Flux into decompsition cascade

Upon fragmentation and release from the litter pool, carbon is transferred into the labile, lignin and cellulose decomposition pools. These pools are vertically resolved in the biogeochemistry model. The movement of carbon into each vertical layer is obviously different for above- and below-ground fragmenting pools. For each layer z and chemical litter type i, we derive a flux from ED into the decomposition cascade as $ED_{lit,i,z}$ (kGC m^{-2} s^{-1})

where t_c is the time conversion factor from years to seconds, $f_{lab,l}$, $f_{cel,l}$ and $f_{lig,l}$ are the fractions of labile, cellulose and lignin in leaf litter, and $f_{lab,r}$, $f_{cel,r}$ and $f_{lig,r}$ are their counterparts for root matter. Similarly, l_{prof}, $r_{f,prof}$and $r_{c,prof}$ are the fractions of leaf, coarse root and fine root matter that are passed into each vertical soil layer z, derived from the CLM(BGC) model.

Table 1.19: Parameters needed for litter model.

Parameter Symbol	Parameter Name	Units	indexed by
$\alpha_{cwd,lsc}$	Maximum fragmentation rate of CWD	y^{-1}	
α_{litter}	Maximum fragmentation rate of leaf litter	y^{-1}	
α_{root}	Maximum fragmentation rate of fine root litter	y^{-1}	
$f_{lab,l}$	Fraction of leaf mass in labile carbon pool	none	
$f_{cel,l}$	Fraction of leaf mass in cellulose carbon pool	none	
$f_{lig,l}$	Fraction of leaf mass in lignin carbon pool	none	
$f_{lab,r}$	Fraction of root mass in labile carbon pool	none	
$f_{cel,r}$	Fraction of root mass in cellulose carbon pool	none	
$f_{lig,r}$	Fraction of root mass in lignin carbon pool	none	
$l_{prof,z}$	Fraction of leaf matter directed to soil layer z	none	soil layer
$r_{c,prof,z}$	Fraction of coarse root matter directed to soil layer z	none	soil layer
$r_{f,prof,z}$	Fraction of fine root matter directed to soil layer z	none	soil layer

1.16 Disturbance

FATES allows disturbance through three processes: (1) mortality of canopy trees, (2) fire, (3) anthropogenic disturbance. Each of these is discussed in more detail below. For the case of canopy tree mortality, some fraction of the crown area f_d of deceased trees is used to generate newly-disturbed patch area, while the rest $(1 - f_d)$ remains in the existing patch. Thus varying f_d from zero to 1 can lead to three different cases of how mortlaity leads to disturbance. If $f_d = 1$, then all canopy area is converted into newly-disturbed patch area, and a fraction of understory trees equal to the ratio of dying-tree crown are a to the patches area are moved to the newly-disturbed patch, at which time they are promoted to the canopy of the new patch; this is labeled below as the 'Pure ED' case. For those trees that are moved to the new patch, some fraction of these will die due to impacts from the disturbance process itself, this fraction i_d is currently a global parameter for all individual-tree disturbance processes, with a default value of 0.55983. If $f_d = 0$, then no disturbance occurs and all mortality is accomodated by promotion of trees from the understory to the canopy within a patch; this is the structure of the PPA formulation as described in *Purves et al. 2008*, and is labelled below as 'Pure PPA'. If $0 > f_d > 1$, then some both processes of promotion within a patch and promotion into a new patch occur. A special case of this is when all trees that would be moved into the new patch are killed in the process, thus guaranteeing that newly-disturbed patches are devoid of any surviving trees; this is blabelled below as the 'bare-ground intermediate case'.

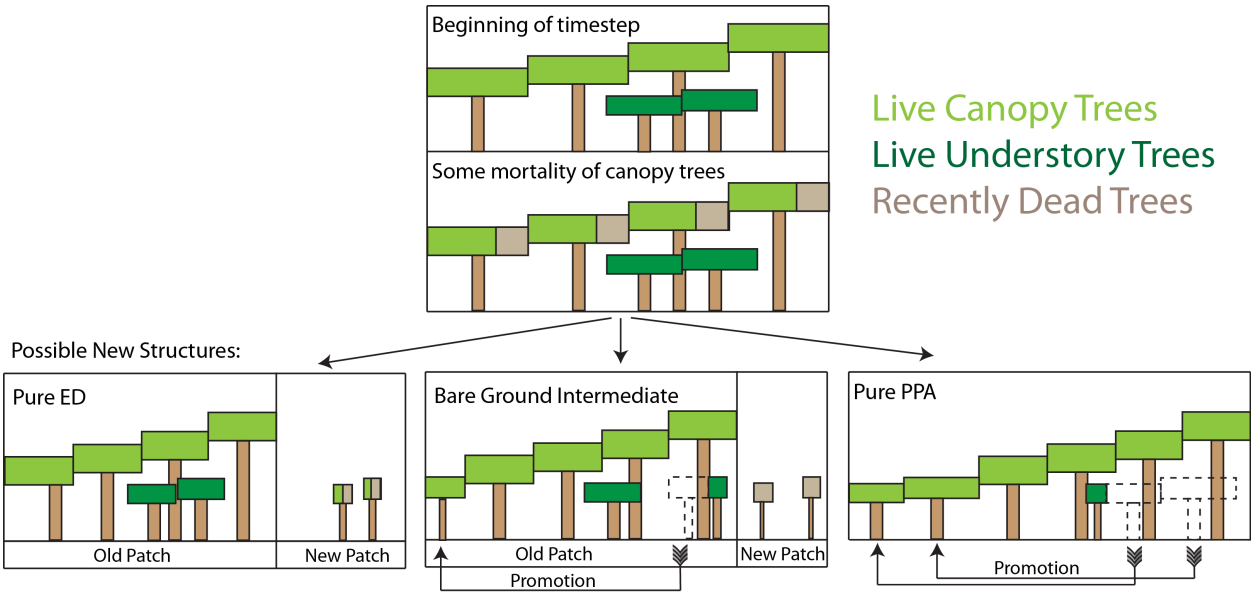

1.17 Plant Mortality

Total plant mortality per cohort $M_{t,coh}$, (fraction year^{-1}) is simulated as the sum of several additive terms,

$$M_{t,coh} = M_{b,coh} + M_{cs,coh} + M_{hf,coh} + M_{f,coh} + M_{i,coh} + M_{fr,coh} + M_{s,coh} + M_{a,coh},$$

where M_b is the background mortality that is unaccounted by any of the other mortality rates and is fixed at a constant PFT-dependent rate in the parameter file.

M_{cs} is the carbon starvation derived mortality, which is a function of the non-structural carbon storage term $C_{store,coh}$ and the 'target' leaf biomass, $\grave{C}_{leaf,coh}$, as follows:

$$M_{cs} = \begin{cases} M_{cs,max}(1 - C_{store,coh}/\grave{C}_{leaf,coh}) & C_{store,coh} < \grave{C}_{leaf,coh} \\ 0 & C_{store,coh} >= \grave{C}_{leaf,coh} \end{cases}$$

where $M_{cs,max}$ is the maximum rate of carbon storage mortality parameter, or the maximum rate of trees in a landscape that will die when their carbon stores are exhausted. This parameter is needed to scale from individual-level mortality simulation to grid-cell average conditions.

Thus FATES implicitly assumes that there is a critical storage pool $C_{store,coh,critical} = \grave{C}_{leaf,coh}$ that sets the total-plant storage level where mortality begins; the implied parameter $C_{store,coh,critical}/\grave{C}_{leaf,coh} = 1$ could be made explicit, but we left this as an implicit parameter here due to the generally weak data constraints on it at present. Because both the increase in mortality and the decrease in respiration (see section 'Respiration') begin when $C_{store,coh}$ drops below $\grave{C}_{leaf,coh}$, and $\grave{C}_{store,coh} = r_{store}\grave{C}_{leaf,coh}$, the parameter $r_{store} - 1$, thus sets the size of the carbon storage buffer that determines how much cumulative negative NPP a plant can experience before it begins to suffer from carbon starvation.

Mechanistic simulation of hydraulic failure is not undertaken on account of it's mechanistic complexity (see *McDowell et al. 2013* for details). Instead, we use a proxy for hydraulic failure induced mortality ($M_{hf,coh}$) that uses a water potential threshold beyond mortality is triggered, such that the tolerance of low water potentials is a function of plant functional type (as expressed via the ψ_c parameter). For each day that the aggregate water potential falls below a threshold value, a set fraction of the trees are killed. The aggregation of soil moisture potential across the root zone is

expressed using the β function. We thus determine plant mortality caused by extremely low water potentials as

$$M_{hf,coh} = \begin{cases} S_{m,ft} & \text{for } \beta_{ft} < 10^{-6} \\ 0.0 & \text{for } \beta_{ft} >= 10^{-6}. \end{cases}$$

The threshold value of 10^{-6} represents a state where the average soil moisture potential is within 10^{-6} of the wilting point (a PFT specific parameter $\theta_{w,ft}$).

$M_{f,coh}$ is the fire-induced mortality, as described in the fire modelling section.

Impact mortality M_{i,coh} occurs to understory trees that are kille dduring the process of disturbance, as described above.

$M_{s,coh}$ and $M_{a,coh}$ are size- and age-dependent mortality respectively. These terms model a gradual increase in mortality rate with either cohort DBH (cm) or cohort age. We model $M_{s,coh}$ as:

$$M_{s,coh} = \frac{1}{1 + e^{(-r_s*(DBH-p_s))}}$$

where DBH is diameter at breast height in cm, r_s is the rate that mortality increases with DBH, and p_s is the inflection point of the curve, i.e. the DBH at which annual mortality rate has increased to 50%. We model $M_{a,coh}$ as :

$$M_{a,coh} = \frac{1}{1 + e^{(-r_a*(age-p_a))}}$$

where age is cohort age in years, r_a is the rate that mortality increases with age, and p_a is the inflection point of the curve, i.e. the age at which annual mortality rate has increased to 50%.

Cohort age is not tracked in default FATES. In order to have age-dependent mortality on, set the flag use_fates_cohort_age_tracking to .true. in the FATES namelist options. To turn on either size- or age-dependent mortality set the p and r parameters to sensible values in the FATES parameter file.

Table 1.20: Parameters needed for mortality model.

Parameter Symbol	Parameter Name	Units	indexed by
$S_{m,ft}$	Stress Mortality Scaler	none	
$l_{targ,ft}$	Target carbon storage fraction	none	ft

1.18 Fire (SPITFIRE)

The influence of fire on vegetation is estimated using the SPITFIRE model, which has been modified for use in ED following it's original implementation in the LPJ-SPITFIRE model (*Thonicke et al. 2010*, *Pfeiffer et al. 2013*). This model as described is substantially different from the existing CLM4.5 fire model *Li et al. 2012*, however, further developments are intended to increase the merging of SPITFIRE's natural vegetation fire scheme with the fire suppression, forest-clearing and peat fire estimations in the existing model. The coupling to the ED model allows fires to interact with vegetation in a size-structured manner, so small fires can burn only understorey vegetation. Also, the patch structure and representation of succession in the ED model allows the model to track the impacts of fire on different forest stands, therefore removing the problem of area-averaging implicit in area-based DGVMs. The SPITFIRE approach has also been coupled to the LPJ-GUESS individual-based model (Forrest et al. in prep) and so this is not the only implementation of this type of scheme in existence.

The SPITFIRE model operates at a daily timestep and at the patch level, meaning that different litter pools and vegetation charecteristics of open and closed forests can be represented effectively (we omit the *patch* subscript throughout for simplicity).

1.18.1 Properties of fuel load

Many fire processes are impacted by the properties of the litter pool in the SPITFIRE model. There are one live (live grasses) and five dead fuel categories (dead leaf litter and four pools of coarse woody debris). Coarse woody debris is classified into 1h, 10h, 100h, and 1000h fuels, defined by the order of magnitude of time required for fuel to lose (or gain) 63% of the difference between its current moisture content and the equilibrium moisture content under defined atmospheric conditions. *Thonicke et al. 2010*. For the purposes of describing the behaviour of fire, we introduce a new index 'fuel class' *fc*, the values of which correspond to each of the six possible fuel categories as follows.

fc index	Fuel type	Drying Time
1	dead grass	n/a
2	twigs	1h fuels
3	small branches	10h fuel
4	large branches	100h fuel
5	stems and trunks	1000h fuel
6	live grasses	n/a

1.18.2 Nesterov Index

Dead fuel moisture ($moist_{df,fc}$), and several other properties of fire behaviour, are a function of the 'Nesterov Index' (N_I) which is an accumulation over time of a function of temperature and humidity (Eqn 5, *Thonicke et al. 2010*),

$$N_I = \sum \max(T_d(T_d - D), 0)$$

where T_d is the daily mean temperature in ^{o}C and D is the dew point calculated as .

$$\upsilon = \frac{17.27 T_d}{237.70 + T_d} + \log(RH/100)$$

$$D = \frac{237.70\upsilon}{17.27 - \upsilon}$$

where RH is the relative humidity (%).

On days when the total precipitation exceeds 3.0mm, the Nesterov index accumulator is reset back to zero.

1.18.3 Fuel properties

Total fuel load $F_{tot,patch}$ for a given patch is the sum of the above ground coarse woody debris and the leaf litter, plus the alive grass leaf biomass $b_{l,grass}$ multiplied by the non-mineral fraction (1-M_f).

$$F_{tot,patch} = \left(\sum_{fc=1}^{fc=5} CWD_{AG,fc} + l_{litter} + b_{l,grass} \right) (1 - M_f)$$

Many of the model behaviours are affected by the patch-level weighted average properties of the fuel load. Typically, these are calculated in the absence of 1000-h fuels because these do not contribute greatly to fire spread properties.

Dead Fuel Moisture Content

Dead fuel moisture is calculated as

$$moist_{df,fc} = e^{-\alpha_{fmc,fc} N_I}$$

where $\alpha_{fmc,fc}$ is a parameter defining how fuel moisture content varies between the first four dead fuel classes.

Live grass moisture Content

The live grass fractional moisture content($moist_{lg}$) is a function of the soil moisture content. (Equation B2 in *Thonicke et al. 2010*)

$$moist_{lg} = \max(0.0, \frac{10}{9}\theta_{30} - \frac{1}{9})$$

where θ_{30} is the fractional moisture content of the top 30cm of soil.

Patch Fuel Moisture

The total patch fuel moisture is based on the weighted average of the different moisture contents associated with each of the different live grass and dead fuel types available (except 1000-h fuels).

$$F_{m,patch} = \sum_{fc=1}^{fc=4} \frac{F_{fc}}{F_{tot}} moist_{df,fc} + \frac{b_{l,grass}}{F_{tot}} moist_{lg}$$

Effective Fuel Moisture Content

Effective Fuel Moisture Content is used for calculations of fuel consumed, and is a function of the ratio of dead fuel moisture content $M_{df,fc}$ and the moisture of extinction factor, $m_{ef,fc}$

$$E_{moist,fc} = \frac{moist_{fc}}{m_{ef,fc}}$$

where the m_{ef} is a function of surface-area to volume ratio.

$$m_{ef,fc} = 0.524 - 0.066 \log_{10} \sigma_{fc}$$

Patch Fuel Moisture of Extinction

The patch 'moisture of extinction' factor (F_{mef}) is the weighted average of the m_{ef} of the different fuel classes

$$F_{mef,patch} = \sum_{fc=1}^{fc=5} \frac{F_{fc}}{F_{tot}} m_{ef,fc} + \frac{b_{l,grass}}{F_{tot}} m_{ef,grass}$$

Patch Fuel Bulk Density

The patch fuel bulk density is the weighted average of the bulk density of the different fuel classes (except 1000-h fuels).

$$F_{bd,patch} = \sum_{fc=1}^{fc=4} \frac{F_{fc}}{F_{tot}} \beta_{fuel,fc} + \frac{b_{l,grass}}{F_{tot}} \beta_{fuel,lgrass}$$

where $\beta_{fuel,fc}$ is the bulk density of each fuel size class (kG m^{-3})

Patch Fuel Surface Area to Volume

The patch surface area to volume ratio (F_σ) is the weighted average of the surface area to volume ratios (σ_{fuel}) of the different fuel classes (except 1000-h fuels).

$$F_\sigma = \sum_{fc=1}^{fc=4} \frac{F_{fc}}{F_{tot}} \sigma_{fuel,fc} + \frac{b_{l,grass}}{F_{tot}} \sigma_{fuel,grass}$$

1.18.4 Forward rate of spread

For each patch and each day, we calculate the rate of forward spread of the fire ros_f (nominally in the direction of the wind).

$$ros_f = \frac{i_r x_i (1 + \phi_w)}{F_{bd,patch} e_{ps} q_{ig}}$$

e_{ps} is the effective heating number ($e^{\frac{-4.528}{F_{\sigma,patch}}}$). q_{ig} is the heat of pre-ignition ($581 + 2594 F_m$). x_i is the propagating flux calculated as (see *Thonicke et al. 2010* Appendix A).

$$x_i = \frac{e^{0.792 + 3.7597 F_{\sigma,patch}^{0.5} (\frac{F_{bd,patch}}{p_d} + 0.1)}}{192 + 7.9095 F_{\sigma,patch}}$$

ϕ_w is the influence of windspeed on rate of spread.

$$\phi_w = c b_w^b . \beta^{-e}$$

Where b, c and e are all functions of surface-area-volume ratio $F_{\sigma,patch}$: $b = 0.15988 F_{\sigma,patch}^{0.54}$, $c = 7.47 e^{-0.8711 F_{\sigma,patch}^{0.55}}$, $e = 0.715 e^{-0.01094 F_{\sigma,patch}}$. $b_w = 196.86 W$ where W is the the windspeed in ms^{-1}, and $\beta = \frac{F_{bd}/p_d}{0.200395 F_{\sigma,patch}^{-0.8189}}$ where p_d is the particle density (513).

i_r is the reaction intensity, calculated using the following set of expressions (from *Thonicke et al. 2010* Appendix A).:

$$\begin{aligned}
i_r &= \Gamma_{opt} F_{tot} H d_{moist} d_{miner} \\
d_{moist} &= \max\Big(0.0, (1 - 2.59 m_w + 5.11 m_w^2 - 3.52 m_w^3)\Big) \\
m_w &= \frac{F_{m,patch}}{F_{mef,patch}} \\
\Gamma_{opt} &= \Gamma_{max} \beta^a \lambda \\
\Gamma_{max} &= \frac{1}{0.0591 + 2.926 F_{\sigma,patch}^{-1.5}} \\
\lambda &= e^{a(1-\beta)} \\
a &= 8.9033 F_{\sigma,patch}^{-0.7913}
\end{aligned}$$

Γ_{opt} is the residence time of the fire, and d_{miner} is the mineral damping coefficient (=0.174 $S_e^{-0.19}$, where S_e is 0.01 and so = d_{miner} 0.41739).

1.18.5 Fuel Consumption

The fuel consumption (fraction of biomass pools) of each dead biomass pool in the area affected by fire on a given day ($f_{c,dead,fc}$) is a function of effective fuel moisture $E_{moist,fc}$ and size class *fc* (Eqn B1, B4 and B5, *Thonicke et al. 2010*). The fraction of each fuel class that is consumed decreases as its moisture content relative to its moisture of extinction ($E_{moist,fc}$) increases.

$$f_{cdead,fc} = \max\Big(0, \min(1, m_{int,mc,fc} - m_{slope,mc,fc} E_{moist,fc})\Big)$$

m_{int} and m_{slope} are parameters, the value of which is modulated by both size class fc and by the effective fuel moisture class mc, defined by $E_{moist,fc}$. m_{int} and m_{slope} are defined for low-, mid-, and high-moisture conditions, the boundaries of which are also functions of the litter size class following *Peterson and Ryan 1986* (page 802). The fuel burned, $f_{cground,fc}$ (Kg m^{-2} day^{-1}) iscalculated from $f_{cdead,fc}$ for each fuel class:

$$f_{cground,fc} = f_{c,dead,fc}(1 - M_f)\frac{F_{fc}}{0.45}$$

Where 0.45 converts from carbon to biomass. The total fuel consumption, $f_{ctot,patch}$(Kg m^{-2}), used to calculate fire intensity, is then given by

$$f_{ctot,patch} = \sum_{fc=1}^{fc=4} f_{c,ground,fc} + f_{c,ground,lgrass}$$

There is no contribution from the 1000 hour fuels to the patch-level $f_{ctot,patch}$ used in the fire intensity calculation.

1.18.6 Fire Intensity

Fire intensity at the front of the burning area ($I_{surface}$, kW m^{-2}) is a function of the total fuel consumed ($f_{ctot,patch}$) and the rate of spread at the front of the fire, ros_f (m min^{-1}) (Eqn 15 *Thonicke et al. 2010*)

$$I_{surface} = \frac{0.001}{60} f_{energy} f_{ctot,patch} ros_f$$

where f_{energy} is the energy content of fuel (Kj/Kg - the same, 18000 Kj/Kg for all fuel classes). Fire intensity is used to define whether an ignition is successful. If the fire intensity is greater than 50Kw/m then the ignition is successful.

1.18.7 Fire Duration

Fire duration is a function of the fire danger index with a maximum length of $F_{dur,max}$ (240 minutes in *Thonicke et al. 2010* Eqn 14, derived from Canadian Forest Fire Behaviour Predictions Systems)

$$D_f = \min\left(F_{dur,max}, \frac{F_{dur,max}}{1 + F_{dur,max} e^{-11.06 fdi}}\right)$$

1.18.8 Fire Danger Index

Fire danger index (*fdi*) is a representation of the effect of meteorological conditions on the likelihood of a fire. It is calculated for each gridcell as a function of the Nesterov Index . *fdi* is calculated from NI as

$$fdi = 1 - e^{\alpha N_I}$$

where α = 0.00037 following *Venevsky et al. 2002*.

1.18.9 Area Burned

Total area burnt is assumed to be in the shape of an ellipse, whose major axis f_{length} (m) is determined by the forward and backward rates of spread (ros_f and ros_b respectively).

$$f_{length} = F_d(ros_b + ros_f)$$

ros_b is a function of ros_f and windspeed (Eqn 10 *Thonicke et al. 2010*)

$$ros_b = ros_f e^{-0.012W}$$

The minor axis to major axis ratio (i.e. the length-to-breadth ratio) l_b of the ellipse is determined by the windspeed. If the windspeed (W) is less than 16.67 m min^{-1} (i.e., 1 km hr $^{-1}$) then $l_b = 1$. Otherwise (Eqn 12 and 13, *Thonicke et*

al. 2010, Eqn 79 and 80 Canadian Forest Fire Behavior Prediction System Ont.Inf.Rep. ST-X-3, 1992, as corrected in errata reported in Information Report GLC-X-10 by Bottom et al., 2009)

$$l_b = \left\{ \begin{array}{ll} 1.0 + 8.729(1.0 - e^{-0.108W})^{2.155}, & f_{tree} > 0.55 \\ 1.1 * (3.6W^{0.0464}), & f_{tree} <= 0.55 \end{array} \right\}$$

f_{grass} and f_{tree} are the fractions of the patch surface covered by grass and trees respectively.

The total area burned (A_{burn} in m^2) is therefore (Eqn 11, *Thonicke et al. 2010*)

$$A_{burn} = \frac{n_f \frac{3.1416}{4l_b}(f_{length}^2))}{10000}$$

where n_f is the number of fires.

1.18.10 Crown Damage

c_k is the fraction of the crown which is consumed by the fire. This is calculated from scorch height H_s, tree height h and the crown fraction parameter F_{crown} (Eqn 17 *Thonicke et al. 2010*):

$$c_k = \left\{ \begin{array}{ll} 0 & \text{for } H_s < (h - hF_{crown}) \\ 1 - \frac{h - H_s}{h - F_{crown}} & \text{for } h > H_s > (h - hF_{crown}) \\ 1 & \text{for } H_s > h \end{array} \right.$$

The scorch height H_s (m) is a function of the fire intensity, following *Byram, 1959*, and is proportional to a plant functional type specific parameter $\alpha_{s,ft}$ (Eqn 16 *Thonicke et al. 2010*):

$$H_s = \sum_{FT=1}^{NPFT} \alpha_{s,p} \cdot f_{biomass,ft} I_{surface}^{0.667}$$

where $f_{biomass,ft}$ is the fraction of the above-ground biomass in each plant functional type.

1.18.11 Cambial Damage and Kill

The cambial kill is a function of the fuel consumed $f_{c,tot}$, the bark thickness t_b, and τ_l, the duration of cambial heating (minutes) (Eqn 8, *Peterson and Ryan 1986*):

$$\tau_l = \sum_{fc=1}^{fc=5} 39.4 F_{p,c} \frac{10000}{0.45}(1 - (1 - f_{c,dead,fc})^{0.5})$$

Bark thickness is a linear function of tree diameter dbh_{coh}, defined by PFT-specific parameters $\beta_{1,bt}$ and $\beta_{2,bt}$ (Eqn 21 *Thonicke et al. 2010*):

$$t_{b,coh} = \beta_{1,bt,ft} + \beta_{2,bt,ft} dbh_{coh}$$

The critical time for cambial kill, τ_c (minutes) is given as (Eqn 20 *Thonicke et al. 2010*):

$$\tau_c = 2.9 t_b^2$$

The mortality rate caused by cambial heating τ_{pm} of trees within the area affected by fire is a function of the ratio between τ_l and τ_c (Eqn 19, *Thonicke et al. 2010*):

$$\tau_{pm} = \left\{ \begin{array}{ll} 1.0 & \text{for } \tau_1/\tau_c \geq 2.0 \\ 0.563(\tau_l/\tau_c)) - 0.125 & \text{for } 2.0 > \tau_1/\tau_c \geq 0.22 \\ 0.0 & \text{for } \tau_1/\tau_c < 0.22 \end{array} \right.$$

Table 1.21: Parameters needed for fire model.

Parameter Symbol	Parameter Name	Units	indexed by
$\beta_{1,bt}$	Intercept of bark thickness function	mm	*FT*
$\beta_{2,bt}$	Slope of bark thickness function	mm cm^{-1}	*FT*
F_{crown}	Ratio of crown height to total height	none	*FT*
α_{fmc}	Fuel moisture parameter	^{o}C $^{-2}$	*fc*
β_{fuel}	Fuel Bulk Density	kG m^{-3}	*fc*
$\sigma_{fuel,fc}$	Surface area to volume ratio	cm $^{-1}$	*fc*
m_{int}	Intercept of fuel burned	none	fc, moisture class
m_{slope}	Slope of fuel burned	none	fc, moisture class
M_f	Fuel Mineral Fraction		
$F_{dur,max}$	Maximum Duration of Fire	Minutes	
f_{energy}	Energy content of fuel	kJ/kG	
α_s	Flame height parameter		*FT*

1.19 Wood Harvest (The selective logging module)

Over half of all tropical forests have been cleared or logged, and almost half of standing old-growth tropical forests are designated by national forest services for timber production (Sist et al., 2015). Disturbances that result from logging are known to cause forest degradation at the same magnitude as deforestation each year in terms of both geographic extent and intensity, with widespread collateral damage to remaining trees, vegetation and soils, leading to disturbance to water, energy, and carbon cycling, as well as ecosystem integrity (*Keller et al., 2004*; *Asner et al., 2004*).

The selective logging module in FATES mimics the ecological, biophysical, and biogeochemical processes following a logging event. The module (1) specifies the timing and areal extent of a logging event; (2) calculates the fractions of trees that are damaged by direct felling, collateral damage, and infrastructure damage, and adds these size-specific plant mortality types to FATES; (3) splits the logged patch into disturbed and intact new patches; (4) applies the calculated survivorship to cohorts in the disturbed patch; and (5) transports harvested logs off-site by adding the remaining necromass from damaged trees into coarse woody debris and litter pool.

1.19.1 Logging practices

The logging module struture and parameterization is based on detailed field and remote sensing studies (*Putz et al., 2008*; *Asner et al., 2004*; *Pereira Jr et al., 2002*; *Asner et al., 2005*; *Feldpausch et al., 2005*). Logging infrastructure including roads, skids, trails, and log decks are represented (Figure 1.17.1). The construction of log decks used to store logs prior to road transport leads to large canopy openings but their contribution to landscape-level gap dynamics is small. In contrast, the canopy gaps caused by tree felling are small but their coverage is spatially extensive at the landscape scale. Variations in logging practices significantly affect the level of disturbance to tropical forest following logging (*Pereira Jr et al., 2002*; *Macpherson et al., 2012*; *Dykstra, 2002*; *Putz et al., 2008*.

Logging operations in the tropics are often carried out with little planning, and typically use heavy machinery to access the forests accompanied by construction of excessive roads and skid trails, leading to unnecessary tree fall and compaction of the soil. We refer to these typical operations as conventional logging (CL). In contrast, reduced impact logging (RIL) is a practice with extensive pre-harvest planning,where trees are inventoried and mapped out for the most efficient and cost-effective harvest and seed trees are deliberately left on site to facilitate faster recovery. Through planning, the construction of skid trails and roads, soil compaction and disturbance can be minimized. Vines connecting trees are cut and tree-fall directions are controlled to reduce damages to surrounding trees. Reduced impact

logging results in consistently less disturbance to forests than conventional logging (*Pereira Jr et al. 2002*; *Putz et al. 2008*).

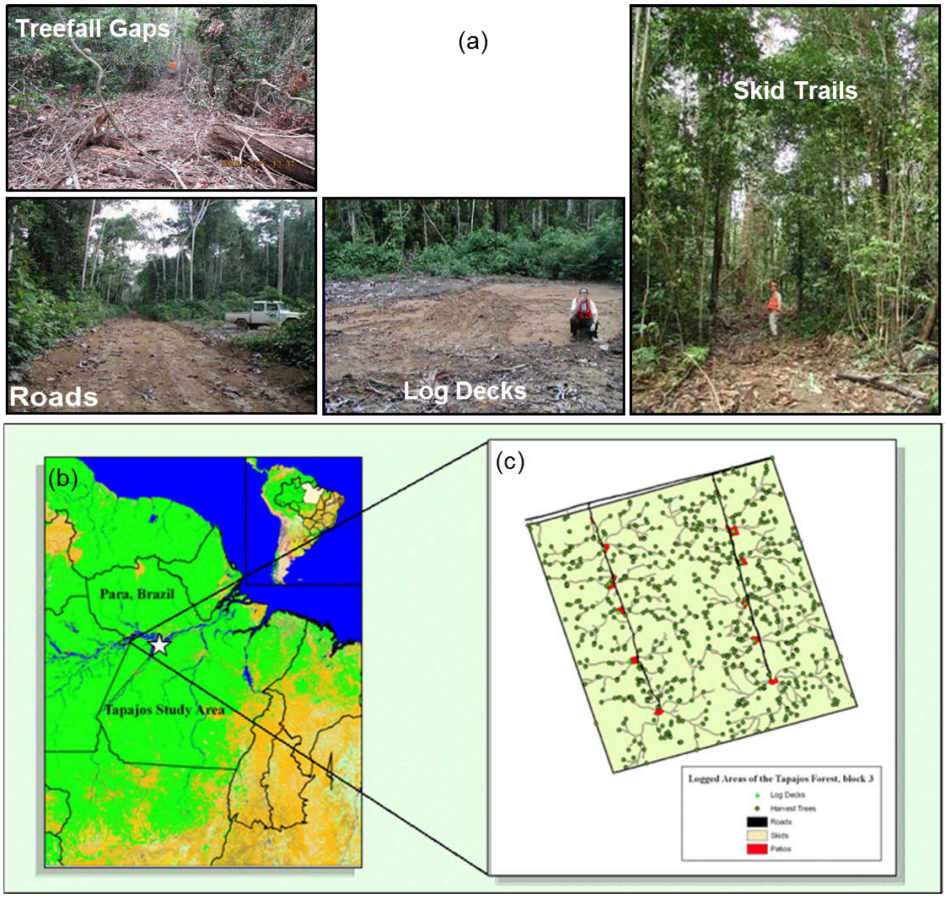

Figure 1.17.1. (a) Landscape components of selective logging; (b) location of the Tapajos National Forest in the Amazon; and (c) a typical logging block showing tree-fall location, skid trail, road, and log deck coverages. Panels (b) and (c) are from *Asner et al.* (2008).

1.19.2 Mortality associated with logging

The FATES logging module was designed to represent a range of logging practices in field operations at a landscape level. Once logging events are activated, we define three types of mortality associated with logging practices: direct-felling mortality ($lmort_{direct}$), collateral mortality ($lmort_{collateral}$), and mechanical mortality ($lmort_{mechanical}$). The direct felling mortality represents the fraction of trees selected for harvesting that are greater or equal to a diameter threshold (this threshold is defined by the diameter at breast height (DBH) = 1.3 m denoted as DBH_{min}); collateral mortality denotes the fraction of adjacent trees that killed by felling of the harvested trees; and the mechanical mortality represents the fraction of trees killed by construction of log decks, skid trails and roads for accessing the harvested trees, as well as storing and transporting logs offsite (Figure 1.17.1a). In a logging operation, the loggers typically avoid large trees when they build log decks, skids, and trails by knocking down relatively small trees as it is not economical to knock down large trees. Therefore, we implemented another DBH threshold, $DBH_{max_{infra}}$, so that only a fraction of trees $<= DBH_{max_{infra}}$ (called mechanical damage fraction) are removed for building infrastructure (*Feldpausch et al., 2005*).

1.19.3 Patch dynamics following logging disturbance

To capture the disturbance mechanisms and degree of damage associated with logging practices at the landscape level, we apply the mortality types following a workflow designed to correspond to field operations. In FATES, as illustrated in Figure 1.17.2., individual trees of all plant functional types (PFTs) in one patch are grouped into cohorts of similar-sized trees, whose size and population sizes evolve in time through processes of recruitment, growth, and mortality. As described abve, cohorts are organized into canopy and understory layers, which are subject to different light conditions (Figure 1.17.2a). When logging activities occur, the canopy trees and a portion of big understory trees lose their crown coverage through direct felling for harvesting logs, or as a result of collateral and mechanical damages ((Figure 1.17.2b). The fractions of (only the) canopy trees affected by the three mortality mechanisms are then summed up to specify the areal percentages of an old (undisturbed) and a new (disturbed) patch caused by logging in the patch fission process (Figure 1.17.2c). After patch fission, the canopy layer over the disturbed patch is removed, while that over the undisturbed patch stays untouched (Figure 1.17.2d). In the undisturbed patch, the survivorship of understory trees is calculated using an understory death fraction consistent with whose default value corresponds to that used for natural disturbance (i_d, 0.559). To differentiate logging from natural disturbance, a slightly elevated, logging-specific understory death fraction is applied in the disturbed patch instead at the time of the logging event. Based on data from field surveys over logged forest plots in southern Amazon (*Feldpausch et al., 2005*), understory death fraction corresponding to logging is now set to be 0.65 as the default, but can be modified via the FATES parameter file (Figure 1.17.2e). Therefore, the logging operations will change the forest from the undisturbed state shown in Figure 1.17.2a to a disturbed state in Figure 1.17.2f in the logging module. It is worth mentioning that the newly generated patches are tracked according to age since disturbance and will be merged with other patches of similar canopy structure following the patch fusion processes in FATES in later time steps of a simulation, pending the inclusion of separate land-use fractions for managed and unmanaged forest.

1.19.4 Flow of necromass following logging disturbance

Logging operations affect forest structure and composition, and also carbon cycling (Palace et al., 2008) by modifying the live biomass pools and flow of necromass (Figure 1.17.3). Following a logging event, the logged trunk products from the harvested trees are transported off-site (as an added carbon pool for resource management in the model), while their branches enter the coarse woody debris (CWD) pool, and their leaves and fine roots enter the litter pool. Similarly, trunks and branches of the dead trees caused by collateral and mechanical damages also become CWD, while their leaves and fine roots become litter. Specifically, the densities of dead trees as a result of direct felling, collateral, and mechanical damages in a cohort are calculated as follows:

$$D_{direct} = lmort_{direct} * n/A$$

$$D_{collateral} = lmort_{collateral} * n/A$$

$$D_{mechanical} = lmort_{mechanical} * n/A$$

where A stands for the area of the patch being logged, and n is the number of individuals in the cohort where the mortality types apply (i.e., as specified by the size thresholds, DBH_{min} and $DBH_{max_{infra}}$). For each cohort, we denote $D_{indirect} = D_{collateral} + D_{mechanical}$ and $D_{total} = D_{direct} + D_{indirect}$, respectively.

Leaf litter ($Litter_{leaf}, [kgC]$) and root litter ($Litter_{root}, [kgC]$) at the cohort level are then calculated as:

$$Litter_{leaf} = D_{total} * B_{leaf} * A$$

$$D_{leaf} = D_{total} * (B_{root} + B_{store}) * A$$

where B_{leaf}, B_{root}, B_{store} are live biomass in leaves and fine roots, and stored biomass in the labile carbon reserve in all individual trees in the cohort of interest.

Following the existing CWD structure in FATES (*Fisher et al., 2015*), CWD in the logging module is first separated into two categories: above-ground CWD and below-ground CWD. Within each category, four size classes are tracked

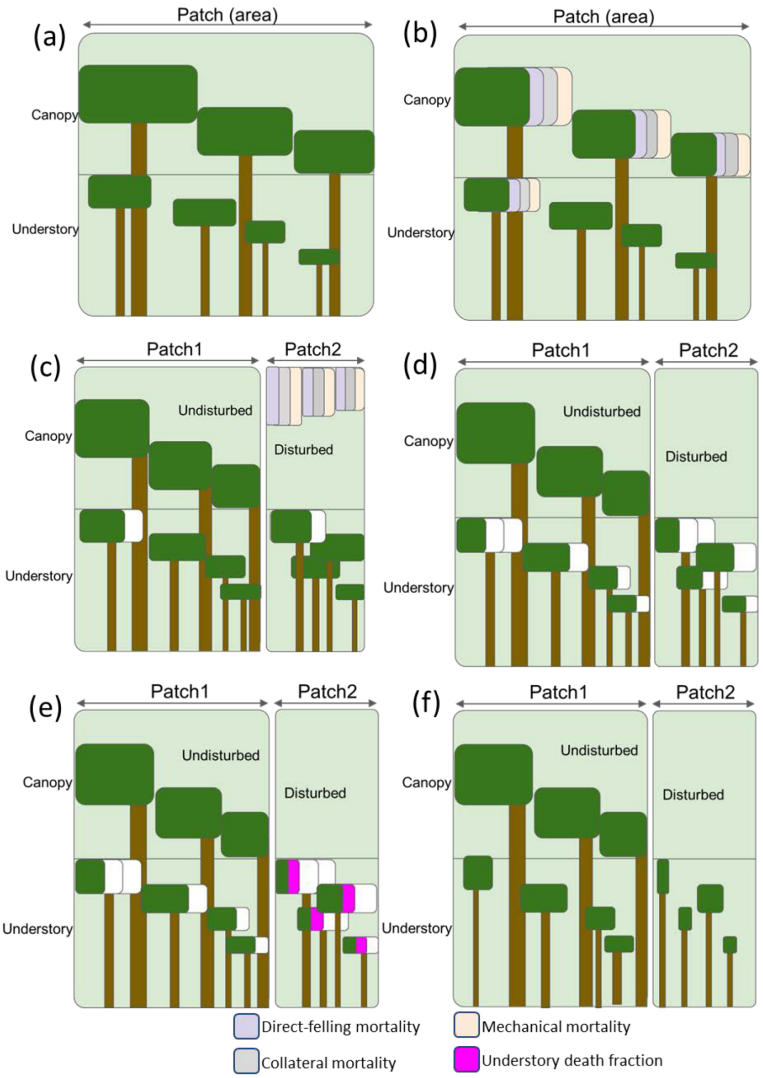

Figure 1.17.2. The mortality types (direct-felling, mechanical, and collateral) and patch generating process in the FATES logging module. The white fraction in (c), (d), (f) indicates mortality associated with other disturbances in FATES. (a) Canopy and understory layers in each cohort in FATES; (b) Mortality applied at the time of a logging event; (c) the patch fission process following a given logging event; (d) canopy removal in the disturbed patch following the logging event; (e) calculate the understory survivorship based on the understory death fraction in each patch; (f) the final states of the intact and disturbed patches.

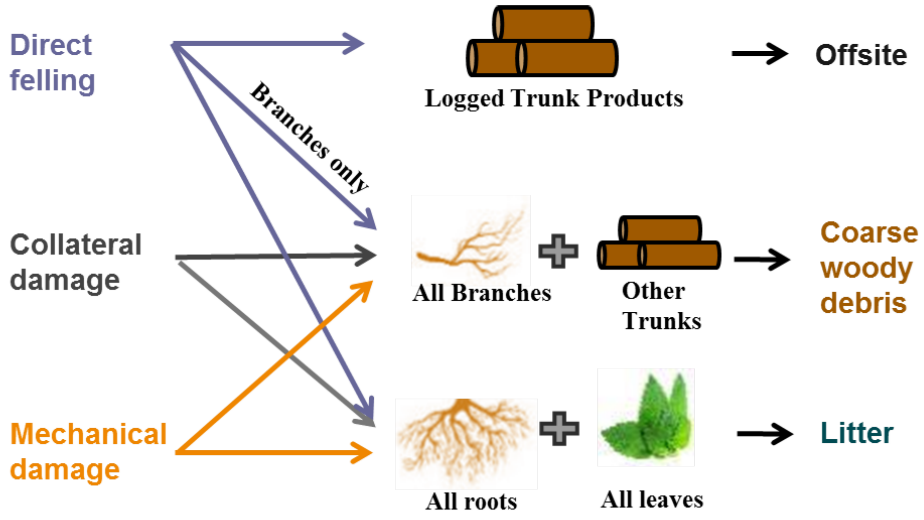

Figure 1.17.3. The flow of necromass following logging.

based on their source, following *Thonicke et al. (2010)*: trunks, large branches, small branches and twigs. Above-ground CWD from trunks ($CWD_{trunk_{agb}}, [kgC]$) and large branches/small branches/twig ($CWD_{branch_{agb}}, [kgC]$) are calculated as follows:

$$CWD_{trunk_{agb}} = D_{indiect} * AGB_{stem} * f_{trunk} * A$$

$$CWD_{branch_{agb}} = D_{total} * AGB_{stem} * f_{branch} * A$$

where AGB_{stem} is the amount of above ground stem biomass in the cohort, f_{trunk} and f_{branch} represent the fraction of trunks and large branches/small branches/twig. Similarly, the below-ground CWD from trunks ($CWD_{trunk_{bg}}, [kgC]$) and branches/twig ($CWD_{branch_{bg}}, [kgC]$) are calculated as follows:

$$CWD_{trunk_{bg}} = D_{total} * B_{root_{bg}} * f_{trunk} * A$$

$$CWD_{branch_{bg}} = D_{total} * B_{root_{bg}} * f_{branch} * A$$

where $B_{croot}[kgC]$ is the amount of coarse root biomass in the cohort. Site-level total litter and CWD inputs can then be obtained by integrating the corresponding pools over all the cohorts in the site. To ensure mass conservation,

$$\delta_B = \delta_{Litter} + \delta_{CWD} + trunk_{product}$$

where δ_B is total loss of biomass due to logging, δ_{litter} and δ_{CWD} are the increments in litter and CWD pools, and $trunk_{product}$ represents harvested logs shipped offsite.

Following the logging event, the forest structure and composition in terms of cohort distributions, as well as the live biomass and necromass pools are updated. Following this logging event update to forest structure, the native processes simulating physiology, growth and competition for resources in and between cohorts resume. Since the canopy layer is removed in the disturbed patch, the existing understory trees are promoted to the canopy layer, but, in general, the canopy is incompletely filled in by these newly-promoted trees, and thus the canopy does not fully close. Therefore, more light can penetrate and reach the understory layer in the disturbed patch, leading to increases in light-demanding species in the early stage of regeneration, followed by a succession process in which shade tolerant species dominate gradually.

The above describes the case where the canopy is closed (by treees) prior to logging. If this is not the case, some amount of non-tree-occupied canopy area is also moved to the newly-disturbed patch so as to maintain the composition of the undisturbed patch or patches in their original state (albeit in covering a smaller area).

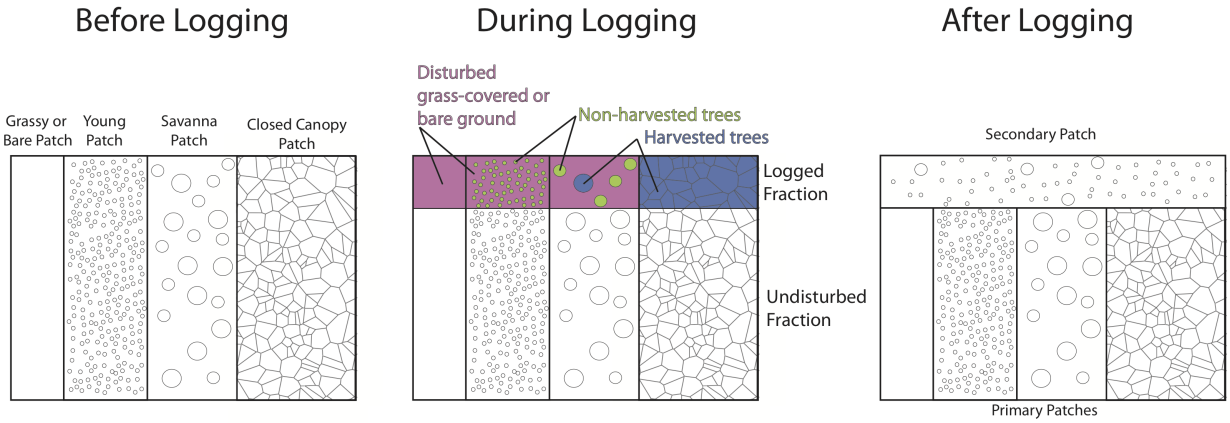

After logging occurs, the patches that have been disturbed are tracked as belonging to secondary lands, and are not fused with patches on primary lands. This allows primary and secondary land areas to be tracked, with possibly different ecological dynamics occuring on each.

. _rst_References:

CHAPTER 2

REFERENCES

Aber, J.D., Melillo, J.M. and McClaugherty, C.A., 1990. Predicting long-term patterns of mass loss, nitrogen dynamics, and soil organic matter formation from initial fime litter chemistry in temperate forest ecosystems. Canadian Journal of Botany, 68: 2201-2208.

Aber, J.D., Goodale, C.L., Ollinger, S.V., Smith, M.-L., Magill, A.H., Martin, M.E., Hallett, R.A., and Stoddard, J.L. 2003. Is nitrogen deposition altering the nitrogen status of northeastern forests? BioScience 53:375-389.

Ali, A. A., C. Xu, A. Rogers, R. A. Fisher, S. D. Wullschleger, E. Massoud, J. A. Vrugt, J. D. Muss, N. McDowell, and J. Fisher, 2016: A global scale mechanistic model of photosynthetic capacity (LUNA V1. 0). Geosci. Mod. Dev., 9:587-606.

Allen, C.B., Will, R.E., and Jacobson, M.A. 2005. Production efficiency and radiation use efficiency of four tree species receiving irrigation and fertilization. Forest Science 51:556-569.

Anderson, E.A. 1976. A point energy and mass balance model of a snow cover. NOAA Technical Report NWS 19, Office of Hydrology, National Weather Service, Silver Spring, MD.

André, J.-C., Goutorbe, J.-P., and Perrier, A. 1986. HAPEX-MOBILHY: A hydrologic atmosphere experiment for the study of water budget and evaporation flux at the climatic scale. Bull. Amer. Meteor. Soc. 67:138-144.

Andrén, O. and Paustian, K., 1987. Barley straw decomposition in the field: a comparison of models. Ecology 68:1190-1200.

Arah, J.R.M. and Stephen, K.D., 1998. A model of the processes leading to methane emission from peatland. Atmos. Environ. 32:3257-3264.

Arah, J. and Vinten, A., 1995. Simplified models of anoxia and denitrification in aggregated and simple-structured soils. European Journal of Soil Science 46:507-517.

Arendt, A., et al. 2012. Randolph Glacier Inventory: A Dataset of Global Glacier Outlines Version: 1.0, Global Land Ice Measurements from Space, Boulder Colorado, USA. Digital Media.

Arora, V.K. and Boer, G.J. 2005. Fire as an interactive component of dynamic vegetation models. J. Geophys. Res. 110:G02008. DOI:10.1029/2005JG000042.

Arya, S.P. 2001. Introduction to Meteorology. Academic Press, San Diego, CA.

Asner, G.P., Wessman, C.A., Schimel, D.S., and Archer, S. 1998. Variability in leaf and litter optical properties: implications for BRDF model inversions using AVHRR, MODIS, and MISR. Remote Sens. Environ. 63:243-257.

Asner, G. P., Keller, M., Pereira, J. R., Zweede, J. C., and Silva, J. N. M. 2004. Canopy damage and recovery after selective logging in amazonia: field and satellite studies, Ecological Applications, 14, 280-298, 10.1890/01-6019.

Asner, G. P., Knapp, D. E., Broadbent, E. N., Oliveira, P. J. C., Keller, M., and Silva, J. N. 2005. Selective Logging in the Brazilian Amazon, Science, 310, 480.

Axelsson, E., and Axelsson, B. 1986. Changes in carbon allocation patterns in spruce and pine trees following irrigation and fertilization. Tree Phys. 2:189-204.

Atkin OK, Bloomfield KJ, Reich PB, Tjoelker MG, Asner GP, Bonal D et al (2015) Global variability in leaf respiration in relation to climate, plant functional types and leaf traits. New Phytologist 206:614–636

Leaf Respiration in Terrestrial Biosphere Models. In Plant Respiration: Metabolic Fluxes and Carbon Balance, Advances in Photosynthesis and Respiration 43, G. Tcherkez, J. Ghashghaie (eds.) Springer International Publishing AG 2017

Badger, A.M., and Dirmeyer, P.A., 2015. Climate response to Amazon forest replacement by heterogeneous crop cover. Hydrol. Earth. Syst. Sci. 19:4547- 4557.

Baird, A.J., Beckwith, C.W., Waldron, S. and Waddington, J.M., 2004. Ebullition of methane-containing gas bubbles from near-surface Sphagnum peat. Geophys. Res. Lett. 31. DOI:10.1029/2004GL021157.

Baldocchi, D., et al. 2001. FLUXNET: A new tool to study the temporal and spatial variability of ecosystem-scale carbon dioxide, water vapor, and energy flux densities. Bull. Amer. Meteor. Soc. 82:2415-2433.

Barbottin, A., Lecomte, C., Bouchard, C., and Jeuffroy, M.-H. 2005. Nitrogen remobilization during grain filling in wheat: Genotypic and environmental effects. Crop Sci. 45:1141-1150.

Batjes, N.H., 2006. ISRIC-WISE derived soil properties on a 5 by 5 arc-minutes global grid. Report 2006/02 (available through : http://www.isric.org)

Berger, A.L. 1978a. Long-term variations of daily insolation and quaternary climatic changes. J. Atmos. Sci. 35:2362-2367.

Berger, A.L. 1978b. A simple algorithm to compute long-term variations of daily or monthly insolation. Contribution de l'Institut d'Astronomie et de Géophysique, Université Catholique de Louvain, Louvain-la-Neuve, No. 18.

Berger, A., Loutre, M.-F., and Tricot, C. 1993. Insolation and Earth's orbital periods. J. Geophys. Res. 98:10341-10362.

Berkowitz, B., and Balberg, I. 1992. Percolation approach to the problem of hydraulic conductivity in porous media. Transport in Porous Media 9:275–286.

Beven, K.J., and Kirkby, M.J. 1979. A physically based variable contributing area model of basin hydrology. Hydrol. Sci. Bull. 24:43-69.

Bohren, C. F., and Huffman, D. R. 1983. Absorption and scattering of light by small particles. John Wiley & Sons, New York, NY.

Bonan, G.B. 1996. A land surface model (LSM version 1.0) for ecological, hydrological, and atmospheric studies: Technical description and user's guide. NCAR Technical Note NCAR/TN-417+STR, National Center for Atmospheric Research, Boulder, CO, 150 pp.

Bonan, G.B. 1998. The land surface climatology of the NCAR Land Surface Model coupled to the NCAR Community Climate Model. J. Climate 11:1307-1326.

Bonan, G.B. 2002. Ecological Climatology: Concepts and Applications. Cambridge University Press.

Bonan, G.B., Oleson, K.W., Vertenstein, M., Levis, S., Zeng, X., Dai, Y., Dickinson, R.E., and Yang, Z.-L. 2002a. The land surface climatology of the Community Land Model coupled to the NCAR Community Climate Model. J. Climate 15: 3123-3149.

Bonan, G.B., Levis, S., Kergoat, L., and Oleson, K.W. 2002b. Landscapes as patches of plant functional types: An integrating concept for climate and ecosystem models. Global Biogeochem. Cycles 16: 5.1-5.23.

Bonan, G.B., and Levis, S. 2006. Evaluating aspects of the Community Land and Atmosphere Models (CLM3 and CAM3) using a dynamic global vegetation model. J. Climate 19:2290-2301.

Bonan, G.B., Lawrence P.J., Oleson K.W., Levis S., Jung M., Reichstein M., Lawrence, D.M., and Swenson, S.C. 2011. Improving canopy processes in the Community Land Model (CLM4) using global flux fields empirically inferred from FLUXNET data. J. Geophys. Res. 116, G02014. DOI:10.1029/2010JG001593.

Bonan, G. B., Oleson, K.W., Fisher, R.A., Lasslop, G., and Reichstein, M. 2012. Reconciling leaf physiological traits and canopy flux data: Use of the TRY and FLUXNET databases in the Community Land Model version 4, J. Geophys. Res., 117, G02026. DOI:10.1029/2011JG001913.

Bonan, G.B., Williams, M., Fisher, R.A., and Oleson, K.W. 2014. Modeling stomatal conductance in the earth system: linking leaf water-use efficiency and water transport along the soil–plant–atmosphere continuum, Geosci. Model Dev., 7, 2193-2222, doi:10.5194/gmd-7-2193-2014.

Botta, A et al., 2000. A global prognostic scheme of leaf onset using satellite data. Global Change Biology 6.7, pp. 709-725.

Brun, E. 1989. Investigation of wet-snow metamorphism in respect of liquid water content. Ann. Glaciol. 13:22-26.

Brunke, M. A., P. Broxton, J. Pelletier, D. Gochis, P. Hazenberg, D. M. Lawrence, L. R. Leung, G.-Y. Niu, P. A. Troch, and X. Zeng, 2016: Implementing and Evaluating Variable Soil Thickness in the Community Land Model, Version 4.5 (CLM4.5). J. Clim. 29:3441-3461.

Brzostek, E. R., J. B. Fisher, and R. P. Phillips, 2014. Modeling the carbon cost of plant nitrogen acquisition: Mycorrhizal trade-offs and multipath resistance uptake improve predictions of retranslocation. J. Geophys. Res. Biogeosci., 119, 1684–1697, doi:10.1002/2014JG002660.

Bugmann, H., and Solomon, A.M. 2000. Explaining forest composition and biomass across multiple biogeographical regions. Ecol. Appl. 10:95-114.

Busing, R.T. 2005. Tree mortality, canopy turnover, and woody detritus in old cove forests of the southern Appalachians. Ecology 86:73-84.

Buzan, J.R., Oleson, K., and Huber, M. 2015: Implementation and comparison of a suite of heat stress metrics within the Community Land Model version 4.5, Geosci. Model Dev., 8, 151-170, doi:10.5194/gmd-8-151-2015.

Byram, G.M., 1959. Combustion of forest fuels. In Forest fire: control and use.(Ed. KP Davis) pp. 61-89.

Campbell, G.S., and Norman, J.M. 1998. An Introduction to Environmental Biophysics (2:math:*{}^{nd}* edition). Springer-Verlag, New York.

Castillo, G., Kendra, C., Levis, S., and Thornton, P. 2012. Evaluation of the new CNDV option of the Community Land Model: effects of dynamic vegetation and interactive nitrogen on CLM4 means and variability. J. Climate 25:3702–3714.

Cao, M., Marshall, S. and Gregson, K., 1996. Global carbon exchange and methane emissions from natural wetlands: Application of a process-based model. J. Geophys. Res. 101(D9):14,399-14,414.

Chave et al, 2015. Improved allometric models to estimate the abovegroud biomass of tropical trees. Global Change Biology. V20, p3177-3190.

Chuang Y.L., Oren R., Bertozzi A.L, Phillips N., Katul G.G. 2006. The porous media model for the hydraulic system of a conifer tree: Linking sap flux data to transpiration rate, Ecological Modelling, 191, 447-468, doi:10.1016/j.ecolmodel.2005.03.027.

Churkina, G. et al., 2003. Analyzing the ecosystem carbon dynamics of four European coniferous forests using a biogeochemistry model. Ecosystems, 6: 168-184.

CIESIN: Gridded population of the world version 3 (GPWv3), 2005. Population density grids, Technical report, Socioeconomic Data and Applications Center (SEDAC), Columbia University, Palisades, New York, USA.

Clapp, R.B., and Hornberger, G.M. 1978. Empirical equations for some soil hydraulic properties. Water Resour. Res. 14:601-604.

Clauser, C., and Huenges, E. 1995. Thermal conductivity of rocks and minerals. pp. 105-126. In: T. J. Ahrens (editor) Rock Physics and Phase Relations: A Handbook of Physical Constants. Washington, D.C.

Cleveland, C.C., Townsend, A.R., Schimel, D.S., Fisher, H., Howarth, R.W., Hedin, L.O., Perakis, S.S., Latty, E.F., Von Fischer, J.C., Elseroad, A., and Wasson, M.F. 1999. Global patterns of terrestrial biological nitrogen (N2) fixation in natural ecosystems. Global Biogeochem. Cycles 13:623-645.

Collatz, G.J., Ball, J.T., Grivet, C., and Berry, J.A. 1991. Physiological and environmental regulation of stomatal conductance, photosynthesis, and transpiration: A model that includes a laminar boundary layer. Agric. For. Meteor. 54:107-136.

Collatz, G.J., Ribas-Carbo, M., and Berry, J.A. 1992. Coupled photosynthesis-stomatal conductance model for leaves of C_4 plants. Aust. J. Plant Physiol. 19:519-538.

Colmer, T.D., 2003. Long-distance transport of gases in plants: a perspective on internal aeration and radial oxygen loss from roots. Plant Cell and Environment 26:17-36.

Conway, H., Gades, A., and Raymond, C.F. 1996. Albedo of dirty snow during conditions of melt. Water Resour. Res. 32:1713-1718.

Cosby, B.J., Hornberger, G.M., Clapp, R.B., and Ginn, T.R. 1984. A statistical exploration of the relationships of soil moisture characteristics to the physical properties of soils. Water Resour. Res. 20:682-690.

Crawford, T. W., Rendig, V. V., and Broadent, F. E. 1982. Sources, fluxes, and sinks of nitrogen during early reproductive growth of maize (Zea mays L.). Plant Physiol. 70:1645-1660.

Dahlin, K., R. Fisher, and P. Lawrence, 2015: Environmental drivers of drought deciduous phenology in the Community Land Model. Biogeosciences, 12:5061-5074.

Dai, Y., and Zeng, Q. 1997. A land surface model (IAP94) for climate studies. Part I: formulation and validation in off-line experiments. Adv. Atmos. Sci. 14:433-460.

Dai, Y., et al. 2001. Common Land Model: Technical documentation and user's guide [Available online at http://climate.eas.gatech.edu/dai/clmdoc.pdf].

Dai, Y., Zeng, X., Dickinson, R.E., Baker, I., Bonan, G.B., Bosilovich, M.G., Denning, A.S., Dirmeyer, P.A., Houser, P.R., Niu, G., Oleson, K.W., Schlosser, C.A., and Yang, Z.-L. 2003. The Common Land Model. Bull. Amer. Meteor. Soc. 84:1013-1023.

Dai, Y., Dickinson, R.E., and Wang, Y.-P. 2004. A two-big-leaf model for canopy temperature, photosynthesis, and stomatal conductance. J. Climate 17:2281-2299.

Dai, A., and Trenberth, K.E. 2002. Estimates of freshwater discharge from continents: Latitudinal and seasonal variations. J. Hydrometeor. 3:660-687.

DeFries, R.S., Hansen, M.C., Townshend, J.R.G., Janetos, A.C., and Loveland, T.R. 2000. A new global 1-km dataset of percentage tree cover derived from remote sensing. Global Change Biol. 6:247-254.

Degens, B. and Sparling, G., 1996. Changes in aggregation do not correspond with changes in labile organic C fractions in soil amended with ^{14}C-glucose. Soil Biology and Biochemistry, 28(4/5): 453-462.

de Kauwe, D.A., Kala, J., Lin, Y.-S., Pitman, A.J., Medlyn, B.E., Duursma, R.A., Abramowitz, G., Wang, Y.-P., Miralles, D.G. 2015. A test of an optimal stomatal conductance scheme within the CABLE land surface model. Geosci. Model Dev. 8(2):431-452.

de Vries, D.A. 1963. Thermal Properties of Soils. In: W.R. van Wijk (editor) Physics of the Plant Environment. North-Holland, Amsterdam.

Dickinson, R.E. 1983. Land surface processes and climate-surface albedos and energy balance. Adv. Geophys. 25:305-353.

Dickinson, R.E., Henderson-Sellers, A., and Kennedy, P.J. 1993. Biosphere-Atmosphere Transfer Scheme (BATS) version 1e as coupled to the NCAR Community Climate Model. NCAR Technical Note NCAR/TN-387+STR. National Center for Atmospheric Research, Boulder, CO.

Dickinson, R.E., Oleson, K.W., Bonan, G., Hoffman, F., Thornton, P., Vertenstein, M., Yang, Z.-L., and Zeng, X. 2006. The Community Land Model and its climate statistics as a component of the Community Climate System Model. J. Climate 19:2302-2324.

Dingman, S.L. 2002. Physical Hydrology. Second Edition. Prentice Hall, NJ.

Dirmeyer, P.A., Dolman, A.J., and Sato, N. 1999. The pilot phase of the Global Soil Wetness Project. Bull. Amer. Meteor. Soc. 80:851-878.

Dobson, J.E., Bright, E.A., Coleman, P.R., Durfee, R.C., and Worley, B.A. 2000. LandScan: A global population database for estimating populations at risk. Photogramm. Eng. Rem. Sens. 66:849-857.

Dorman, J.L., and Sellers, P.J. 1989. A global climatology of albedo, roughness length and stomatal resistance for atmospheric general circulation models as represented by the simple biosphere model (SiB). J. Appl. Meteor. 28:833-855.

Dougherty, R.L., Bradford, J.A., Coyne, P.I., and Sims, P.L. 1994. Applying an empirical model of stomatal conductance to three C4 grasses. Agric. For. Meteor. 67:269-290.

Drewniak, B., Song, J., Prell, J., Kotamarthi, V.R., and Jacob, R. 2013. Modeling agriculture in the Community Land Model. Geosci. Model Dev. 6:495-515. DOI:10.5194/gmd-6-495-2013.

Dykstra, D. P. 2002. Reduced impact logging: concepts and issues, Applying Reduced Impact Logging to Advance Sustainable Forest Management, 23-39.

Dunfield, P., Knowles, R., Dumont, R. and Moore, T.R., 1993. Methane Production and Consumption in Temperate and Sub-Arctic Peat Soils - Response to Temperature and Ph. Soil Biology & Biochemistry 25:321-326.

Entekhabi, D., and Eagleson, P.S. 1989. Land surface hydrology parameterization for atmospheric general circulation models including subgrid scale spatial variability. J. Climate 2:816-831.

Fang, X. and Stefan, H.G., 1996. Long-term lake water temperature and ice cover simulations/measurements. Cold Regions Science and Technology 24:289-304.

Farouki, O.T. 1981. The thermal properties of soils in cold regions. Cold Regions Sci. and Tech. 5:67-75.

Farquhar, G.D., von Caemmerer, S., and Berry, J.A. 1980. A biochemical model of photosynthetic CO_2 assimilation in leaves of C_3 species. Planta 149:78-90.

Farquhar, G.D., and von Caemmerer, S. 1982. Modeling of photosynthetic response to environmental conditions. pp. 549-587. In: O.L. Lange, P.S. Nobel, C.B. Osmond, and H. Zeigler (editors) Encyclopedia of Plant Physiology. Vol. 12B. Physiological Plant Ecology. II. Water Relations and Carbon Assimilation. Springer-Verlag, New York.

Feldpausch, T. R., Jirka, S., Passos, C. A. M., Jasper, F., and Riha, S. J. 2005. When big trees fall: Damage and carbon export by reduced impact logging in southern Amazonia, Forest Ecology and Management, 219, 199-215, https://doi.org/10.1016/j.foreco.2005.09.0035.

Ferrari, J.B., 1999. Fine-scale patterns of leaf litterfall and nitrogen cycling in an old-growth forest. Canadian Journal of Forest Research, 29: 291-302.

Firestone, M.K. and Davidson, E.A. 1989. Exchange of Trace Gases between Terrestrial Ecosystems and the Atmosphere. In: M.O. Andreae and D.S. Schimel (Editors). John Wiley and Sons, pp. 7-21.

Fisher, J. B., S. Sitch, Y. Malhi, R. A. Fisher, C. Huntingford, and S.-Y. Tan, 2010. Carbon cost of plant nitrogen acquisition: A mechanistic, globally applicable model of plant nitrogen uptake, retranslocation, and fixation. Global Biogeochem. Cycles, 24, GB1014, doi:10.1029/2009GB003621.

Fisher, R. A., S. Muszala, M. Verteinstein, P. Lawrence, C. Xu, N. G. McDowell, R. G. Knox, C. Koven, J. Holm, B. M. Rogers, A. Spessa, D. Lawrence, and G. Bonan, 2015: Taking off the training wheels: the properties of a dynamic

vegetation model without climate envelopes, CLM4.5(ED). Geosci. Model Dev., 8: 3593-3619, doi:10.5194/gmd-8-3593-2015.

Fisher, R.A., C.D. Koven, W.R.L. Anderegg, et al., 2018: Vegetation demographics in Earth System Models: A review of progress and priorities. Glob Change Biol. 2018;24:35–54. https://doi.org/10.1111/gcb.13910

Flanner, M.G., and Zender. C.S. 2005. Snowpack radiative heating: Influence on Tibetan Plateau climate. Geophys. Res. Lett. 32:L06501. DOI:10.1029/2004GL022076.

Flanner, M.G., and Zender, C.S. 2006. Linking snowpack microphysics and albedo evolution. J. Geophys. Res. 111:D12208. DOI:10.1029/2005JD006834.

Flanner, M.G., Zender, C.S., Randerson, J.T., and Rasch, P.J. 2007. Present day climate forcing and response from black carbon in snow. J. Geophys. Res. 112:D11202. DOI:10.1029/2006JD008003.

Flatau, P.J., Walko, R.L., and Cotton, W.R. 1992. Polynomial fits to saturation vapor pressure. J. Appl. Meteor. 31:1507-1513.

Foley, J.A. et al., 1996. An integrated biosphere model of land surface processes, terrestrial carbon balance, and vegetation dynamics. Global Biogeochemical Cycles 10.4, pp. 603-628.

Friedl, M.A., McIver, D.K., Hodges, J.C.F., Zhang, X.Y., Muchoney, D., Strahler, A.H., Woodcock, C.E., Gopal, S., Schneider, A., Cooper, A., Baccini, A., Gao, F., and Schaaf, C. 2002. Global land cover mapping from MODIS: algorithms and early results. Remote Sens. Environ. 83:287-302.

Frolking, S., et al. 2001. Modeling Northern Peatland Decomposition and Peat Accumulation. Ecosystems. 4:479-498.

Fyllas, N.M. et al., 2014. Analysing Amazonian forest productivity using a new individual and trait- based model (TFS v. 1). Geoscientific Model Development 7.4, pp. 1251-1269.

Gallais, A., Coque, M. Quillere, I., Prioul, J., and Hirel, B. 2006. Modeling postsilking nitrogen fluxes in maize (Zea mays) using 15N-labeling field experiments. New Phytologist 172:696-707.

Gallais, A., Coque, M., Gouis, J. L., Prioul, J. L., Hirel, B., and Quillere, I. 2007. Estimating the proportion of nitrogen remobilization and of postsilking nitrogen uptake allocated to maize kernels by Nitrogen-15 labeling. Crop Sci. 47:685-693.

Galloway, J.N., et al. 2004. Nitrogen cycles: past, present, and future. Biogeochem. 70:153-226.

Garcia, R.L., Kanemasu, E.T., Blad, B.L., Bauer, A., Hatfield, J.L., Major, D.A., Reginato, R.J., and Hubbard, K.G. 1988. Interception and use efficiency of light in winter wheat under different nitrogen regimes. Agric. For. Meteor. 44:175-186.

Gardner, W. R. 1960. Dynamic aspects of water availability to plants, Soil Sci., 89, 63–73.

Gash, J.H.C., Nobre, C.A., Roberts, J.M., and Victoria, R.L. 1996. An overview of ABRACOS. pp. 1-14. In: J.H.C. Gash, C.A. Nobre, J.M. Roberts, and R.L. Victoria (editors) Amazonian Deforestation and Climate. John Wiley and Sons, Chichester, England.

Getirana, A. C. V., A. Boone, D. Yamazaki, B. Decharme, F. Papa, and N. Mognard. 2012. The hydrological modeling and analysis platform (HyMAP): Evaluation in the Amazon basin, J. Hydrometeorol., 13, 1641-1665.

Ghimire, B., W. J. Riley, C. D. Koven, M. Mu, and J. T. Randerson, 2016: Representing leaf and root physiological traits in CLM improves global carbon and nitrogen cycling predictions. J. Adv. Mod. Earth Sys. 8: 598-613.

Gholz, H.L., Perry, C.S., Cropper, W.P., Jr. and Hendry, L.C., 1985. Litterfall, decomposition, and nitrogen and phosphorous dynamics in a chronosequence of slash pine (*Pinus elliottii*) plantations. Forest Science, 31: 463-478.

Giglio, L., Csiszar, I., and Justice, C.O. 2006. Global distribution and seasonality of active fires as observed with the Terra and Aqua Moderate Resolution Imaging Spectroradiometer (MODIS) sensors. J. Geophys. Res. 111:G02016. DOI:10.1029/2005JG000142.

Global Soil Data Task 2000. Global soil data products CD-ROM (IGBP-DIS). International Geosphere-Biosphere Programme-Data and Information Available Services [Available online at http://www.daac.ornl.gov].

Gomes, E.P.C., Mantovani, W., and Kageyama, P.Y. 2003. Mortality and recruitment of trees in a secondary montane rain forest in southeastern Brazil. Brazilian Journal of Biology 63:47-60.

Gosz, J.R., Likens, G.E., and Bormann, F.H. 1973. Nutrient release from decomposing leaf and branch litter in the Hubbard Brook Forest, New Hampshire. Ecological Monographs 43:173-191.

Gotangco Castillo C., Levis S., and Thornton P. 2012. Evaluation of the new CNDV option of the Community Land Model: Effects of dynamic vegetation and interactive nitrogen on CLM4 means and variability. J. Climate 25:3702-3714. DOI:10.1175/JCLID-11-00372.1.

Graham, S.T., Famiglietti, J.S., and Maidment, D.R. 1999. Five-minute, 1/2º, and 1º data sets of continental watersheds and river networks for use in regional and global hydrologic and climate system modeling studies. Water Resour. Res. 35:583-587.

Graven, H., C. E. Allison, D. M. Etheridge, S. Hammer, R. F. Keeling, I. Levin, H. A. J. Meijer, M. Rubino, P. P. Tans, C. M. Trudinger, B. H. Vaughn and J. W. C. White, 2017. Compiled records of carbon isotopes in atmospheric CO2 for historical simulations in CMIP6, Geoscientific Model Development, in review. doi: 10.5194/gmd-2017-166.

Grenfell, T.C., and Warren, S.G. 1999. Representation of a nonspherical ice particle by a collection of independent spheres for scattering and absorption of radiation. J. Geophys. Res. 104(D24):37697-37709.

del Grosso, S.J., et al. 2000. General model for N2O and N2 gas emissions from soils due to dentrification. Global Biogeochem. Cycles 14:1045-1060.

Guenther, A., Hewitt, C.N., Erickson, D., Fall, R., Geron, C., Graedel, T., Harley, P., Klinger, L., Lerdau, M., McKay, W.A., Pierce, T., Scholes, B., Steinbrecher, R., Tallamraju, R., Taylor, J., and Zimmerman, P. 1995. A global model of natural volatile organic compound emissions. J. Geophys. Res. 100:8873-8892.

Guenther, A., Karl, T., Harley, P., Wiedinmyer, C., Palmer. P.I., and Geron, C. 2006. Estimates of global terrestrial isoprene emissions using MEGAN (Model of Emissions of Gases and Aerosols from Nature). Atmos. Chem. Phys. 6:3181–3210.

Guenther, A. B., Jiang, X., Heald, C. L., Sakulyanontvittaya, T., Duhl, T., Emmons, L. K., & Wang, X., 2012. The Model of Emissions of Gases and Aerosols from Nature version 2.1 (MEGAN2.1): an extended and updated framework for modeling biogenic emissions, Geosci. Model Dev., 5, 1471–1492. DOI:10.5194.

Hack, J.J., Caron, J.M., Yeager, S.G., Oleson, K.W., Holland, M.M., Truesdale, J.E., and Rasch, P.J. 2006. Simulation of the global hydrological cycle in the CCSM Community Atmosphere Model version 3 (CAM3): mean features. J. Climate 19:2199-2221.

Hansen, M., DeFries, R.S., Townshend, J.R.G., Carroll, M., Dimiceli, C., and Sohlberg, R.A. 2003. Global percent tree cover at a spatial resolution of 500 meters: first results of the MODIS vegetation continuous fields algorithm. Earth Interactions 7:1-15.

Hastings, D.A., Dunbar, P.K., Elphingstone, G.M., Bootz, M., Murakami, H., Maruyama, H., Masaharu, H., Holland, P., Payne, J., Bryant, N.A., Logan, T.L., Muller, J.-P., Schreier, G., and MacDonald, J.S., eds., 1999. The Global Land One-kilometer Base Elevation (GLOBE) Digital Elevation Model, Version 1.0. National Oceanic and Atmospheric Administration, National Geophysical Data Center, 325 Broadway, Boulder, Colorado 80305-3328, U.S.A.

Heald, C.L., Henze, D.K., Horowitz, L.W., Feddema, J., Lamarque, J.-F., Guenther, A., Hess, P.G., Vitt, F., Seinfeld, J.H., Goldstein, A.H., and Fung, I. 2008. Predicted change in global secondary organic aerosol concentrations in response to future climate, emissions, and land use change. J. Geophys. Res. 113:D05211. DOI:10.1029/2007JD009092.

Heald, C.L., Wilkinson, M.J., Monson, R.K., Alo, C.A., Wang, G.L., and Guenther, A. 2009. Response of isoprene emission to ambient CO_2 changes and implications for global budgets. Global Change Biol. 15:1127-1140. DOI:10.1111/j.1365-2486.2008.01802.x

Henderson-Sellers, B. 1985. New formulation of eddy diffusion thermocline models. Appl. Math. Modelling 9:441-446.

Henderson-Sellers, B. 1986. Calculating the surface energy balance for lake and reservoir modeling: A review. Rev. Geophys. 24:625-649.

Henderson-Sellers, A., Yang, Z.-L., and Dickinson, R.E. 1993. The project for intercomparison of land-surface parameterization schemes. Bull. Amer. Meteor. Soc. 74: 1335-1349.

Hostetler, S.W., and Bartlein, P.J. 1990. Simulation of lake evaporation with application to modeling lake level variations of Harney-Malheur Lake, Oregon. Water Resour. Res. 26:2603-2612.

Hostetler, S.W., Bates, G.T., and Giorgi, F. 1993. Interactive coupling of a lake thermal model with a regional climate model. J. Geophys. Res. 98:5045-5057.

Hostetler, S.W., Giorgi, F., Bates, G.T., and Bartlein, P.J. 1994. Lake-atmosphere feedbacks associated with paleolakes Bonneville and Lahontan. Science 263:665-668.

Hou, Z., Huang, M., Leung, L.R., Lin, G., and Ricciuto, D.M. 2012. Sensitivity of surface flux simulations to hydrologic parameters based on an uncertainty quantification framework applied to the Community Land Model. J. Geophys. Res. 117:D15108.

Houlton, B.Z., Wang, Y.P., Vitousek, P.M. and Field, C.B., 2008. A unifying framework for dinitrogen fixation in the terrestrial biosphere. Nature, 454(7202), p.327.

Huang, M., and Liang, X. 2006. On the assessment of the impact of reducing parameters and identification of parameter uncertainties for a hydrologic model with applications to ungauged basins. J. Hydrol. 320:37-61.

Hugelius, G., C. Tarnocai, G. Broll, J.G. Canadell, P. Kuhry, adn D.K. Swanson, 2012. The Northern Circumpolar Soil Carbon Database: spatially distributed datasets of soil coverage and soil carbon storage in the northern permafrost regions. Earth Syst. Sci. Data Discuss., 5, 707-733 (available online at (http://dev1.geo.su.se/bbcc/dev/ncscd/).

Hunt, H.W., Ingham, E.R., Coleman, D.C., Elliott, E.T., and Reid, C.P.P. 1988. Nitrogen limitation of production and decomposition in prairie, mountain meadow, and pine forest. Ecology 69:1009-1016.

Hunt, E.R., Jr. and Running, S.W., 1992. Simulated dry matter yields for aspen and spruce stands in the north american boreal forest. Canadian Journal of Remote Sensing, 18: 126-133.

Hunt, E.R., Jr. et al., 1996. Global net carbon exchange and intra-annual atmospheric CO_2 concentrations predicted by an ecosystem process model and three-dimensional atmospheric transport model. Global Biogeochemical Cycles, 10: 431-456.

Hurtt, G.C., Frolking, S., Fearon, M.G., Moore, B., Shevliakova, E., Malyshev, S., Pacala, S.W., and Houghton, R.A. 2006. The underpinnings of land-use history: three centuries of global gridded land-use transitions, wood-harvest activity, and resulting secondary lands. Global Change Biol. 12:1208-1229.

Hurtt, G.C., et al. 2011. Harmonization of land-use scenarios for the period 1500-2100: 600 years of global gridded annual land-use transitions, wood harvest, and resulting secondary lands. Climatic Change 109:117-161. DOI:10.1007/s10584-011-0153-2.

Idso, S.B. 1981. A set of equations for full spectrum and 8- to 14-μ m and 10.5- to 12.5-μ m thermal radiation from cloudless skies. Water Resour. Res. 17:295-304.

Iiyama, I. and Hasegawa, S., 2005. Gas diffusion coefficient of undisturbed peat soils. Soil Science and Plant Nutrition 51:431-435.

Jacksonetal1996: E., and Schulze, E. D. 1996. A global analysis of root distributions for terrestrial biomes Oecologia 108:389–411. DOI:10.1007/BF00333714.

Jackson, T.L., Feddema, J.J., Oleson, K.W., Bonan, G.B., and Bauer, J.T. 2010. Parameterization of urban characteristics for global climate modeling. Annals of the Association of American Geographers. 100:848-865.

Jenkinson, D. and Coleman, K. 2008. The turnover of organic carbon in subsoils. Part 2. Modelling carbon turnover. European Journal of Soil Science 59:400-413.

Jordan, R. 1991. A One-dimensional Temperature Model for a Snow Cover: Technical Documentation for SNTHERM.89. U.S. Army Cold Regions Research and Engineering Laboratory, Special Report 91-16.

Kattge, J., and Knorr, W. 2007. Temperature acclimation in a biochemical model of photosynthesis: a reanalysis of data from 36 species. Plant Cell Environ. 30:1176-1190. DOI:10.1111/j.1365-3040.2007.01690.x.

Kattge, J., Knorr, W., Raddatz, T., and Wirth C. 2009: Quantifying photosynthetic capacity and its relationship to leaf nitrogen content for global–scale terrestrial biosphere models. Global Change Biol. 15:976–991.

Kavetski, D., Binning, P. and Sloan, S.W., 2002. Noniterative time stepping schemes with adaptive truncation error control for the solution of Richards equation. Water Resources Research, 38(10).

Keller, M., Palace, M., Asner, G.P., Pereira, R., Jr. and Silva, J.N.M., 2004. Coarse woody debris in undisturbed and logged forests in the eastern Brazilian Amazon. Global Change Biology, 10: 784-795.

Kellner, E., Baird, A.J., Oosterwoud, M., Harrison, K. and Waddington, J.M., 2006. Effect of temperature and atmospheric pressure on methane (CH4) ebullition from near-surface peats. Geophys. Res. Lett. 33. DOI:10.1029/2006GL027509.

Kimball, J.S., Thornton, P.E., White, M.A. and Running, S.W. 1997. Simulating forest productivity and surface-atmosphere exchange in the BOREAS study region. Tree Physiology 17:589-599.

Kohyama, T., Suzuki, E., Partomihardjo, T., and Yamada, T. 2001. Dynamic steady state of patch-mosaic tree size structure of a mixed diptocarp forest regulated by local crowding. Ecological Research 16:85-98.

Kourzeneva, E., 2009. Global dataset for the parameterization of lakes in Numerical Weather Prediction and Climate modeling. ALADIN Newsletter, No 37, July-December, 2009, F. Bouttier and C. Fischer, Eds., Meteo-France, Toulouse, France, 46-53.

Kourzeneva, E., 2010: External data for lake parameterization in Numerical Weather Prediction and climate modeling. Boreal Environment Research, 15, 165-177.

Kourzeneva, E., Asensio, H., Martin, E. and Faroux, S., 2012. Global gridded dataset of lake coverage and lake depth for use in numerical weather prediction and climate modelling. Tellus A 64.

Koven, C., et al. 2009. On the formation of high-latitude soil carbon stocks: The effects of cryoturbation and insulation by organic matter in a land surface model. Geophys. Res. Lett. 36: L21501.

Koven, C.D., et al. 2011. Permafrost carbon-climate feedbacks accelerate global warming. Proceedings of the National Academy of Sciences 108:14769-14774.

Koven, C.D. et al. 2013. The effect of vertically-resolved soil biogeochemistry and alternate soil C and N models on C dynamics of CLM4. Biogeosciences Discussions 10:7201-7256.

Koven, C.D. et al. 2015. Permafrost carbon-climate feedback is sensitive to deep soil carbon decomposability but not deep soil nitrogen dynamics. Proceedings of the National Academies of Science, 112, 12, 3752-3757, doi:10.1073/pnas.1415123112

Koven, C.D., G. Hugelius, D.M. Lawrence, and W.R. Wieder, 2017: Higher climatological temperature sensitivity of soil carbon in cold than warm climates. Nature Clim. Change, 7, doi:10.1038/nclimate3421.

Kucharik, C.J., J.M. Norman, and S.T. Gower, 1998. Measurements of branch area and adjusting leaf area index indirect measurements. Agricultural and Forest Meteorology 91.1, pp. 69-88.

Kucharik, C.J., Foley, J.A., Delire, C., Fisher, V.A., Coe, M.T., Lenters, J.D., Young-Molling, C., and Ramankutty, N. 2000. Testing the performance of a dynamic global ecosystem model: water balance, carbon balance, and vegetation structure. Global Biogeochem. Cycles 14: 795–825.

Kucharik, C.J., and Brye, K.R. 2003. Integrated BIosphere Simulator (IBIS) yield and nitrate loss predictions for Wisconsin maize receiving varied amounts of nitrogen fertilizer. Journal of Environmental Quality 32: 247–268.

Ladd, J.N., Jocteur-Monrozier, L. and Amato, M., 1992. Carbon turnover and nitrogen transformations in an alfisol and vertisol amended with [U-^{14}C] glucose and [^{15}N] ammonium sulfate. Soil Biology and Biochemistry, 24: 359-371.

Lamarque, J.-F., et al. 2010. Historical (1850-2000) gridded anthropogenic and biomass burning emissions of reactive gases and aerosols: methodology and application. Atmos. Chem. Phys. Discuss. 10:4963-5019. DOI:10.5194/acpd-10-4963-2010.

Larcher, W. 1995. Physiological Plant Ecology, Springer-Verlag, Berlin Heidelberg.

Lavigne, M.B., and Ryan, M.G. 1997. Growth and maintenance respiration rates of aspen, black spruce, and jack pine stems at northern and southern BOREAS sites. Tree Phys. 17:543-551.

Law, B.E., Sun, O.J., Campbell, J., Van Tuyl, S. and Thornton, P.E. 2003. Changes in carbon storage and fluxes in a chronosequence of ponderosa pine. Global Change Biology, 9: 510-514.

Lawrence, D.M., Thornton, P.E., Oleson, K.W., and Bonan, G.B. 2007. The partitioning of evapotranspiration into transpiration, soil evaporation, and canopy evaporation in a GCM: Impacts on land-atmosphere interaction. J. Hydrometeor. 8:862-880.

Lawrence, D.M., and Slater, A.G. 2008. Incorporating organic soil into a global climate model. Clim. Dyn. 30. DOI:10.1007/s00382-007-0278-1.

Lawrence, D.M., Slater, A.G., Romanovsky, V.E., and Nicolsky, D.J. 2008. The sensitivity of a model projection of near-surface permafrost degradation to soil column depth and inclusion of soil organic matter. J. Geophys. Res. 113:F02011. DOI:10.1029/2007JF000883.

Lawrence, D.M., K.W. Oleson, M.G. Flanner, P.E. Thornton, S.C. Swenson, P.J. Lawrence, X. Zeng, Z.-L. Yang, S. Levis, K. Sakaguchi, G.B. Bonan, and A.G. Slater, 2011. Parameterization improvements and functional and structural advances in version 4 of the Community Land Model. J. Adv. Model. Earth Sys. 3. DOI:10.1029/2011MS000045.

Lawrence, D.M., Hurtt, G.C., Arneth, A., Brovkin, V., Calvin, K.V., Jones, A.D., Jones, C.D., Lawrence, P.J., de Noblet-Ducoudré, N., Pongratz, J., Seneviratne, S.I., and Shevliakova, E. 2016. The Land Use Model Intercomparison Project (LUMIP) contribution to CMIP6: rationale and experimental design. Geosci. Model Dev. 9:2973-2998. DOI:10.5194/gmd-9-2973-2016.

Lawrence, P.J., and Chase, T.N. 2007. Representing a MODIS consistent land surface in the Community Land Model (CLM 3.0). J. Geophys. Res. 112:G01023. DOI:10.1029/2006JG000168.

Lawrence, P.J., and Chase, T.N. 2010. Investigating the climate impacts of global land cover change in the Community Climate System Model. Int. J. Climatol. 30:2066-2087. DOI:10.1002/joc.2061.

Lawrence, P.J., et al. 2012. Simulating the biogeochemical and biogeophysical impacts of transient land cover change and wood harvest in the Community Climate System Model (CCSM4) from 1850 to 2100. J. Climate 25:3071-3095. DOI:10.1175/JCLI-D-11-00256.1.

Lehner, B. and Döll, P., 2004. Development and validation of a global database of lakes, reservoirs and wetlands, J. Hydrol., 296, 1–22.

Lehner, B., Verdin, K. and Jarvis, A., 2008. New global hydrograhy derived from spaceborne elevation data. Eos Trans., AGU, 89, 93 – 94.

Le Page, Y., van der Werf, G.R., Morton, D.C., and Pereira, J.M.C. 2010. Modeling fire-driven deforestation potential in Amazonia under current and projected climate conditions. J. Geophys. Res. 115:G03012. DOI:10.1029/2009JG001190.

Lerman, A., 1979. Geochemical processes: Water and sediment environments. John Wiley and Sons, New York, N.Y.

Letts, M.G., Roulet, N.T., Comer, N.T., Skarupa, M.R., and Verseghy, D.L. 2000. Parametrization of peatland hydraulic properties for the Canadian Land Surface Scheme. Atmos.-Ocean 38:141-160.

Levis, S., Wiedinmyer, C., Bonan, G.B., and Guenther, A. 2003. Simulating biogenic volatile organic compound emissions in the Community Climate System Model. J. Geophys. Res. 108:4659. DOI:10.1029/2002JD003203.

Levis, S., Bonan, G.B., Vertenstein, M., and Oleson, K.W. 2004. The community land model's dynamic global vegetation model (CLM-DGVM): technical description and user's guide. NCAR Technical Note NCAR/TN-459+STR. National Center for Atmospheric Research, Boulder, Colorado. 50 pp.

Levis, S., Thornton, P., Bonan, G., and Kucharik, C. 2009. Modeling land use and land management with the Community Land Model. iLeaps newsletter, No. 7.

Levis, S., Bonan, G., Kluzek, E., Thornton, P., Jones, A., Sacks, W., and Kucharik, C 2012. Interactive crop management in the Community Earth System Model (CESM1): Seasonal influences on land-atmosphere fluxes. J. Climate 25: 4839-4859. DOI:10.1175/JCLI-D-11-00446.1.

Levis, S., Badger, A., Drewniak, B., Nevison, C., Ren, X. 2016. CLMcrop yields and water requirements: avoided impacts by choosing RCP 4.5 over 8.5. Climatic Change. DOI:10.1007/s10584-016-1654-9.

Li, C., Aber, J., Stange, F., Butterbach-Bahl, K. and Papen, H. 2000. A process-oriented model of N2O and NO emissions from forest soils: 1. Model development. J. Geophys. Res. 105(D4):4369-4384.

Li, F., Zeng, X.-D., and Levis, S. 2012a. A process-based fire parameterization of intermediate complexity in a Dynamic Global Vegetation Model. Biogeosciences 9:2761-2780.

Li, F., Zeng, X. D., and Levis, S. 2012b. Corrigendum to "A process-based fire parameterization of intermediate complexity in a Dynamic Global Vegetation Model" published in Biogeosciences, 9, 2761–2780, 2012". Biogeosciences 9: 4771-4772.

Li, F., Levis, S., and Ward, D. S. 2013a. Quantifying the role of fire in the Earth system – Part 1: Improved global fire modeling in the Community Earth System Model (CESM1). Biogeosciences 10:2293-2314.

Li, F., and Lawrence, D. 2017. Role of fire in the global land water budget during the 20th century through changing ecosystems. J. Clim. 30: 1894-1908.

Li, H.-Y., Huang, M., Tesfa, T., Ke, Y., Sun, Y., Liu, Y., and Leung, L. R. 2013b. A subbasin-based framework to represent land surface processes in an Earth System Model, Geosci. Model Dev. Discuss. 6:2699-2730. DOI:10.5194/gmdd-6-2699-2013.

Li, H., Huang, M., Wigmosta, M.S., Ke, Y., Coleman, A.M., Leung, L.R., Wang, A., and Ricciuto, D.M. 2011. Evaluating runoff simulations from the Community Land Model 4.0 using observations from flux towers and a mountainous watershed. J. Geophys. Res. 116:D24120. DOI:10.1029/2011JD016276.

Li, H., L. Leung, A. Getirana, M. Huang, H. Wu, Y. Xu, J. Guo and N. Voisin. 2015a. Evaluating global streamflow simulations by a physically-based routing model coupled with the Community Land Model, J. of Hydromet., 16(2):948-971, doi: 10.1175/JHM-D-14-0079.1

Li, H., L. Leung, T. Tesfa, N. Voisin, M. Hejazi, L. Liu, Y. Liu, J. Rice, H. Wu, and X. Yang. 2015. Modeling stream temperature in the Anthropocene: An earth system modeling approach, J. Adv. Model. Earth Syst., 7, doi:10.1002/2015MS000471.

Liang, X., Lettenmaier, D.P., Wood, E.F., and Burges, S.J. 1994. A simple hydrologically based model of land surface water and energy fluxes for GSMs. J. Geophys. Res. 99(D7):14,415–14,428.

Lichstein, J.W. and S.W. Pacala, 2011. Local diversity in heterogeneous landscapes: quantitative assessment with a height-structured forest metacommunity model'. Theoretical Ecology 4.2, pp. 269-281.

Lipscomb, W., and Sacks, W. 2012. The CESM land ice model documentation and user's guide. 46 pp. [Available online at http://www.cesm.ucar.edu/models/cesm1.1/cism/].

Lischke, H. et al., 2006. TreeMig: a forest-landscape model for simulating spatio-temporal patterns from stand to landscape scale. Ecological Modelling 199.4, pp. 409-420. 41

Lloyd, J. and Taylor, J.A., 1994. On the temperature dependence of soil respiration. Functional Ecology, 8: 315-323.

Lloyd, J., et al. 2010. Optimisation of photosynthetic carbon gain and within-canopy gradients of associated foliar traits for Amazon forest trees. Biogeosci. 7:1833-1859. DOI:10.5194/bg-7-1833-2010.

Lobell, D.B., Bala, G., and Duffy, P.B. 2006. Biogeophysical impacts of cropland management changes on climate. Geophys. Res. Lett. 33:L06708. DOI:10.1029/2005GL025492.

Lombardozzi, D.L., Bonan, G.B., Smith, N.G., Dukes, J.S. 2015. Temperature acclimation of photosynthesis and respiration: A key uncertainty in the carbon cycle-climate feedback. Geophys. Res. Lett. 42:8624-8631.

Loveland, T.R., Reed, B.C., Brown, J.F., Ohlen, D.O., Zhu, Z., Yang, L., and Merchant, J.W. 2000. Development of a global land cover characteristics database and IGBP DISCover from 1 km AVHRR data. Int. J. Remote Sens. 21:1303-1330.

Lowe, P.R. 1977. An approximating polynomial for the computation of saturation vapor pressure. J. Appl. Meteor. 16:100-103.

Luo, Y., Hui, D., and Zhang, D. 2006. Elevated CO2 stimulates net accumulations of carbon and nitrogen in land ecosystems: a meta-analysis. Ecology 87:53-63.

Magill, A.H. et al., 1997. Biogeochemical response of forest ecosystems to simulated chronic nitrogen deposition. Ecological Applications, 7: 402-415.

Mahowald, N.M., Muhs, D.R., Levis, S., Rasch, P.J., Yoshioka, M., Zender, C.S., and Luo, C. 2006. Change in atmospheric mineral aerosols in response to climate: last glacial period, pre-industrial, modern and doubled CO_2 climates. J. Geophys. Res. 111:D10202. DOI:10.1029/2005JD006653.

Makela, A. 2002. Derivation of stem taper from the pipe model theory in a carbon balance framework. Tree Phys. 22:891-905.

Mao, J., Thornton, P.E., Shi, X., Zhao, M., and Post, W.M. 2012. Remote sensing evaluation of CLM4 GPP for the period 2000 to 2009. J. Climate 25:5327-5342.

Mao, J., Shi, X., Thornton, P.E., Hoffman, F.M., Zhu, Z., and Ranga B. Myneni, R.B. 2013. Global latitudinal-asymmetric vegetation growth trends and their driving mechanisms: 1982-2009. Remote Sensing 5:1484-1497.

Martin, J.P., Haider, K. and Kassim, G., 1980. Biodegradation and stabilization after 2 years of specific crop, lignin, and polysaccharide carbons in soils. Soil Science Society of America Journal 44:1250-1255.

Martinez Cano, I., Muller-Landau, H. C., Wright, S. J., Bohlman, S. A. and Pacala S. W., 2019. Tropical tree height and crown allometries for the Barro Colorado Nature Monument, Panama: a comparison of alternative hierarchical models incorporating interspecific variation in relation to life history traits. Biogeosciences 16(4):847-862.

Mary, B., Fresneau, C., Morel, J.L. and Mariotti, A., 1993. C and N cycling during decomposition of root mucilage, roots and glucose in soil. Soil Biology and Biochemistry 25:1005-1014.

McDowell, N.G. et al., 2013. Evaluating theories of drought-induced vegetation mortality using a multimodel experiment framework. New Phytologist 200.2, pp. 304-321.

McGuire, A.D., Melillo, J.M., Joyce, L.A., Kicklighter, D.W., Grace, A.L., Moore III, B., and Vorosmarty, C.J. 1992. Interactions between carbon and nitrogen dynamics in estimating net primary productivity for potential vegetation in North America. Global Biogeochem. Cycles 6:101-124.

Macpherson, A. J., Carter, D. R., Schulze, M. D., Vidal, E., and Lentini, M. W. 2012. The sustainability of timber production from Eastern Amazonian forests, Land Use Policy, 29, 339-350, https://doi.org/10.1016/j.landusepol.2011.07.004.

Medlyn, B.E., Duursma, R.A., Eamus, D., Ellsworth, D.S., Prentice, I.C., Barton, C.V.M., Crous, K.Y., De Angelis, P., Freeman, M., and Wingate, L., 2011. Reconciling the optimal and empirical approaches to modelling stomatal conductance. Global Change Biology, 17: 2134–2144. doi:10.1111/j.1365-2486.2010.02375.x

Melzer, E., and O'Leary, M.H. 1987. Anapleurotic CO2 Fixation by Phosphoenolpyruvate Carboxylase in C3 Plants. Plant. Physiol. 84:58.

Miller, J.R., Russell, G.L., and Caliri, G. 1994. Continental-scale river flow in climate models. J. Climate 7:914-928.

Millington, R. and Quirk, J.P., 1961. Permeability of Porous Solids. Transactions of the Faraday Society 57:1200-1207.

Mironov, D. et al., 2010. Implementation of the lake parameterisation scheme FLake into the numerical weather prediction model COSMO. Boreal Environment Research 15:218-230.

Mitchell, T.D., and Jones, P.D. 2005. An improved method of constructing a database of monthly climate observations and associated high-resolution grids. Int. J. Climatol. 25:693-712.

Moldrup, P. et al. 2003. Modeling diffusion and reaction in soils: X. A unifying model for solute and gas diffusivity in unsaturated soil. Soil Science 168:321-337.

Moorcroft, P.R., G.C. Hurtt, and S.W. Pacala, 2001. A method for scaling vegetation dynamics: the ecosystem demography model ED. Ecological monographs 71.4, pp. 557-586.

Myneni, R.B., et al. 2002. Global products of vegetation leaf area and fraction absorbed PAR from year one of MODIS data. Remote Sens. Environ. 83:214-231.

Neff, J.C., Harden, J.W. and Gleixner, G. 2005. Fire effects on soil organic matter content, composition, and nutrients in boreal interior Alaska. Canadian Journal of Forest Research-Revue Canadienne De Recherche Forestiere 35:2178-2187.

Neitsch, S.L., Arnold, J.G., Kiniry, J.R., and Williams J.R. 2005. Soil and Water Assessment Tool, Theoretical Documentation: Version 2005. Temple, TX. USDA Agricultural Research Service and Texas A&M Blackland Research Center.

Negron-Juarez, R. Koven, C.D., Riley, W.J., Knox, R.G., Chambers, J.Q. 2015. Environmental Research Letters 10:064017. DOI:10.1088/1748-9326/10/6/064017.

Nemani, R.R., and Running, S.W. 1996. Implementation of a hierarchical global vegetation classification in ecosystem function models. J. Veg. Sci. 7:337-346.

Niinemets, U., Kull, O., and Tenhunen, J.D. 1998. An analysis of light effects on foliar morphology, physiology, and light interception in temperate deciduous woody species of contrasting shade tolerance. Tree Phys. 18:681-696.

Niu, G.-Y., Yang, Z.-L., Dickinson, R.E., and Gulden, L.E. 2005. A simple TOPMODEL-based runoff parameterization (SIMTOP) for use in global climate models. J. Geophys. Res. 110:D21106. DOI:10.1029/2005JD006111.

Niu, G.-Y., and Yang, Z.-L. 2006. Effects of frozen soil on snowmelt runoff and soil water storage at a continental scale. J. Hydrometeor. 7:937-952.

Niu, G.-Y., Yang, Z.-L., Dickinson, R.E., Gulden, L.E., and Su, H. 2007. Development of a simple groundwater model for use in climate models and evaluation with Gravity Recovery and Climate Experiment data. J. Geophys. Res. 112:D07103. DOI:10.1029/2006JD007522.

Niu, G.-Y., and Yang, Z.-L. 2007. An observation-based formulation of snow cover fraction and its evaluation over large North American river basins. J. Geophys. Res. 112:D21101. DOI:10.1029/2007JD008674.

Norman, J.M., 1979. Modeling the complete crop canopy. Modification of the Aerial Environment of Crops, pp. 249-280.

O'Brien, S.T., S. T., Hubbell, S. P., Spiro, P., Condit, R., and Foster, R. B. 1995. Diameter, Height, Crown, and Age Relationship in Eight Neotropical Tree Species, Ecology, 76: 1926–1939.

Oikawa, S., Hikosaka, K. and Hirose, T., 2005. Dynamics of leaf area and nitrogen in the canopy of an annual herb, Xanthium canadense. Oecologia, 143: 517-526.

Oke, T. 1987. Boundary Layer Climates (2:math:*{}^{nd}* edition). Routledge, London and New York.

Oleson, K.W., and Bonan, G.B. 2000. The effects of remotely-sensed plant functional type and leaf area index on simulations of boreal forest surface fluxes by the NCAR land surface model. J. Hydrometeor. 1:431-446.

Oleson, K.W., Dai, Y., Bonan, G., Bosilovich, M., Dickinson, R., Dirmeyer, P., Hoffman, F., Houser, P., Levis, S., Niu, G.-Y., Thornton, P., Vertenstein, M., Yang, Z.-L., and Zeng. X. 2004. Technical description of the Community Land

Model (CLM). NCAR Technical Note NCAR/TN-461+STR. National Center for Atmospheric Research, Boulder, Colorado. 173 pp.

Oleson, K.W., Niu, G.-Y., Yang, Z.-L., Lawrence, D.M., Thornton, P.E., Lawrence, P.J., Stöckli, R., Dickinson, R.E., Bonan, G.B., Levis, S., Dai, A., and Qian, T. 2008a. Improvements to the Community Land Model and their impact on the hydrological cycle. J. Geophys. Res. 113:G01021. DOI:10.1029/2007JG000563.

Oleson, K.W., Bonan, G.B., Feddema, J., Vertenstein, M., and Grimmond, C.S.B. 2008b. An urban parameterization for a global climate model. 1. Formulation and evaluation for two cities. J. Appl. Meteor. Clim. 47:1038-1060.

Oleson, K.W., Bonan, G.B., Feddema, J., and Vertenstein, M. 2008c. An urban parameterization for a global climate model. 2. Sensitivity to input parameters and the simulated urban heat island in offline simulations. J. Appl. Meteor. Clim. 47:1061-1076.

Oleson, K.W., et al. 2010a. Technical description of version 4.0 of the Community Land model (CLM). NCAR Technical Note NCAR/TN-478+STR, National Center for Atmospheric Research, Boulder, CO, 257 pp.

Oleson, K.W., Bonan, G.B., Feddema, J., Vertenstein, M., and Kluzek, E. 2010b. Technical description of an urban parameterization for the Community Land Model (CLMU). NCAR Technical Note NCAR/TN-480+STR, National Center for Atmospheric Research, Boulder, CO, 169 pp.

Oleson, K.W., et al. 2013. Technical description of version 4.5 of the Community Land Model (CLM). NCAR Technical Note NCAR/TN-503+STR, National Center for Atmospheric Research, Boulder, CO, 420 pp.

Olson, J.S., 1963. Energy storage and the balance of producers and decomposers in ecological systems. Ecology 44:322-331.

Olson, D.M., Dinerstein, E., Wikramanayake, E.D., Burgess, N.D., Powell, G.V.N., Underwood, E.C., D'Amico, J.A., Itoua, I., Strand, H. E., Morrison, J. C., Loucks, C. J., Allnutt, T. F., Ricketts, T. H., Kura, Y., Lamoreux, J. F., Wettengel, W. W., Heda, P., and Kassem, K. R., 2001. Terrestrial ecoregions of the world a new map of life on earth, Bioscience, 51, 933–938.

Orchard, V.A. and Cook, F.J., 1983. Relationship between soil respiration and soil moisture. Soil Biology and Biochemistry, 15: 447-453.

Owen, P.R. 1964. Saltation of uniform grains in air. J. Fluid Mech. 20:225-242.

Ozdogan, M., Rodell, M., Beaudoing, H.K., and Toll, D.L. 2010. Simulating the effects of irrigation over the United States in a land surface model based on satellite-derived agricultural data. Journal of Hydrometeorology 11:171-184.

Page, S.E., Siegert, F., Rieley, J.O., Boehm, H-D.V., Jaya, A., and Limin, S. 2002. The amount of carbon released from peat and forest fires in Indonesia in 1997. Nature 420:61-65.

Panofsky, H.A., and Dutton, J.A. 1984. Atmospheric Turbulence: Models and Methods for Engineering Applications. John Wiley and Sons, New York.

Parton, W., Stewart, J. and Cole, C., 1988. Dynamics of C, N, P And S in Grassland Soils - A Model. Biogeochemistry 5:109-131.

Parton, W.J., et al. 1993. Observations and modeling of biomass and soil organic matter dynamics for the grassland biome worlwide. Global Biogeochemical Cycles 7:785-809.

Parton, W. et al. 1996. Generalized model for N2 and N2O production from nitrification and denitrification. Global Biogeochemical Cycles 10:401-412.

Parton, W.J. et al. 2001. Generalized model for NOx and N2O emissions from soils. J. Geophys. Res. 106(D15):17403-17419.

Paterson, W.S.B., 1994. The Physics of Glaciers. Elsevier Science Inc., New York, 480 pp.

Pelletier, J. D., P. D. Broxton, P. Hazenberg, X. Zeng, P. A. Troch, G. Y. Niu, Z. Williams, M. A. Brunke, and D. Gochis, 2016: A gridded global data set of soil, intact regolith, and sedimentary deposit thicknesses for regional and global land surface modeling. J. Adv. Mod. Earth Sys. 8:41-65.

Pereira Jr, R., Zweede, J., Asner, G. P., and Keller, M. 2002. Forest canopy damage and recovery in reduced-impact and conventional selective logging in eastern Para, Brazil, Forest Ecology and Management, 168, 77-89, http://dx.doi.org/10.1016/S0378-1127(01)00732-0.

Peterson, D.L. and K.C. Ryan, 1986. Modeling postfire conifer mortality for long-range planning. Environmental Management 10.6, pp. 797-808.

Petrescu, A.M.R. et al. 2010. Modeling regional to global CH4 emissions of boreal and arctic wetlands. Global Biogeochemical Cycles, 24(GB4009).

Pfeiffer, M., A. Spessa, and J.O. Kaplan, 2013. A model for global biomass burning in preindustrial time: LPJ-LMfire (v1. 0). Geoscientific Model Development 6.3, pp. 643-685.

Philip, J.R. 1957. Evaporation, and moisture and heat fields in the soil. J. Meteor. 14:354-366.

Piao, S.L., et al. 2012. The carbon budget of terrestrial ecosystems in East Asia over the last two decades. Biogeosciences 9:3571-3586.

Pivovarov, A.A., 1972. Thermal Conditions in Freezing Lakes and Reservoirs. John Wiley, New York.

Pollmer, W.G., Eberhard, D., Klein, D., and Dhillon, B.S. 1979. Genetic control of nitrogen uptake and translocation in maize. Crop Sci. 19:82-86.

Pomeroy, J. W., D. M. Gray, K. R. Shook, B. Toth, R. L. H. Essery, A. Pietroniro, and N. Hedstrom. 1998. An evaluation of snow accumulation and ablation processes for land surface modelling. Hydrol. Process. 12:2339–2367.

Poorter, L., L. Bongers and F. Bongers. 2006. Architecture of 54 moist-forest tree species: Traits, trade-offs, and functional groups. Ecology, 87(5): 1289-1301.

Portmann, F.T., Siebert, S., and Döll, P. 2010. MIRCA2000 - Global monthly irrigated and rainfed crop areas around the year 2000: A new high-resolution data set for agricultural and hydrological modeling. Global Biogeochem. Cycles. 24, GB1011. DOI:10.1029/2008GB003435.

Press, W.H., Teukolsky, S.A., Vetterling, W.T., and Flannery, B.P. 1992. Numerical Recipes in FORTRAN: The Art of Scientific Computing. Cambridge University Press, New York.

Prigent, C., Papa, F., Aires, F., Rossow, W.B. and Matthews, E. 2007. Global inundation dynamics inferred from multiple satellite observations, 1993-2000. J. Geophys. Res. 112(D12).

Pritchard, M.S., Bush, A.B.G., and Marshall, S.J. 2008. Neglecting ice-atmosphere interactions underestimates ice sheet melt in millennial-scale deglaciation simulations. Geophys. Res. Lett. ** 35:L01503. DOI:10.1029/2007GL031738.

Purves, D.W. et al., 2008. Predicting and understanding forest dynamics using a simple tractable model. Proceedings of the National Academy of Sciences 105.44, pp. 17018-17022.

Putz, F. E., Sist, P., Fredericksen, T., and Dykstra, D., 2008. Reduced-impact logging: Challenges and opportunities, Forest Ecology and Management, 256, 1427-1433, https://doi.org/10.1016/j.foreco.2008.03.036.

Qian, T et al., 2006. Simulation of global land surface conditions from 1948 to 2004: Part I: Forcing data and evaluations. J. Hydrometeorology 7, pp. 953-975.

Ramankutty, N., and Foley, J. A., 1998. Characterizing patterns of global land use: An analysis of global croplands data. Global Biogeochemical Cycles, 12, 667-685.

Ramankutty, N., Evan, A., Monfreda, C., and Foley, J.A. 2008. Farming the Planet. Part 1: The Geographic Distribution of Global Agricultural Lands in the Year 2000. Global Biogeochem. Cycles. 22:GB1003. DOI:10.1029/2007GB002952.

Randlett, D.L., Zak, D.R., Pregitzer, K.S., and Curtis, P.S. 1996. Elevated atmospheric carbon dioxide and leaf litter chemistry: Influences on microbial respiration and net nitrogen mineralization. Soil Sci. Soc. Am. J. 60:1571-1577.

Rastetter, E.B., Ryan, M.G., Shaver, G.R., Melillo, J.M., Nadelhoffer, K.J., Hobbie, J.E., and Aber, J.D. 1991. A general biogeochemical model describing the responses of the C and N cycles in terrestrial ecosystems to changes in CO2, climate and N deposition. Tree Phys. 9:101-126.

Rastner, P., Bolch, T., Mölg, N., Machguth, H., and Paul, F., 2012. The first complete glacier inventory for the whole of Greenland, The Cryosphere Discuss., 6, 2399-2436, 10.5194/tcd-6-2399-2012.

Riley, W. J., Z. M. Subin, D. M. Lawrence, S. C. Swenson, M. S. Torn, L. Meng, N. Mahowald, and P. Hess, 2011a. Barriers to predicting global terrestrial methane fluxes: Analyses using a methane biogeochemistry model integrated in CESM. Biogeosciences, 8, 1925–1953. DOI:10.5194/bg-8-1925-2011.

Riley, W.J. et al. 2011b. CLM4Me, a Methane Biogeochemistry Model Integrated in CESM, Land and Biogeochemistry Model Working Group Meeting, Boulder, CO.

Roesch, A., M. Wild, H. Gilgen, and A. Ohmura. 2001. A new snow cover fraction parametrization for the ECHAM4 GCM, Clim. Dyn., 17:933–946.

Rogers, A., B. E. Medlyn, J. S. Dukes, G. Bonan, S. Caemmerer, M. C. Dietze, J. Kattge, A. D. Leakey, L. M. Mercado, and U. Niinemets, 2017: A roadmap for improving the representation of photosynthesis in Earth system models. New Phytologist, 213:22-42.

Ryan, M. G. 1991. A simple method for estimating gross carbon budgets for vegetation in forest ecosystems. Tree Phys. 9:255-266.

Running, S.W. and Coughlan, J.C., 1988. A general model of forest ecosystem processes for regional applications. I. Hydrological balance, canopy gas exchange and primary production processes. Ecological Modelling, 42: 125-154.

Running, S.W. et al., 1989. Mapping regional forest evapotranspiration and photosynthesis by coupling satellite data with ecosystem simlation. Ecology, 70: 1090-1101.

Running, S.W. and Gower, S.T., 1991. FOREST BGC, A general model of forest ecosystem processes for regional applications. II. Dynamic carbon allocation and nitrogen budgets. Tree Physiology, 9: 147-160.

Running, S.W. and Hunt, E.R., Jr., 1993. Generalization of a forest ecosystem process model for other biomes, BIOME-BGC, and an applicationfor global-scale models. In: J.R. Ehleringer and C. Field (Editors), Scaling Physiological Processes: Leaf to Globe. Academic Press, San Diego, CA, pp. 141-158.

Sacks, W. J., Cook, B. I., Buenning, N., Levis, S., and Helkowski, J. H. 2009. Effects of global irrigation on the near-surface climate. Climate Dyn., 33, 159–175. DOI:10.1007/s00382-008-0445-z.

Saggar, S., Tate, K.R., Feltham, C.W., Childs, C.W. and Parshotam, A., 1994. Carbon turnover in a range of allophanic soils amended with ^{14}C-labelled glucose. Soil Biology and Biochemistry, 26: 1263-1271.

Sakaguchi, K., and Zeng, X. 2009. Effects of soil wetness, plant litter, and under-canopy atmospheric stability on ground evaporation in the Community Land Model (CLM3.5). J. Geophys. Res. 114:D01107. DOI:10.1029/2008JD010834.

Sato, H., A. Itoh, and T. Kohyama, 2007. SEIB-DGVM: A new Dynamic Global Vegetation Model using a spatially explicit individual-based approach. Ecological Modelling 200.3, pp. 2793307.

Saldarriaga, J.G. et al., 1998. Journal of Ecology vol 76 p938-958.

Schaaf, C.B., Gao, F., Strahler, A.H., Lucht, W., Li, X., Tsang, T., Strugnell, N.C., Zhang, X., Jin, Y., and Muller, J.-P. 2002. First operational BRDF, albedo nadir reflectance products from MODIS. Remote Sens. Environ. 83:135-148.

Schlesinger, W.H., 1997. Biogeochemistry: an analysis of global change. Academic Press, London, 588 pp.

Schnell, S. and King, G.M., 1996. Responses of methanotrophic activity in soils and cultures to water stress. Applied and Environmental Microbiology 62:3203-3209.

Segers, R., 1998. Methane production and methane consumption: a review of processes underlying wetland methane fluxes. Biogeochemistry 41:23-51.

Sellers, P.J. 1985. Canopy reflectance, photosynthesis and transpiration. Int. J. Remote Sens. 6:1335-1372.

Sellers, P.J., Mintz, Y., Sud, Y.C., and Dalcher, A. 1986. A simple biosphere model (SiB) for use within general circulation models. J. Atmos. Sci. 43:505-531.

Sellers, P.J., Hall, F.G., Asrar, G., Strebel, D.E., and Murphy, R.E. 1988. The First ISLSCP Field Experiment (FIFE). Bull. Amer. Meteor. Soc. 69:22-27.

Sellers, P.J., Berry, J.A., Collatz, G.J., Field, C.B., and Hall, F.G. 1992. Canopy reflectance, photosynthesis, and transpiration. III. A reanalysis using improved leaf models and a new canopy integration scheme. Remote Sens. Environ. 42:187-216.

Sellers, P.J., et al. 1995. The Boreal Ecosystem-Atmosphere Study (BOREAS): An overview and early results from the 1994 field year. Bull. Amer. Meteor. Soc. 76:1549-1577.

Sellers, P.J., Randall, D.A., Collatz, G.J., Berry, J.A., Field, C.B., Dazlich, D.A., Zhang, C., Collelo, G.D., and Bounoua, L. 1996. A revised land surface parameterization (SiB2) for atmospheric GCMs. Part I: Model formulation. J. Climate 9:676-705.

Sellers, Piers J et al. (1996). A revised land surface parameterization (SiB2) for atmospheric GCMs. Part II: The generation of global fields of terrestrial biophysical parameters from satellite data. Journal of climate 9.4, pp. 706-737.

Shi, X., Mao, J., Thornton, P.E., and Huang, M. 2013. Spatiotemporal patterns of evapotranspiration in response to multiple environmental factors simulated by the Community Land Model. Environ. Res. Lett. 8:024012.

Shi, M., J. B. Fisher, E. R. Brzostek, and R. P. Phillips, 2016: Carbon cost of plant nitrogen acquisition: global carbon cycle impact from an improved plant nitrogen cycle in the Community Land Model. Glob. Change Biol., 22:1299-1314.

Shiklomanov, I.A. 2000. Appraisal and assessment of world water resources. Water International 25:11-32.

Siebert, S., Döll, P., Hoogeveen, J., Faures, J.M., Frenken, K., Feick, S., 2005. Development and validation of the global map of irrigation areas. Hydrol Earth Syst Sc 9:535–547

Simard, M., Pinto, N., Fisher, J.B., and Baccini, A. (2011), Mapping forest canopy height globally with spaceborne lidar. J. Geophys. Res., 116, G04021, doi:10.1029/2011JG001708.

Simpson, R.J., Lambers, H., and Dalling, M.J. 1983. Nitrogen redistribution during grain growth in wheat (Triticum avestivum L.). Plant Physiol. 71:7-14.

Sitch, S et al. (2003). Evaluation of ecosystem dynamics, plant geography and terrestrial carbon cycling in the LPJ dynamic global vegetation model. Global Change Biology 9.2, pp. 161-185.

Sivak, M. 2013. Air conditioning versus heating: climate control is more energy demanding in Minneapolis than in Miami. Environ. Res. Lett., 8, doi:10.1088/1748-9326/8/1/014050.

Smith, B., I.C. Prentice, and M.T. Sykes, 2001. Representation of vegetation dynamics in the modelling of terrestrial ecosystems: comparing two contrasting approaches within European climate space. Global Ecology and Biogeography 10.6, pp. 621-637.

Smith, A.M.S., Wooster, M.J., Drake, N.A., Dipotso, F.M. and Perry, G.L.W., 2005. Fire in African savanna: Testing the impact of incomplete combustion on pyrogenic emissions estimates. Ecological Applications, 15: 1074-1082.

Smith, A.M. and M. Stitt, 2007. Coordination of carbon supply and plant growth. Plant, cell & environment 30.9, pp. 1126-1149.

Sollins, P., 1982. Input and decay of coarse woody debris in coniferous stands in western Oregon and Washington. Canadian Journal of Forest Research, 12: 18-28.

Son, Y. and Gower, S.T., 1991. Aboveground nitrogen and phosphorus use by five plantation-grown trees with different leaf longevities. Biogeochemistry, 14: 167-191.

Sørensen, L.H., 1981. Carbon-nitrogen relationships during the humification of cellulose in soils containing different amounts of clay. Soil Biology and Biochemistry, 13: 313-321.

Sperry, J.S., Adler, F.R., Campbell, G.S. and Comstock, J.P. 1998. Limitation of plant water use by rhizosphere and xylem conductance: results from a model. Plant, Cell & Environment, 21: 347–359. doi:10.1046/j.1365-3040.1998.00287.x

Sperry, J.S. and Love, D.M. 2015. What plant hydraulics can tell us about responses to climate-change droughts. New Phytol, 207: 14–27. doi:10.1111/nph.13354

Sprugel, D.G., Ryan, M.G., Brooks, J.R., Vogt, K.A., and Martin, T.A. 1995. Respiration from the organ level to stand level. pp. 255-299. In: W. K. Smith and T. M. Hinkley (editors) Resource Physiology of Conifers. Academic Press, San Diego,CA.

Stauffer, D., and Aharony, A. 1994. Introduction to Percolation Theory. Taylor and Francis, London.

Still, C.J., Berry, J.A., Collatz, G.J., and DeFries, R.S. 2003. Global distribution of C3 and C4 vegetation: carbon cycle implications. Global Biogeochem. Cycles 17:1006. DOI:10.1029/2001GB001807.

Stöckli, R., Lawrence, D.M., Niu, G.-Y., Oleson, K.W., Thornton, P.E., Yang, Z.-L., Bonan, G.B., Denning, A.S., and Running, S.W. 2008. Use of FLUXNET in the Community Land Model development. J. Geophys. Res. 113:G01025. DOI:10.1029/2007JG000562.

Strack, M., Kellner, E. and Waddington, J.M., 2006. Effect of entrapped gas on peatland surface level fluctuations. Hydrological Processes 20:3611-3622.

Strahler, A.H., Muchoney, D., Borak, J., Friedl, M., Gopal, S., Lambin, E., and Moody. A. 1999. MODIS Land Cover Product: Algorithm Theoretical Basis Document (Version 5.0). Boston University, Boston.

Stull, R.B. 1988. An Introduction to Boundary Layer Meteorology. Kluwer Academic Publishers, Dordrecht.

Subin, Z.M., Riley, W.J. and Mironov, D. 2012a. Improved lake model for climate simulations, J. Adv. Model. Earth Syst., 4, M02001. DOI:10.1029/2011MS000072.

Subin, Z.M., Murphy, L.N., Li, F., Bonfils, C. and Riley, W.J., 2012b. Boreal lakes moderate seasonal and diurnal temperature variation and perturb atmospheric circulation: analyses in the Community Earth System Model 1 (CESM1). Tellus A, North America, 64.

Sun, Y., Gu, L., and Dickinson, R. E. 2012. A numerical issue in calculating the coupled carbon and water fluxes in a climate model, J. Geophys. Res., 117, D22103. DOI:10.1029/2012JD018059.

Swenson, S.C., Lawrence, D.M., and Lee, H. 2012. Improved Simulation of the Terrestrial Hydrological Cycle in Permafrost Regions by the Community Land Model. JAMES, 4, M08002. DOI:10.1029/2012MS000165.

Swenson, S.C. and Lawrence, D.M. 2012. A New Fractional Snow Covered Area Parameterization for the Community Land Model and its Effect on the Surface Energy Balance. JGR, 117, D21107. DOI:10.1029/2012JD018178.

Swenson, S.C., and D. M. Lawrence. 2014. Assessing a dry surface layer-based soil resistance parameterization for the Community Land Model using GRACE and FLUXNET-MTE data. JGR, 119, 10, 299–10,312, DOI:10.1002/2014JD022314.

Swenson, S.C., and D. M. Lawrence. 2015. A GRACE-based assessment of interannual groundwater dynamics in the Community Land Model. WRR, 51, doi:10.1002/2015WR017582.

Ta, C.T. and Weiland, R.T. 1992. Nitrogen partitioning in maize during ear development. Crop Sci. 32:443-451.

Tang, J.Y. and Riley, W.J. 2013. A new top boundary condition for modeling surface diffusive exchange of a generic volatile tracer: Theoretical analysis and application to soil evaporation. Hydrol. Earth Syst. Sci. 17:873-893.

Tarnocai, C., Kettles, I. M., and Lacelle, B., 2011. Peatlands of Canada, Geological Survey of Canada, Open File 6561, CD-ROM. DOI:10.495/288786.

Taylor, B.R., Parkinson, D. and Parsons, W.F.J., 1989. Nitrogen and lignin content as predictors of litter decay rates: A microcosm test. Ecology, 70: 97-104.

Thomas R.Q., Brookshire E.N., Gerber S. 2015. Nitrogen limitation on land: how can it occur in Earth system models? Global Change Biology, 21, 1777-1793, doi:10.1111/gcb.12813.

Thonicke, K., Venevsky, S., Sitch, S., and Cramer, W. 2001. The role of fire disturbance for global vegetation dynamics: coupling fire into a Dynamic Global Vegetation Model. Global Ecology and Biogeography 10:661-667.

Thonicke, K. et al., 2010. The influence of vegetation, fire spread and fire behaviour on biomass burning and trace gas emissions: results from a process-based model. Biogeosciences 7.6, pp. 1991-2011.

Thornton, P.E., 1998. Regional ecosystem simulation: combining surface- and satellite-based observations to study linkages between terrestrial energy and mass budgets. Ph.D. Thesis, The University of Montana, Missoula, 280 pp.

Thornton, P.E., Law, B.E., Gholz, H.L., Clark, K.L., Falge, E., Ellsworth, D.S., Goldstein, A.H., Monson, R.K., Hollinger, D., Falk, M., Chen, J., and Sparks, J.P. 2002. Modeling and measuring the effects of disturbance history and climate on carbon and water budgets in evergreen needleleaf forests. Agric. For. Meteor. 113:185-222.

Thornton, P.E., and Rosenbloom, N.A. 2005. Ecosystem model spin-up: estimating steady state conditions in a coupled terrestrial carbon and nitrogen cycle model. Ecological Modelling 189:25-48.

Thornton, P.E., and Zimmermann, N.E. 2007. An improved canopy integration scheme for a land surface model with prognostic canopy structure. J. Climate 20:3902-3923.

Thornton, P.E., Lamarque, J.-F., Rosenbloom, N.A., and Mahowald, N.M. 2007. Influence of carbon-nitrogen cycle coupling on land model response to CO_2 fertilization and climate variability. Global Biogeochem. Cycles 21:GB4018.

Thornton, P.E., Doney, S.C., Lindsay, K., Moore, J.K., Mahowald, N., Randerson, J.T., Fung, I., Lamarque, J.F., Feddema, J.J., and Lee, Y.H. 2009. Carbon-nitrogen interactions regulate climate-carbon cycle feedbacks: results from an atmosphere-ocean general circulation model. Biogeosci. 6:2099-2120.

Tian, H. et al. 2010. Spatial and temporal patterns of CH4 and N2O fluxes in terrestrial ecosystems of North America during 1979-2008: application of a global biogeochemistry model. Biogeosciences 7:2673-2694.

Toon, O.B., McKay, C.P., Ackerman, T.P., and Santhanam, K. 1989. Rapid calculation of radiative heating rates and photodissociation rates in inhomogeneous multiple scattering atmospheres. J. Geophys. Res. 94(D13):16,287-16,301.

Turetsky, M.R., Wieder, R.K., Halsey, L.A., and Vitt, D.H. 2002. Current disturbance and the diminishing peatland carbon sink. Geophys. Res. Lett. 29:1526. DOI:10.1029/2001GL014000.

Turetsky, M.R., Amiro, B.D., Bosch, E., and Bhatti, J.S. 2004. Historical burn area in western Canadian peatlands and its relationship to fire weather indices. Global Biogeochem. Cycles 18:GB4014. DOI:10.1029/2004GB002222.

Tye, A.M., et al. 2005. The fate of N-15 added to high Arctic tundra to mimic increased inputs of atmospheric nitrogen released from a melting snowpack. Global Change Biology 11:1640-1654.

Unland, H.E., Houser, P.R., Shuttleworth, W.J., and Yang, Z.-L. 1996. Surface flux measurement and modeling at a semi-arid Sonoran Desert site. Agric. For. Meteor. 82:119-153.

UNSTAT, 2005. National Accounts Main Aggregates Database, United Nations Statistics Division.

Uriarte, M. et al., 2009. Natural disturbance and human land use as determinants of tropical forest dynamics: results from a forest simulator. Ecological Monographs 79.3, pp. 423-443.

Vallano, D.M. and Sparks, J.P. 2007. Quantifying foliar uptake of gaseous itrogen dioxide using enriched foliar δ^{15} N values. New Phytologist 177:946-955.

van der Werf, G.R., Randerson, J.T., Giglio, L., Collatz, G.J., Mu, M., Kasibhatla, S.P., Morton, D.C., DeFries, R.S., Jin, Y., van Leeuwen, T.T. 2010. Global fire emissions and the contribution of deforestation, savanna, forest, agricultural, and peat fires (1997-2009) Atmos. Chem. Phys. 10:11707-11735.

van Veen, J.A., Ladd, J.N. and Frissel, M.J., 1984. Modelling C and N turnover through the microbial biomass in soil. Plant and Soil, 76: 257-274.

van Kampenhout, L., J.T.M. Lenaerts, W.H. Lipscomb, W.J. Sacks, D.M. Lawrence, A.G. Slater, and M.R. van den Broeke, 2017. Improving the Representation of Polar Snow and Firn in the Community Earth System Model. Journal of Advances in Modeling Earth Systems 9, no. 7: 2583–2600. https://doi.org/10.1002/2017MS000988.

Van Tricht, K., Lhermitte, S., Gorodetskaya, I.V. and van Lipzig, N.P.M., 2016. Improving satellite-retrieved surface radiative fluxes in polar regions using a smart sampling approach. The Cryosphere 10:2379-2397. doi:10.5194/tc-10-2379-2016

Van Vuuren, D.P., Lucas, P.S., and Hilderink, H.B.M., 2006. Downscaling drivers of global environmental change: enabling use of global SRES scenarios at the national and grid levels, Report 550025001, Netherlands Environmental Assessment Agency, 45 pp.

Vanninen, P., and Makela, A. 2005. Carbon budget for Scots pine trees: effects of size, competition and site fertility on growth allocation and production. Tree Phys. 25:17-30.

Venevsky, S. et al., 2002. Simulating fire regimes in human-dominated ecosystems: Iberian Peninsula case study. Global Change Biology 8.10, pp. 984-998.

Verdin, K. L., and S. K. Greenlee, 1996. Development of continental scale digital elevation models and extraction of hydrographic features, paper presented at the Third International Conference/Workshop on Integrating GIS and Environmental Modeling, Santa Fe, New Mexico, 21–26 January, Natl. Cent. for Geogr. Inf. and Anal., Santa Barbara, Calif.

Vionnet, V., E. Brun, S. Morin, A. Boone, S. Faroux, P. Le Moigne, E. Martin, and J.-M. Willemet. The Detailed Snowpack Scheme Crocus and Its Implementation in SURFEX v7.2. GMD 5, no. 3 (May 24, 2012): 773-91. https://doi.org/10.5194/gmd-5-773-2012.

Viovy, N. 2011. CRUNCEP dataset. [Description available at http://dods.extra.cea.fr/data/p529viov/cruncep/readme.htm. Data available at http://dods.extra.cea.fr/store/p529viov/cruncep/V4_1901_2011/].

Vitousek, P.M., and Howarth, R.W. 1991. Nitrogen limitation on land and in the sea: How can it occur? Biogeochem. 13:87-115.

Walter, B.P., Heimann, M. and Matthews, E., 2001. Modeling modern methane emissions from natural wetlands 1. Model description and results. J. Geophys. Res. 106(D24):34189-34206.

Wania, R., Ross, I. and Prentice, I.C. 2009. Integrating peatlands and permafrost into a dynamic global vegetation model: 2. Evaluation and sensitivity of vegetation and carbon cycle processes. Global Biogeochem. Cycles 23.

Wania, R., Ross, I. and Prentice, I.C. 2010. Implementation and evaluation of a new methane model within a dynamic global vegetation model LPJ-WHyMe v1.3. Geoscientific Model Development Discussions 3:1-59.

Wang, A., and Zeng, X. 2009. Improving the treatment of vertical snow burial fraction over short vegetation in the NCAR CLM3. Adv. Atmos. Sci. 26:877-886. DOI:10.1007/s00376-009-8098-3.

Weng, E.S. et al., 2014. Scaling from individuals to ecosystems in an Earth System Model using a mathematically tractable model of height-structured competition for light. Biogeosciences Discussions 11.12, pp. 17757-17860.

White, M.A., Thornton, P.E., and Running, S.W. 1997. A continental phenology model for monitoring vegetation responses to interannual climatic variability. Global Biogeochem. Cycles 11:217-234.

White, M.A., Thornton, P.E., Running, S.W., and Nemani, R.R. 2000. Parameterization and sensitivity analysis of the Biome-BGC terrestrial ecosystem model: net primary production controls. Earth Interactions 4:1-85.

Wieder, W. R., Cleveland, C. C., Lawrence, D. M., and Bonan, G. B. 2015. Effects of model structural uncertainty on carbon cycle projections: biological nitrogen fixation as a case study. Environmental Research Letters, 10(4), 044016.

Williams, M., Rastetter, E.B., Fernandes, D.N., Goulden, M.L., Wofsy, S.C., Shaver, G.R., Melillo, J.M., Munger, J.W., Fan, S.M. and Nadelhoffer, K.J. 1996. Modelling the soil-plant-atmosphere continuum in a Quercus–Acer stand at Harvard Forest: the regulation of stomatal conductance by light, nitrogen and soil/plant hydraulic properties. Plant, Cell & Environment, 19: 911–927. doi:10.1111/j.1365-3040.1996.tb00456.x

Wiscombe, W.J., and Warren, S.G. 1980. A model for the spectral albedo of snow. I. Pure snow. J. Atmos. Sci. 37:2712-2733.

Wood, E.F., Lettenmaier, D.P., and Zartarian, V.G. 1992. A land-surface hydrology parameterization with subgrid variability for general circulation models. J. Geophys. Res. 97(D3):2717–2728. DOI:10.1029/91JD01786.

World Bank, 2004. World development indicators 2004, Oxford University Press, New York, 416 pp.

Wu, H., J. S. Kimball, N. Mantua, and J. Stanford, 2011: Automated upscaling of river networks for macroscale hydrological modeling. Water Resour. Res., 47, W03517, doi:10.1029/2009WR008871.

Wu, H., J. S. Kimball, H. Li, M. Huang, L. R. Leung, and R. F. Adler, 2012. A New Global River Network Database for Macroscale Hydrologic modeling, Water Resour. Res., 48, W09701, doi:10.1029/2012WR012313.

Xiaodong, Y. and H.H. Shugart, 2005. FAREAST: a forest gap model to simulate dynamics and patterns of eastern Eurasian forests. Journal of Biogeography 32.9, pp. 1641-1658.

Xu, C., R. Fisher, S. D. Wullschleger, C. J. Wilson, M. Cai, and N. G. McDowell, 2012: Toward a mechanistic modeling of nitrogen limitation on vegetation dynamics. PloS one, 7:e37914.

Yang, Z.-L. 1998. Technical note of a 10-layer soil moisture and temperature model. Unpublished manuscript.

Zender, C.S., Bian, H., and Newman, D. 2003. Mineral dust entrainment and deposition (DEAD) model: Description and 1990s dust climatology. ** J. Geophys. Res. 108(D14):4416. DOI:10.1029/2002JD002775.

Zeng, X., and Dickinson, R.E. 1998. Effect of surface sublayer on surface skin temperature and fluxes. J.Climate 11:537-550.

Zeng, X., Zhao, M., and Dickinson, R.E. 1998. Intercomparison of bulk aerodynamic algorithms for the computation of sea surface fluxes using the TOGA COARE and TAO data. J. Climate 11:2628-2644.

Zeng, X. 2001. Global vegetation root distribution for land modeling. J. Hydrometeor. 2:525-530.

Zeng, X., Shaikh, M., Dai, Y., Dickinson, R.E., and Myneni, R. 2002. Coupling of the Common Land Model to the NCAR Community Climate Model. J. Climate 15:1832-1854.

Zeng, X., Dickinson, R.E., Barlage, M., Dai, Y., Wang, G., and Oleson, K. 2005. Treatment of under-canopy turbulence in land models. J. Climate 18:5086-5094.

Zeng, X., and Wang, A. 2007. Consistent parameterization of roughness length and displacement height for sparse and dense canopies in land models. J. Hydrometeor. 8:730-737.

Zeng, X., and Decker, M. 2009. Improving the numerical solution of soil moisture-based Richards equation for land models with a deep or shallow water table. J. Hydrometeor. 10:308-319.

Zeng, X., Zeng, X., and Barlage, M. 2008. Growing temperate shrubs over arid and semiarid regions in the Community Land Model - Dynamic Global Vegetation Model. Global Biogeochem. Cycles 22:GB3003. DOI:10.1029/2007GB003014.

Zhang, Y., Li, C.S., Trettin, C.C., Li, H. and Sun, G., 2002. An integrated model of soil, hydrology, and vegetation for carbon dynamics in wetland ecosystems. Global Biogeochemical Cycles 16. DOI:10.1029/2001GB001838.

Zhuang, Q., et al. 2004. Methane fluxes between terrestrial ecosystems and the atmosphere at northern high latitudes during the past century: A retrospective analysis with a process-based biogeochemistry model. Global Biogeochemical Cycles 18. DOI:10.1029/2004GB002239.

Zilitinkevich, S.S. 1970. Dynamics of the Atmospheric Boundary Layer. Leningrad Gidrometeor.

CHAPTER 3

INDICES AND TABLES

- genindex
- modindex
- search